공학박사학위논문

변환 탄성 기법을 이용한 유도초음파 클로킹의 설계와 응력 차단에의 응용

Engineering of Elastic Cloaking in Thin Plates by Using Transformation Elasticity and its Practical Application for Stress Shielding

2014년 8월

서울대학교 대학원

기계항공공학부

이 민 경

Abstract

Engineering of Elastic Cloaking in Thin Plates by Using Transformation Elasticity and its Practical Application for Stress Shielding

Minkyung Lee
School of Mechanical and Aerospace Engineering
The Graduate School
Seoul National University

This work is concerned with the realization of an elastic cloaking by transformation elasticity and its applications to stress shielding. Transformation methods have been widely used as new tools to manipulate electromagnetic or acoustic waves, but its use for elastic waves is very limited. The main reason for limited development in elastic problems is that an elastic medium has two characteristic stiffness parameters such as bulk and shear moduli. In particular, the shear modulus has no counterpart in electromagnetic/acoustic media and its existence makes it difficult to use transformation methods in elastic media because it results in form-variance under coordinate transformation. In other words, the coordinate transformation in elasticity produces extra coupling terms not existing in the original un-transformed coordinate systems. Therefore, it is impossible to realize devices with the exact material properties by using transformation elasticity.

As a means to relieve this difficulty or weaken the effects of the extra terms on wave behavior under the coordinate transformation, we first examine if the extra terms can become sufficiently small for practical applications if transformation equations are properly selected. Here, our focus mainly lies in stress shielding around a cracked or stress-concentrated region without significantly altering the original elastic wave propagation pattern around the target region.

Towards these efforts, we first show that the transformation by conformal mapping can diminish the effects of the extra terms because the extra terms related to one of the stiffness parameters identically disappear. This finding is confirmed both numerically and experimentally through a cloaking example. We propose to realize the cloaking by engineering gradient-index phononic crystals. Then, we extend the elastic cloaking as a tool for stress mitigation in a zone of stress concentration. We call this unprecedented development “stress bandage” or “stress meta-bandage” because reinforcement with a finite ring of which property is designed by transformation elasticity works as if it were a “stress-relieving” bandage. We show that the idea of stress bandage indeed works and reduces stress concentration by guiding elastic waves around a crack or a hole. At the same time, the original stress wave flow nearby is only slightly affected. Our simulation results are supported by actual experimental results, confirming the effectiveness of the proposed stress bandage idea based on the transformation elasticity method.

Keywords : transformation elasticity, elastic cloaking, stress bandage, wave manipulation

Student Number : 2010-31318

Contents

List of Tables

List of Figures

Chapter 1.

Introduction

1.1 Research Motivation

An invisibility cloaking has been a fascinating subject as much as it has been one of the most frequently appearing materials in novels and movies. It had been an imaginary and implausible device until its working principles was proposed by Pendry in 2006 [1]. Ref. [1] proposed transformation electromagnetics as a method of realizing the cloaking devices, in which electromagnetic waves can propagate along the curved path around a certain space inside it. It is realizable by arranging materials of gradually changing properties (permittivity and permeability in transformation electromagnetics) around the cloaked space, and these materials comprise an invisibility cloaking. As well as the cloaking, various devices can be composed to control waves by combining several materials.

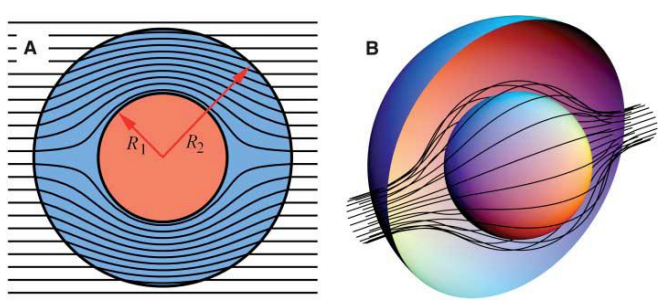

Fig. 1. 1 Schematic diagram of invisibility cloakings by Pendry *et al*.[1]

Since transformation electromagnetic was suggested in 2006, many efforts were made to establish the principles and realization methodologies of the devices engineered through transformation methods. For example, Leonhardt transformed a space where optical waves propagate by using conformal mapping, which is a special case of transformation electromagnetics [2]. Moreover, in order to realized the invisibility cloaking proposed in Ref. [1], split ring resonators(SRRs) were used [3]. Gradually changing size of SRR controlled the distribution of permeability within the cloaking device, and electromagnetic waves consequently changed their velocities and directions along curved paths. Cummer *et al*. suggested another methodology to realize the invisibility cloaking [4]. A multilayer structure composed of two different isotropic materials was adopted to satisfy anisotropic distributions of the permeability and the permittivity required for the invisibility cloaking device. Another multilayer-structured electromagnetic cloaking was experimentally examined in Ref. [5], which had been suggested before in Ref. [3].

Much more researches on transformation electromagnetics have been actively conducted due to its advantages. One of the greatest advantages is that directions and speeds of waves can be shifted within a continuous medium, in contrast with straightness of wave direction in a general medium. In order to take advantage of this point, transformation methods for acoustic waves, elastic waves and heat transfer were developed as well. Especially, the governing equations for acoustic waves in a transformed space are easily derived because the physics of acoustic waves are quite similar to that of electromagnetic waves (i.e. the Maxwell's equations). Acoustic governing equations were derived by

comparing acoustic properties with electromagnetic properties used in the Maxwell's equations in Ref. [6]. Furthermore, the realizing methodologies that used for electromagnetic waves can be directly applied to acoustic waves. Since directions and propagating velocities of waves can be freely changed even in a continuum by using transformation methods, they are thought to be promising techniques for controlling various kinds of waves and thus, many devices including cloaking have been designed and realized.

Meanwhile, there have been attempts to apply transformation methods to elastic waves. However, it was turned out that transformation elasticity is quite different from transformation electromagnetic/acoustics in that, unlike electromagnetic/acoustic governing equations, the elastic governing equations cannot keep the form-invariance under transformation and results in extra terms that do not exist in the original space [7]. These features cause toughness in realizing devices that manipulate elastic waves by using transformation elasticity. In spite of this difficulty, transformation elasticity is still a desirable technique for controlling unwanted vibrations and elastic waves propagating in solid structures as shown in Fig. 1.2. The devices can be widely used for guidance, avoidance or dissipation of elastic waves and consequently, aeronautic, ship and car industries could benefit from such deliberately engineered devices. Therefore, a breakthrough to overcome the difficulties in transformation elasticity is strongly required.

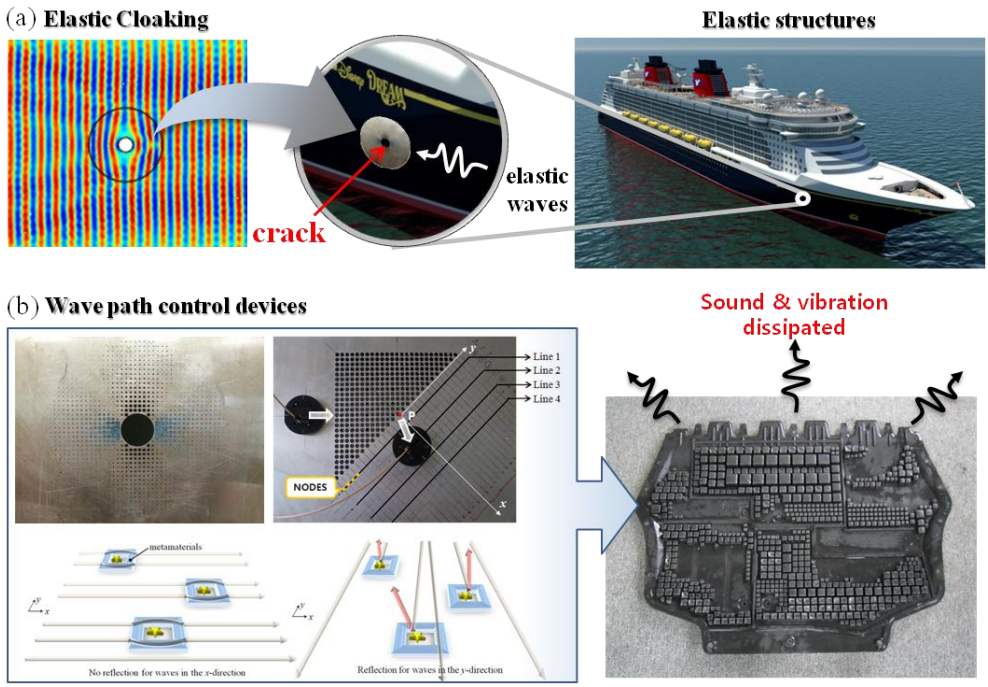

Fig. 1. 2 Elastic wave control devices applicable to solid structures. (a) stress shielding by using cloakings in elastic structures (b) various devices proposed by Lee *et al*. [8, 9] that can be applied to vibration dissipation in engine undercovers.

Motivated by this issue, an innovative way to overcome the inherent difficulties of transformation elasticity will be proposed. Before the detailed researches, it might be recommended to review the principles and the characteristics of transformation methods and the devices designed through them. In this process, the objectives of this thesis will be clarified.

1.2 Transformation Methods

1.2.1 Principle of Transformation Methods

The basic concept of transformation methods is to distort the space where waves propagate as presented in Fig. 1.3. Then the material properties of the original medium such as permeability or density changes as well as the grid lines are deformed. In the transformed (physical) space, the changed material properties lead the waves along the distorted paths. The distorted paths are determined in the way that all the points a certain ray passes in the original space correspond to the points the ray passes in the transformed space. In other words, waves propagate along the deformed path that are designated by the transformation equation and the original straight paths. Figure 1.3 shows the transformation process for cloakings [10]. A hole opened by a screwdriver is transformed to a circular space, around which a ray can be guided. Finally, no waves can penetrate into the circular space and it is cloaked. The space around the circular space (cloaked space) is set to be a design domain for the cloaking device and the device should retain appropriate distribution of material properties. In this case, the distributions of permeability and permittivity are changed for electromagnetic wave propagation.

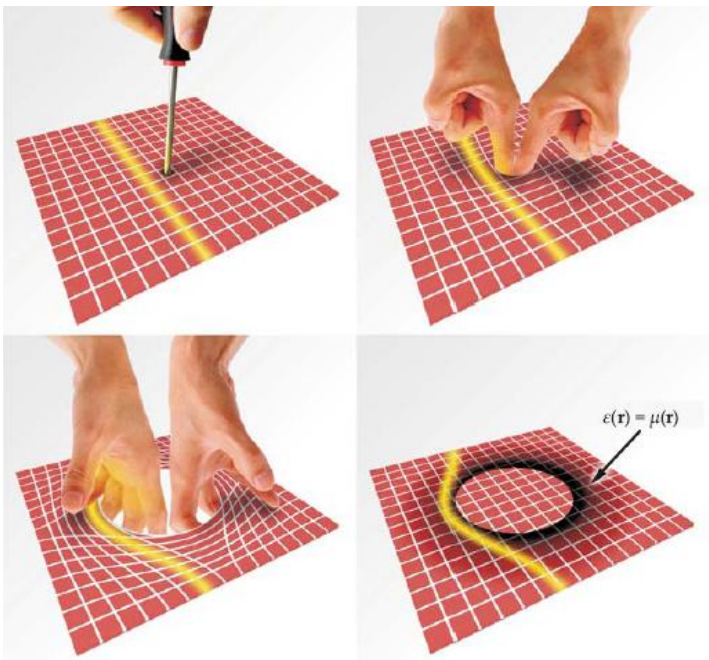

Fig. 1. 3 Process of distorting spaces for wave control by Wegener *et al*.[9]

There are innumerable kinds of transformation for manipulation of wave propagation. Figure 1.4 is a set of additional examples that explain how the wave paths change by space transformation. As mentioned before, the paths of a wave in the original and the transformed space correspond to each other [11]. Figure 1.4 (a) and (b) are the original and the transformed space of cloaking devices which are relevant to the cloaking presented in Fig. 1.1 and Fig. 1.3. Figure 1.4(d) is conformally transformed from Fig. 1.4(c) like Ref. [2] which results in transformed material properties that are less extreme. Another kind of cloaking devices is introduced in Fig. 1.4(e) and Fig. 1.4(f), which is generally called cloaking carpets.

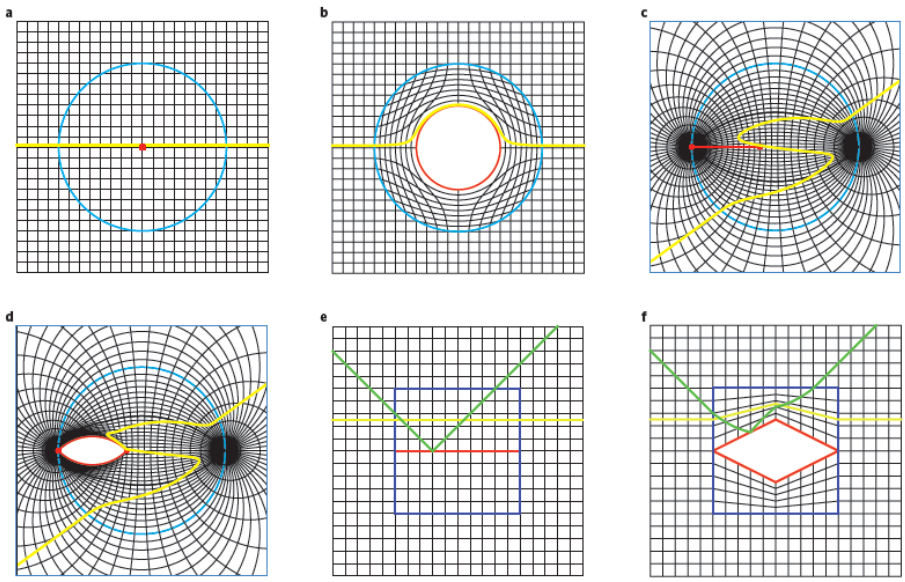

Fig. 1. 4 Various types of transformation by Chen *et al*. [11]. The original spaces a, c, e correspond to the transformed space b, d, f.

1.2.2 Devices engineered by Transformation methods

In addition to invisibility cloaking (electromagnetic cloakings), cloakings for other kinds of waves have been designed. In case of acoustic cloakings, the required density and bulk modulus are in the same form with the permeability and the permittivity of the electromagnetic cloaking [6]. Cheng *et al*., Cummer *et al*. and Torrent *et al*. suggested multilayered structures to achieve the acoustic cloakings by borrowing the methods used in realizing the electromagnetic cloaking [12-16]. Broadband acoustic cloaking for 52~64 kHz was realized using a planar network of acoustic circuits machined in an Aluminum plate that controls the fluid properties by changing widths and depths of the

circuits [17]. Other acoustic cloaks were manufactured and experimented in Ref. [18-20].

As electromagnetic cloakings and acoustic cloakings became realizable, many devices were studied besides invisibility cloakings. Newly designed wave controlling devices designed by transformation methods include wave rotators [21-23], cloaking carpets [24-33], wave benders [33-38], wave collimators [39], etc. Furthermore, any wave control device can be designed, provided a proper mapping equation between the original space and the transformation is formulated.

There have been great efforts to manufacture materials used for devices designed through transformation elasticity, especially elastic cloakings. The difficulty of transformation elastics comes from shear moduli of elastic materials. Unlike electromagnetic materials and acoustic materials, an elastic body requires shear force transverse to the direction of deformation when an external force is applied. Shear modulus G indicates the extent of required shear force per unit strain [40]. It produces extra coupling terms to the elastic governing equation under transformation and general materials cannot make up for the extra terms. To resolve this problem, a lot of researches were conducted. Brun *et al*. showed that a cylindrical cloak for in-plane coupled shear and pressure waves works well in a special case where the elastic governing equation, the Navier equation keeps its form in spite of geometric change [41]. But the stiffness of the cloaking has severe anisotropy that is practically unrealistic. Farhat *et al*. also proved that, for the out-of-plane displacement, the elastodynamic equation can be simplified [42]. Therefore, flexural

waves in thin plates were governed only by spatially varying quantities of the stiffness tensor and the density of a medium. To obtain the homogenized elastic parameters, six different materials were combined to form a multilayered structure. The performance of the designed cloaking was proved computationally [43, 44] and experimentally [45]. To fundamentally resolve the problem of shear modulus, Milton suggested in Ref. [7] the concept of *pentamode materials* which has relatively large bulk modulus than shear modulus so that they are almost regarded as gases or liquids. A diamond lattice of solid linkages proposed by Milton is one of the pentamode materials. This structure was manufactured and examined in Ref. [46]. It showed a fairly large ratio of bulk modulus to shear modulus (*B/G* ratio) in the range of $>10^3$ were accessible but the stability of the structure got deteriorated because the linkage elements touch each other only at their point-like tips. The connection tips should be thickened to keep substantial stability, which is a trade off against the *B/G* ratio and the performance of the material. Norris discussed Cosserat materials which do not display minor symmetry [47], but they are impossible to realize for the present.

As discussed above, there have been numerous studies and attempts to engineer manufacturable elastic materials to be used for elastic wave control devices, no satisfactory material has been presented because previous models are applicable only to a certain wave modes or too unstable for practical uses. It would be advisable to take a close look at the characteristics and the fundamental causes of difficulties in realization of transformation elasticity.

1.2.3 Characteristics of transformation elasticity

As mentioned before, the main cause of peculiarity of transformation elasticity over transformation electromagnetics/acoustics is that elastic media has shear modulus, and shear moduli of elastic media arouse a special kind of polarization of waves [40]. Since solids have nonzero shear modulus unlike ideal gases and liquids, transformation elasticity is of different nature from transformation electromagnetic/acoustics. For instance, additional deformation is concerned in elongation or compression of elastic body and vice versa. This leads to the form variance under coordinate transformations. The equation of motion of general elastic media is given as

$$\nabla \cdot \left(C \nabla u \right) = \rho \frac{\partial^2 u}{\partial t^2}, \tag{1.1}$$

where C, ρ and u denote the stiffness tensor, the density of the medium and the displacement vector, respectively. After the coordinate transformation, however, the governing equation becomes

$$\nabla' \cdot \left(C' \nabla' u' + S' u' \right) = D' \nabla' u' + \rho' \frac{\partial'^2 u'}{\partial' t'^2}, \tag{1.2}$$

where prime notations mean that the physical quantities are expressed in the transformed space. As can be seen, the extra terms $S'u'$ and $D'\nabla'u'$ are added and consequently the form invariance is destroyed.

There are two important remarks on these extra terms. First, no material having S and D is available in nature. Therefore, they should be minimized to an ignorable extent for

engineering wave control devices by using transformation elasticity. Second, the material properties in transformation elasticity comprise of more various kinds of geometric variables. When deriving the required material properties in transformation electromagnetics/acoustics, only the 1st order derivatives of mapping equations are involved. On the other hand, not only the 1st order derivatives, but also the 2nd order derivatives of a mapping equation are required to obtain the material properties including the extra terms. If the 2nd order derivatives go zero, the medium in the transformed space behaves like fluid and the extra terms are eliminated (Detailed derivation of this point will be discussed later). Therefore the minimization of the 2nd order derivatives of the mapping equations contributes to diminution of the extra terms. The magnitude of shear modulus and the 2nd order derivatives are two key variables to decrease of the extra terms in transformation elasticity. The difference between two ways is that, as shown in Ref. [46], the increase of instability is inevitable in the case of decreasing of shear modulus, while robust structures might be permitted in the case of decreasing the magnitudes of the 2nd order derivatives. In this point of view, the objectives of this thesis can be embodied in detail.

1.3 Research Objectives and coverage

As explained above, the motivation and the objectives of the thesis are apparent; needed is a methodology to design materials for engineering elastic wave control devices that can be applied to various wave modes and have a substantial stability by using

transformation elasticity. Thus, a way to design safe and versatile materials suitable for transformation elasticity should be found and experimentally verified. Moreover, practical applications of the engineered wave control devices should be sought to give value to them. Since elastic cloaking can block elastic wave propagation in a certain region of an elastic body, they are expected to relieve the stress concentration by placing the stress-concentrated point inside the cloaking area. To accomplish these objectives, the following issues should be discussed in depth.

- **How to minimize the extra terms in transformation elasticity?**

As discussed above, it is desirable to minimize the extra terms appearing in Eq. (1.2) because they are nonexistent at least in the materials found in nature. Since control of the extra terms by decreasing the magnitude of shear modulus may accompany instability of structures, decreasing the 2nd order derivatives of a mapping equation is ideal. Therefore, a methodology to diminish the 2nd order derivatives should be studied. The resolution of this step will pave the way to the feasibility of devices for elastodynamic waves including elastic cloaking.

- **How to realize the wave control devices?**

When the extra terms are substantially ignorable, it should be discussed how to compose the elastic wave control devices in accordance to the distributions of material properties calculated from the mapping equation. The distributions might be varying depending on the locations in the design domain of the device. The constituent materials need to be sufficiently stable and found in nature.

- **Where to apply and Does it work well?**

Application of the devices designed through transformation elasticity is another important issue in an engineering viewpoint. Since wave control technologies are almost saturated and no further growth is expected currently, the engineered devices will be multipurpose such as stress shielding, sound and vibration dissipation, energy harvesting, etc. Of them, we are engrossed in the mitigation of concentrated stress that can threaten the structural health with the elastic wave control devices.

1.4 Organization of the thesis

In chapter 2, physics of general acoustics and transformation acoustics are discussed in detail as a preliminary study. As transformation acoustics keeps form invariance of its governing equations after transformation, inherent physical properties, wave propagations and requirements of transformation methods can be easily understood through it.

In chapter 3, the physics of transformation elasticity is studied in detail and how it is different from other transformation methods is analyzed. Then conformal transformation is introduced as a key to decreasing the extra terms, the main difficulties of transformation elasticity. Thank to the uniqueness of conformal transformations, parts of extra terms are cancelled each other. To verify the superiority of conformal transformations in small extra terms over general transformations, an index is established

and the distribution of the index inside a design domain is shown for three examples : a cloaking, a wave collimator and a wave bend guider.

Chapter 4 is dedicated to the detailed process of realizing elastic cloakings in thin plates by using conformal transformations. Various kinds of phononic crystals (PCs) are used in combination to design the cloaking. The governing equation of motion in transformation elasticity is simplified in chapter 3. The wave speed, the key variable of simplified transformation elasticity, at a certain point in the cloaking device is controlled by the specifications of PC. Then the performance of the designed cloaking is examined numerically and experimentally at a couple of ultrasonic frequency.

In chapter 5, stress shielding at a stress concentration point in solid structures is suggested as an application of elastic cloaking designed above. Even though the cloaking is not embedded in a plate, the cloakings in a form of patch on the surfaces of elastic body might be able to relax stress concentration at singular points such as cracks or notches.

Finally, the concluding remarks of this thesis are mentioned in chapter 6.

Chapter 2.

Directional Cloaking by Transformation Acoustics

2.1 Chapter Overview

In this chapter, transformation acoustics and relevant governing equations will be derived. The general governing equations in acoustic media are induced to begin with, and then the governing equations in the transformed space are following when an arbitrary mapping equation is given. In this process, form invariance of the governing equations under transformation will be clearly proved. The distributions of required material properties are also investigated; bulk modulus and density are the constituent variables in transformation acoustics. If the design domain has the distributions of the bulk modulus and the density calculated from the mapping equation, it can be regarded as an acoustic wave control device.

The overview of transformation acoustics might be helpful in the comprehension of characteristics of wave propagation in the transformed space and the derivation of material properties. Furthermore, it is much easier to understand the physics of transformation elasticity on the basis of this chapter because transformation elasticity is basically an extension of transformation electromagnetics/acoustics.

2.2 Acoustic Governing Equations

To deduce the equation of motion of the fluid, the equations of continuity and the Euler's equation should be derived above all. For an elemental spatially fixed volume fluid, the rate of mass flow into and out of the volume resulting from fluid flowing in the x direction is shown in Fig. 2.1. It is assumed that, before transformation, the density and bulk modulus of medium is homogeneous and isotropic like water or air.

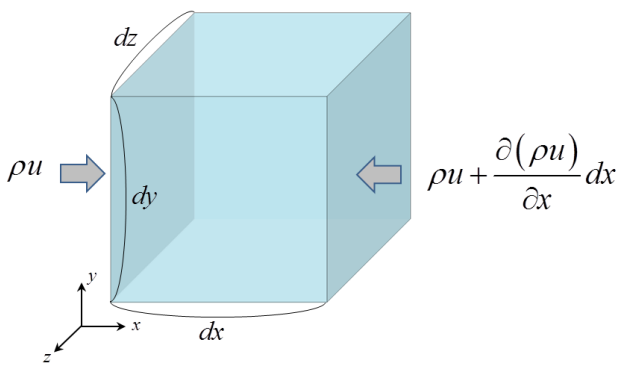

Fig. 2. 1 An elemental fixed volume of fluid flowing in the x direction. A similar diagram can be drawn for the y and z directions.

Then the net influx of mass within the volume in the x direction is expressed as [48]

$$\left[\rho v_x - \left(\rho v_x + \frac{\partial(\rho v_x)}{\partial x}dx\right)\right]dydz = -\frac{\partial(\rho v_x)}{\partial x}dV \tag{2.1}$$

where v_x is the particle velocity in the x direction and the infinitesimal cubic volume element $dV = dx\,dy\,dz$. Similar equations in the y and z direction can be

expressed, so that the total influx is

$$-\left(\frac{\partial(\rho v_x)}{\partial x}+\frac{\partial(\rho v_y)}{\partial y}+\frac{\partial(\rho v_z)}{\partial z}\right)dV=-\nabla\cdot\left(\rho\bar{v}\right)dV \tag{2.2}$$

where v_y and v_z are the velocities in the y and z direction, respectively and the velocity vector is written as $\bar{v}=\begin{pmatrix} v_x & v_y & v_z \end{pmatrix}^T$. Since the volume is unchanged, mass increase in the volume is

$$\frac{dm}{dt}=\frac{d(\rho V)}{dt}=\frac{\partial V}{\partial t}d\rho \tag{2.3}$$

Then the net influx is equal to the rate of mass increase, and Eq. (2.2) turns to

$$\frac{\partial\rho}{\partial t}+\nabla\cdot\left(\rho\bar{v}\right)=0 \tag{2.4}$$

This indicates the equation of continuity of fluid flowing.

The next is Euler's equation, the equation of force applied to a mass of fluid. When pressures in the x direction are applied to both sides of the cubic element shown in Fig. 2.1, the net force experienced by the element in the x direction, dF_x is

$$dF_x=\left[P-\left(P+\frac{\partial P}{\partial x}dx\right)\right]dydz=-\frac{\partial P}{\partial x}dV \tag{2.5}$$

This force accelerates the element according to Newton's second law, so dF_x is also expressed as [49]

$$dF_x=a\,dm=\frac{dv_x}{dt}\rho dV \tag{2.6}$$

By combining Eq. (2.5) and Eq. (2.6) and involving the forces in other directions,

$$\nabla P + \rho \frac{d\bar{v}}{dt} = 0 \tag{2.7}$$

Pressure and density of fluid changes little compared to the static values P_0 and ρ_0 when associated with propagation In this case, the following relation

$$B = c^2 \rho \tag{2.8}$$

where B and c are bulk modulus and fluid velocity, is obtained.

In order to combine the above equations, Eq. (2.7) is taken the divergence and Eq. (2.4) is taken time-derivative. Those two results yield

$$\nabla^2 P = \frac{\rho}{B} \frac{\partial^2 P}{\partial t^2} = \frac{1}{c^2} \frac{\partial^2 P}{\partial t^2} \tag{2.9}$$

which is called Helmholtz equation. It shows the propagation of acoustic wave because the differential term by space is related to the counterpart by time.

In case density of fluid is in a tensor form, although it is implausible for general fluids, the density in the 3-dimensional space is defined as

$$\underline{\rho} = \begin{bmatrix} \rho_{xx} & \rho_{xy} & \rho_{xz} \\ \rho_{yx} & \rho_{yy} & \rho_{yz} \\ \rho_{zx} & \rho_{zy} & \rho_{zz} \end{bmatrix} \tag{2.10}$$

General fluid is a special case of Eq. (2.10) where the diagonal terms are identical and the off-diagonal terms are all zero.

$$\underline{\rho}_{general} = \begin{bmatrix} \rho & 0 & 0 \\ 0 & \rho & 0 \\ 0 & 0 & \rho \end{bmatrix} = \rho \underline{I} = \rho \tag{2.11}$$

The reciprocal of density of general fluid is simply $1/\rho$ and the reciprocal of a diagonal density tensor including scalar density of general fluid is

$$\underline{\rho}^{-1} = \begin{bmatrix} \rho & 0 & 0 \\ 0 & \rho & 0 \\ 0 & 0 & \rho \end{bmatrix}^{-1} = \begin{bmatrix} 1/\rho & 0 & 0 \\ 0 & 1/\rho & 0 \\ 0 & 0 & 1/\rho \end{bmatrix} = \left[\frac{1}{\rho}\right] = \frac{1}{\rho} \tag{2.12}$$

Therefore, the reciprocal density tensor $[1/\rho]$ is commonly regarded as the inverse of a density tensor, not the tensor of which components are simply reciprocal values of the corresponding components of the density tensor, i.e.

$$\left[\frac{1}{\rho}\right] \triangleq \begin{bmatrix} \rho_{xx} & \rho_{xy} & \rho_{xz} \\ \rho_{yx} & \rho_{yy} & \rho_{yz} \\ \rho_{zx} & \rho_{zy} & \rho_{zz} \end{bmatrix}^{-1} = \underline{\rho}^{-1} \tag{2.13}$$

Using the space-varying tensorial density and bulk modulus, the governing equation of fluid motion is complicated than Eq. (2.9) as

$$\nabla \cdot \left[\frac{1}{\rho(x)} \nabla P \right] = \frac{1}{\kappa(x)} \frac{\partial^2 P}{\partial t^2} \tag{2.14}$$

As can be seen from Eq. (2.14), density and bulk modulus are dependent only on space, while the pressure field P is time- and space-varying, $P = P(x,t)$. If density and bulk modulus are regarded as isotropic and homogeneous, i.e. invariant at any point, Eq. (2.14) is identical to Eq. (2.9), the general Helmholtz equation. The material properties in

the governing equation after transformation, however, are usually space-varying. Therefore, the governing equation in the form of Eq. (2.14) is rather helpful.

If the pressure field is time harmonic, i.e. $P = P_0 e^{i\omega t}$ where ω is angular frequency of harmonic waves, Eq. (2.14) turns to be irrelevant to time, resulting in

$$\nabla \cdot \left[\frac{1}{\rho(x)} \nabla P(x) \right] = -\frac{\omega^2}{\kappa(x)} P(x) \tag{2.15}$$

2.3 Governing Equations and Material Properties in Transformation Acoustics

Transformation acoustics is based on the form invariance of acoustic wave governing equation under coordinate transformation. The 2-dimentional transformation acoustics is treated here starting from Eq. (2.15). All notations after transformation are primed for distinction from those before the transformation. Then the $x - y$ space is the original space filled with isotropic homogeneous medium and waves generally propagate straight. Meanwhile, the $x' - y'$ space, the transformed space is a physical space where transformation media devices are working. In this space, waves propagate along the points that are mapped from the points waves passed in the original space. In other words, waves go along the transformed grid lines like Fig. 2.2.

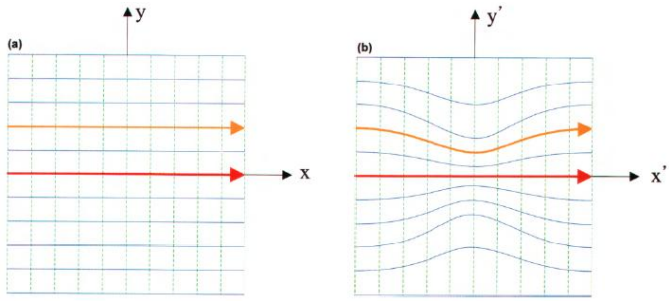

Fig. 2. 2 An example of change of wave trajectories under coordinate transformation by Kwon *et al*. [50] (a) the original Cartesian coordinates with two parallel waves (b) the transformed coordinates with two waves flowing along the curved paths.

In a physical view, the distributions of medium properties changed by mapping equations practically manipulate wave paths. Therefore, the first step for transformation is to find an appropriate mapping equation. The mapping equation is a mean of translocating the points from the original space to the transformed space. The coordinates of the transformed points are defined as

$$x' = f(x, y), \quad y' = g(x, y) \tag{2.16}$$

To keep the form invariance of Eq. (2.11), the waves in the transformed space should be governed by the equation in the form of

$$\nabla' \cdot \left[\frac{1}{\rho'(x')} \nabla' P'(x') \right] = -\frac{\omega^2}{\kappa'(x')} P'(x') \tag{2.17}$$

where $P'(x')$ in the transformed space is exactly identical to $P(x)$ in the original space. The medium properties $\left[1/\rho'(x')\right]$ and $\kappa'(x')$ are drawn in the process of transforming Eq. (2.15) into Eq. (2.17).

The Jacobian matrix J, which is the indication of the extent of deformation is

$$J = \begin{bmatrix} \frac{\partial x'}{\partial x} & \frac{\partial x'}{\partial y} \\ \frac{\partial y'}{\partial x} & \frac{\partial y'}{\partial y} \end{bmatrix} \tag{2.18}$$

The nabla operator used in Eq. (2.15) is $\nabla = \begin{bmatrix} \frac{\partial}{\partial x} & \frac{\partial}{\partial y} \end{bmatrix}$ while that used in Eq. (2.17) is $\nabla' = \begin{bmatrix} \frac{\partial}{\partial x'} & \frac{\partial}{\partial y'} \end{bmatrix}$.

If the term inside the bracket in the left-hand side of Eq. (2.15) are defined as [51]

$$j(x) \triangleq \frac{1}{\rho(x)} \nabla p(x), \tag{2.19}$$

the gradient of pressure field is

$$\nabla p = \frac{\partial p}{\partial x_i} = \frac{\partial x_k'}{\partial x_i} \frac{\partial p}{\partial x_k'} = J_{ki} \frac{\partial p}{\partial x_k'}, \tag{2.20}$$

and finally the left-hand side of Eq. (2.15) changes to

$$\nabla \cdot \left[\frac{1}{\rho(x)} \nabla p(x) \right] = \nabla \cdot j = \frac{\partial j_i}{\partial x_i} = \frac{\partial x_k'}{\partial x_i} \frac{\partial j_i}{\partial x_k'} = J_{ki} \frac{\partial j_i}{\partial x_k'} \tag{2.21}$$

Equation (2.20) can be expressed by using the nabla operator as

$$J_{ki} \frac{\partial p}{\partial x_k'} = J^T \nabla' p(x) \tag{2.22}$$

Meanwhile, from the fact that the cofactor matrix of the inverse of the Jacobian matrix

J^{-1} is $\frac{1}{\det J} J^T$, the following identity can be drawn.

$$\frac{\partial}{\partial x_k'}\left(\frac{1}{\det J}\frac{\partial x_k'}{\partial x_i}\right)=0 \tag{2.23}$$

The term in the parenthesis of Eq. (2.23) can be re-written by using the Levi-Civita tensor ε_{ijk} as

$$\frac{1}{\det J}\frac{\partial x_k'}{\partial x_i}=\varepsilon_{klm}\varepsilon_{irs}\frac{\partial x_r}{\partial x_l'}\frac{\partial x_s}{\partial x_m'} \tag{2.24}$$

Then it can be derived from Eq. (2.23) and Eq. (2.24) that

$$\begin{aligned}\frac{\partial}{\partial x_k'}\left(\frac{1}{\det J}\frac{\partial x_k'}{\partial x_i}\right)&=\frac{\partial}{\partial x_k'}\left(\varepsilon_{klm}\varepsilon_{irs}\frac{\partial x_r}{\partial x_l'}\frac{\partial x_s}{\partial x_m'}\right)\\&=\varepsilon_{klm}\varepsilon_{irs}\left(\frac{\partial^2 x_r}{\partial x_k'\partial x_l'}\frac{\partial x_s}{\partial x_m'}+\frac{\partial x_r}{\partial x_l'}\frac{\partial^2 x_s}{\partial x_k'\partial x_m'}\right)=0\end{aligned} \tag{2.25}$$

By using Eq. (2.25), Eq. (2.21) is transformed as

$$\nabla\cdot j=J_{ki}\frac{\partial j_i}{\partial x_k'}=\det J\frac{\partial}{\partial x_k'}\left(\frac{J_{ki}j_i}{\det J}\right)=\det J\nabla'\cdot\left(\frac{Jj}{\det J}\right) \tag{2.26}$$

Inserting Eq. (2.26) and Eq. (2.22) into j in Eq. (2.21) result in

$$\begin{aligned}\nabla\cdot j&=\det J\nabla'\cdot\left[\frac{1}{\det J}Jj\right]\\&=\det J\nabla'\cdot\left[\frac{1}{\det J}J\frac{1}{\rho}J^T\nabla' P(x)\right]\\&=\det J\nabla'\cdot\left[\frac{1}{\det J}J\frac{1}{\rho}J^T\nabla' P'(x')\right]\end{aligned} \tag{2.27}$$

It can replace the left-hand side of Eq. (2.15).

$$\det J \nabla' \cdot \left[\frac{1}{\det J} J \frac{1}{\rho} J^T \nabla' P'(x') \right] = -\frac{\omega^2}{\kappa(x)} P(x) = -\frac{\omega^2}{\kappa(x)} P'(x') \tag{2.28}$$

Both sides can be divided by $\det J$ so that it is in the similar form with Eq. (2.17), then it turns to

$$\nabla' \cdot \left[\frac{1}{\det J} J \frac{1}{\rho} J^T \nabla' P'(x') \right] = -\frac{\omega^2}{\det J \kappa(x)} P'(x') \tag{2.29}$$

From Eq. (2.29), the density tensor and the bulk modulus required for the transformation devices are identified. Comparison of Eq. (2.29) and Eq. (2.17) gives

$$\left[\frac{1}{\rho'(x')} \right] = \frac{J \left[\frac{1}{\rho(x)} \right] J^T}{\det J} = \frac{JJ^T}{\det J \cdot \rho(x)} = \frac{JJ^T}{\det J \cdot \rho_0} \tag{2.30}$$

$$\kappa'(x') = \det J \cdot \kappa(x) = \det J \cdot \kappa_0 \tag{2.31}$$

where ρ_0 and κ_0 are the density and the bulk modulus of medium in the original space. Transformation acoustics, as mentioned before, impose the heterogeneous anisotropic density in the reciprocal matrix and the heterogeneous isotropic bulk modulus in a scalar form. It should be remarked that the reciprocal density $[1/\rho]$ is not $\begin{bmatrix} 1/\rho_{xx} & 1/\rho_{xy} \\ 1/\rho_{xy} & 1/\rho_{yy} \end{bmatrix}$, but $\begin{bmatrix} \rho_{xx} & \rho_{xy} \\ \rho_{xy} & \rho_{yy} \end{bmatrix}^{-1}$ and in the general case, the reciprocal density matrix is expressed as Eq. (2.13) because the density in the original space is unity. After the transformation, however, the density of medium is in a tensorial form and has

different value depending on directions. Consequently, the velocity of the waves propagating in the medium can vary along different directions [14].

$$c_{ij}^2 = \frac{\kappa}{\rho_{ij}} \tag{2.32}$$

Especially the cloaking, the most popular and intriguing device by using transformation methods, is based on the radial compression in cylindrical coordinates. The material properties required to realize an acoustic cloaking can be drawn following the above mentioned process. For cloaking, a circular region in the original space is transformed to a torus which has a hollow space inside it. Objects inside the inner space can be cloaked by avoiding outside waves. The detailed studies on the cloaking are included in Appendix A.

Chapter 3.

Methodology for Realizable Materials in Transformation Elasticity

3.1 Chapter Overview

In this chapter, transformation elasticity suggested in [7] is reviewed over all. It is sufficiently told that, in Chap. 2, waves propagate along the transformed grid lines in the transformed space and the continuously varying material properties play a practical role in controlling waves. This property of transformation methods is also true in transformation elasticity. However, as mentioned in Chap. 1, the equation of motion of elastic body is unable to keep its form under transformation (see Eq. (1.2)). The main factor of this form variance is the existence of shear modulus of solids. The governing equations and the material properties transformed in transformation elasticity are derived to see how those in transformation elasticity are different from the counterparts in transformation electromagnetics/acoustics. The virtual work theory is used to derive the governing equation in transformation elasticity. In this process, new terms appear, which are not found in materials in nature and have to be minimized for realization. Several models to overcome this difficulty have been suggested. Among them, there is an elastic cloaking that can be applied only to a selective mode of elastic waves. Meanwhile, a special kind of materials, pentamode materials are developed to behave like fluid without shear modulus, but they have too vulnerable a structure to be used for practical use.

Another approach to overcome this difficulty is proposed here: *conformal transformation*, in which coordinates are treated in a complex plane. Conformal transformation has been used in various coordinate transformation including transformation electromagnetics/acoustics, but it has hardly used in transformation elasticity. Especially, its characteristics with regard to the reduction of the extra terms have never been clarified. Detailed progresses of simplification of material properties and dramatic decrease of the extra terms of transformation elasticity are derived in this chapter.

To confirm the superiority of conformal transformation to other general transformations in decreasing the extra terms of transformation elasticity, three examples are shown; elastic cloakings, elastic wave collimators and elastic wave benders. In each case, two different transformations are exerted to the original space to engineer the devices that have a similar dimension and functionality in controlling elastic wave propagation. Here, an index is set up to show the portion of the extra terms and the distributions of the index in each device are presented. Conformal transformation generally produces smaller values of the index. To confirm if the extra terms are small enough, the performances of the devices designed with and without the extra terms are numerically simulated and compared. Finally, it is verified that the magnitude of the extra terms are sufficiently minimized by conformal transformation. Therefore, the ultimate purpose of minimization of the extra terms is achieved.

3.2 Governing Equations and Material Properties in Transformation Elasticity

To thoroughly understand the difference between the governing equations in the original and the transformed spaces and the terms defined in each space, the basics of elasticity [52, 53] is introduced in the first place.

In the 3-dimensional space where three orthogonal directions in the Cartesian coordinate system are denoted by x, y and z, and the displacements in these directions are u, v and w, a strain tensor $\underline{\varepsilon}$ is defined as

$$\varepsilon_{ij} = \frac{1}{2}\left(\frac{\partial u_j}{\partial x_i} + \frac{\partial u_i}{\partial x_j}\right), \tag{3.1}$$

$$\underline{\varepsilon} = \begin{bmatrix} \varepsilon_{xx} & \varepsilon_{xy} & \varepsilon_{xz} \\ \varepsilon_{yx} & \varepsilon_{yy} & \varepsilon_{yz} \\ \varepsilon_{zx} & \varepsilon_{zy} & \varepsilon_{zz} \end{bmatrix} = \begin{bmatrix} \frac{\partial u}{\partial x} & \frac{1}{2}\left(\frac{\partial v}{\partial x} + \frac{\partial u}{\partial y}\right) & \frac{1}{2}\left(\frac{\partial w}{\partial x} + \frac{\partial u}{\partial z}\right) \\ \frac{1}{2}\left(\frac{\partial v}{\partial x} + \frac{\partial u}{\partial y}\right) & \frac{\partial v}{\partial y} & \frac{1}{2}\left(\frac{\partial w}{\partial y} + \frac{\partial v}{\partial z}\right) \\ \frac{1}{2}\left(\frac{\partial w}{\partial x} + \frac{\partial u}{\partial z}\right) & \frac{1}{2}\left(\frac{\partial w}{\partial y} + \frac{\partial v}{\partial z}\right) & \frac{\partial w}{\partial z} \end{bmatrix} \tag{3.2}$$

and it can be expressed in the vector form of the gradient of displacements as

$$\nabla \bar{u} = \bar{\varepsilon} = \begin{bmatrix} \varepsilon_{xx} & \varepsilon_{yy} & \varepsilon_{zz} & 2\varepsilon_{xy} & 2\varepsilon_{yz} & 2\varepsilon_{zx} \end{bmatrix}^T \tag{3.3}$$

Equation (3.3) is composed only of 6 components out of 9 components in Eq. (3.2) because of the symmetry. In the same manner, stress tensor $\underline{\sigma}$ is also written in two

different forms.

$$\underline{\sigma} = \begin{bmatrix} \sigma_{xx} & \sigma_{xy} & \sigma_{xz} \\ \sigma_{yx} & \sigma_{yy} & \sigma_{yz} \\ \sigma_{zx} & \sigma_{zy} & \sigma_{zz} \end{bmatrix} \tag{3.4}$$

$$\underline{\sigma} = \begin{bmatrix} \sigma_{xx} & \sigma_{yy} & \sigma_{zz} & \sigma_{xy} & \sigma_{yz} & \sigma_{zx} \end{bmatrix}^T \tag{3.5}$$

Equation (3.3) and Eq. (3.5) are related as a constitutive equation by using a stiffness tensor $\underline{C}$ as

$$\overline{\sigma} = \underline{C} : \overline{\varepsilon} \tag{3.6}$$

where $\underline{C}$ is a material property of solids. This equation shows Hooke's law for continuous media in the 3D space. For all materials in nature, the symmetric relations as following are valid.

$$C_{ijkl} = C_{klij} \tag{3.7}$$

$$C_{ijkl} = C_{jikl} = C_{ijlk} \tag{3.8}$$

Equation (3.7) and Eq. (3.8) are called the major and the minor symmetry of a stiffness tensor, respectively. A stiffness tensor has 36 components generally in 3D space, but they are dependent with each other depending on a material type. Especially for an isotropic material, a stiffness tensor $\underline{C}$ can be expressed only with two components as

$$\underline{C} = \begin{bmatrix} C_{1111} & C_{1122} & C_{1122} & 0 & 0 & 0 \\ C_{1122} & C_{1111} & C_{1122} & 0 & 0 & 0 \\ C_{1122} & C_{1122} & C_{1111} & 0 & 0 & 0 \\ 0 & 0 & 0 & (C_{1111} - C_{1122})/2 & 0 & 0 \\ 0 & 0 & 0 & 0 & (C_{1111} - C_{1122})/2 & 0 \\ 0 & 0 & 0 & 0 & 0 & (C_{1111} - C_{1122})/2 \end{bmatrix} \tag{3.9}$$

By introducing the Lame's constants λ and μ, Eq. (3.9) is rewritten as

$$\underline{C} = \begin{bmatrix} \lambda+2\mu & \lambda & \lambda & 0 & 0 & 0 \\ \lambda & \lambda+2\mu & \lambda & 0 & 0 & 0 \\ \lambda & \lambda & \lambda+2\mu & 0 & 0 & 0 \\ 0 & 0 & 0 & \mu & 0 & 0 \\ 0 & 0 & 0 & 0 & \mu & 0 \\ 0 & 0 & 0 & 0 & 0 & \mu \end{bmatrix} \tag{3.10}$$

Next, based on Newton's 2nd law, $F = ma$, the equation of motion(i.e. momentum equation) of solid can be drawn. Total force exerted on a unit cubic volume by stress field is

$$F_i = \sum \frac{\partial \sigma_{ij}}{\partial x_j} dxdydz \tag{3.11}$$

By combining Eq. (3.6) and Eq. (3.11), the elastic wave equation is completed as following

$$\sum \frac{\partial \sigma_{ij}}{\partial x_j} = \sum \frac{\partial \left(C_{ijkl} \varepsilon_{kl} \right)}{\partial x_j} = \sum \frac{\partial \left(C_{ijkl} \dfrac{\partial u_l}{\partial x_k} \right)}{\partial x_j} = \rho \frac{\partial^2 u_i}{\partial t^2} \tag{3.12}$$

$$\nabla \cdot \left(\underline{C} \nabla \bar{u} \right) = \rho \frac{\partial^2 \bar{u}}{\partial t^2} \tag{3.13}$$

which is the same as Eq. (1.1). For time harmonic waves, $\bar{u} = u \exp(i\omega t)$ can be applied to Eq. (3.13) and the wave equation turns to

$$\nabla \cdot \left(\underline{C} \nabla \bar{u} \right) = -\omega^2 \rho \bar{u} \tag{3.14}$$

This is the equation of motion of solid body in the general elasticity. However, it changes its form under coordinate transformation as Eq. (1.2).

Let us examine thoroughly the expansion of Eq. (1.2) from Eq. (1.1) by transformation [54]. It is assumed that the Jacobian matrix of a mapping equation is used for the transformation of displacement vectors. This feature allows the stress tensor to be symmetric. By transposing the left-hand side of Eq. (3.14) to the right-hand side, the equation of motion at a certain point x is

$$-\nabla \cdot \left(\underline{C}(x) \nabla \bar{u} \right) - \omega^2 \rho(x) \bar{u} = 0 \tag{3.15}$$

For an arbitrary test vector $\bar{v}$, the following is true in the design domain Ω.

$$\int_{\Omega} \left[-\nabla \cdot (\underline{C}(x) \nabla \bar{u}) - \omega^2 \rho(x) \bar{u} \right] \cdot \bar{v} dx = 0 \tag{3.16}$$

The transformation maps the vector fields as

$$\bar{u}'(x') = J^{-T}(x) \bar{u}(x) \tag{3.17}$$

and the test vector is similarly transformed as

$$\bar{v}'(x') = J^{-T}(x) \bar{v}(x) \tag{3.18}$$

The strain changes as

$$\nabla u = \frac{\partial u_j}{\partial x_i} = \frac{\partial \left(u_p J_{pj} \right)}{\partial x_i} = \frac{\partial x'_m}{\partial x_i} \frac{\partial u'_p}{\partial x'_m} J_{pj} + \frac{\partial J_{pj}}{\partial x_i} u'_p = J^T \left(\nabla' u' \right) J + G' u' \tag{3.19}$$

where $G_{ijp} = \dfrac{\partial J_{pj}}{\partial x_i}$ is defined. Using Eq. (3.17) ~ (3.19), (3.16) can be transformed as

$$
\begin{aligned}
0 &= \int_{\Omega}\left[-\nabla\cdot(\underline{C}(x)\nabla\bar{u})-\omega^2\rho(x)\bar{u}\right]\cdot\bar{v}dx \\
&= \int_{\Omega}\left[\underline{C}(x)\nabla\bar{u}:\nabla\bar{v}-\omega^2\rho(x)\bar{u}\cdot\bar{v}\right]dx \\
&= \int_{\Omega'}\left[\underline{C}(x)\left(J^T\nabla'\bar{u}'J+\underline{G}\bar{u}'\right):\left(J^T\nabla'\bar{v}'J+\underline{G}\bar{v}'\right)-\omega^2\rho(x)\left(J^T\bar{u}'\right)\cdot\left(J^T\bar{v}'\right)\right]\frac{1}{\det J}dx' \\
&= \int_{\Omega'}\left[\underline{C}'(x')\nabla'\bar{u}':\nabla'\bar{v}'+\underline{S}'(x')\bar{u}':\nabla'\bar{v}'+\left(\underline{D}'(x')\nabla'\bar{u}'\right)\cdot\bar{v}'-\omega^2\left(\underline{\rho}'(x')\bar{u}'\right)\cdot\bar{v}'\right]dx' \\
&= \int_{\Omega'}\left[-\nabla'\cdot\left(\underline{C}'(x')\nabla'\bar{u}'+\underline{S}'(x')\bar{u}'\right)+\underline{D}'(x')\nabla'\bar{u}'-\omega^2\underline{\rho}'(x')\bar{u}'\right]\cdot\bar{v}'dx'
\end{aligned}
\tag{3.20}
$$

Therefore, the governing equation in the transformed space can be expressed as [7]

$$
\nabla'\cdot\left(\underline{C}'(x')\nabla'\bar{u}'+\underline{S}'(x')\bar{u}'\right)=\underline{D}'(x')\nabla'\bar{u}'-\omega^2\underline{\rho}'(x')\bar{u}' \tag{3.21}
$$

In this process, the density tensor $\underline{\rho}'$, the transformed stiffness tensor $\underline{C}'$, and the newly introduced properties $\underline{S}'$ and $\underline{D}'$ are composed of elements

$$
\rho'_{pq}=\frac{\rho}{\det J}\frac{\partial x'_p}{\partial x_i}\frac{\partial x'_q}{\partial x_i}+\frac{1}{\det J}\frac{1}{(-i\omega)^2}\frac{\partial^2 x'_p}{\partial x_i\partial x_j}C_{ijkl}\frac{\partial^2 x'_q}{\partial x_k\partial x_l} \tag{3.22}
$$

$$
C'_{pqrs}=\frac{1}{\det J}\frac{\partial x'_p}{\partial x_i}\frac{\partial x'_q}{\partial x_j}C_{ijkl}\frac{\partial x'_r}{\partial x_k}\frac{\partial x'_s}{\partial x_l} \tag{3.23}
$$

$$
S'_{pqr}=\frac{1}{\det J}\frac{\partial x'_p}{\partial x_i}\frac{\partial x'_q}{\partial x_j}C_{ijkl}\frac{\partial^2 x'_r}{\partial x_k\partial x_l}=S'_{qpr} \tag{3.24}
$$

$$
D'_{pqr}=\frac{1}{\det J}\frac{\partial^2 x'_p}{\partial x_i\partial x_j}C_{ijkl}\frac{\partial x'_q}{\partial x_k}\frac{\partial x'_r}{\partial x_l}=S'_{qrp} \tag{3.25}
$$

The stiffness tensor and the density are inherent properties of materials, while the newly added terms $\underline{S}'$ and $\underline{D}'$ are not found in the original space and unable to realize.

The dimensions of each term in transformation elasticity are checked. After a transformation, the symmetries of strain and stress tensors are generally broken. Then each in a vector form is presented by 9 components as

$$\nabla' u' = \varepsilon' = \begin{bmatrix} \varepsilon'_{xx} & \varepsilon'_{yy} & \varepsilon'_{zz} & \varepsilon'_{xy} & \varepsilon'_{yx} & \varepsilon'_{yz} & \varepsilon'_{zy} & \varepsilon'_{zx} & \varepsilon'_{xz} \end{bmatrix}^T \quad (3.26)$$

$$\sigma' = \begin{bmatrix} \sigma'_{xx} & \sigma'_{yy} & \sigma'_{zz} & \sigma'_{xy} & \sigma'_{yx} & \sigma'_{yz} & \sigma'_{zy} & \sigma'_{zx} & \sigma'_{xz} \end{bmatrix}^T \quad (3.27)$$

The special case where the Jacobian matrix is applied to transformation of displacement vectors allows the symmetry of stress tensor. A stiffness tensor relating two physical quantities is of (9×9) dimension. Meanwhile, the dimension of the extra terms $\underline{S}'$ and $\underline{D}'$ are (9×3) and (3×9), respectively ((8×2) and (2×8), respectively in the 2D space).

It might be meaningful to expand the governing equation by using the principle of virtual work, where a material undergoes a small imaginary displacement and the external forces conduct virtual work. A weak form of the governing equation can be drawn in this process. For a solid body in equilibrium in an original space,

$$\nabla \cdot \underline{\sigma} + \omega^2 \underline{\rho} \bar{u} = 0 \quad (3.28)$$

$$\underline{\sigma} = \underline{C} \nabla \bar{u} \quad (3.29)$$

are true. If a virtual displacement $\overline{u_{test}}$ is exerted to the body, the volume integral of the inner product of Eq. (3.38) and $\overline{u_{test}}$ is

$$\int_V \overline{u_{test}} \cdot \left(\nabla \cdot \underline{\sigma}\right) dV + \int_V \overline{u_{test}} \cdot \left(\omega^2 \underline{\rho} \bar{u}\right) dV = 0 \tag{3.30}$$

The first term in Eq. (3.30) can be changed from a 3D volume integral to a 2D surface integral by the divergence theorem as

$$\begin{aligned} \int_V \overline{u_{test}} \cdot \left(\nabla \cdot \underline{\sigma}\right) dV &= \int_V \nabla \cdot \left(\underline{\sigma} \cdot \overline{u_{test}}\right) dV - \int_V \underline{\sigma} : \nabla \overline{u_{test}} dV \\ &= \int_S \bar{n} \cdot \underline{\sigma} \cdot \overline{u_{test}} dS - \int_V \underline{\sigma} : \overline{\varepsilon_{test}} dV \\ &= \int_S \bar{t} \cdot \overline{u_{test}} dS - \int_V \underline{\sigma} : \overline{\varepsilon_{test}} dV \end{aligned} \tag{3.31}$$

where S, $\bar{n}$, $\overline{\varepsilon_{test}}$, $\bar{t}$ are the contour of the body, the normal vector on the contour, the strain by the virtual work and the traction force vector on the contour, respectively. By substitution of Eq. (3.31) to Eq. (3.30),

$$\int_S \bar{t} \cdot \overline{u_{test}} dS - \int_V \underline{\sigma} : \overline{\varepsilon_{test}} dV + \int_V \overline{u_{test}} \cdot \left(\omega^2 \underline{\rho} \bar{u}\right) dV = 0 \tag{3.32}$$

can be drawn. Since the cases treated in this thesis have no traction force at surfaces, the following is true before transformation.

$$\begin{aligned} &-\varepsilon_{xx,test}\sigma_{xx} - \varepsilon_{yy,test}\sigma_{yy} - \varepsilon_{zz,test}\sigma_{zz} - 2\varepsilon_{xy,test}\sigma_{xy} - 2\varepsilon_{yz,test}\sigma_{yz} - 2\varepsilon_{zx,test}\sigma_{zx} \\ &+\omega^2 \rho (u_{test} u + v_{test} v + w_{test} w) = 0 \end{aligned} \tag{3.33}$$

As mentioned before, however, stress and strain tensors are generally asymmetric and the density is in a form of tensor in the transformed space. Moreover, the extra terms are concerned, so Eq. (3.33) should be modified to reflect these differences. The transformed governing equations are re-written as

$$\nabla' \cdot \underline{\sigma}' - \underline{D}' \nabla' \bar{u}' + \omega^2 \underline{\rho}' \bar{u}' = 0 \tag{3.34}$$

$$\underline{\sigma}' = \underline{C}'\nabla'\bar{u}' + \underline{S}'\bar{u}' \tag{3.35}$$

Then the components of stress tensor are including $\underline{S}'$ terms as

$$\begin{aligned}\sigma'_{xx} &= C'_{1111}\cdot\varepsilon'_{xx} + C'_{1112}\cdot\varepsilon'_{xy} + C'_{1113}\cdot\varepsilon'_{xz} + C'_{1121}\cdot\varepsilon'_{yx} + C'_{1122}\cdot\varepsilon'_{yy} + C'_{1123}\cdot\varepsilon'_{yz} \\ &+ C'_{1131}\cdot\varepsilon'_{zx} + C'_{1132}\cdot\varepsilon'_{zy} + C'_{1133}\cdot\varepsilon'_{zz} + S'_{111}u' + S'_{112}v' + S'_{113}w'\end{aligned} \tag{3.36a}$$

$$\begin{aligned}\sigma'_{yy} &= C'_{2211}\cdot\varepsilon'_{xx} + C'_{2212}\cdot\varepsilon'_{xy} + C'_{2213}\cdot\varepsilon'_{xz} + C'_{2221}\cdot\varepsilon'_{yx} + C'_{2222}\cdot\varepsilon'_{yy} + C'_{2223}\cdot\varepsilon'_{yz} \\ &+ C'_{2231}\cdot\varepsilon'_{zx} + C'_{2232}\cdot\varepsilon'_{zy} + C'_{2233}\cdot\varepsilon'_{zz} + S'_{221}u' + S'_{222}v' + S'_{223}w'\end{aligned} \tag{3.36b}$$

$$\begin{aligned}\sigma'_{zz} &= C'_{3311}\cdot\varepsilon'_{xx} + C'_{3312}\cdot\varepsilon'_{xy} + C'_{3313}\cdot\varepsilon'_{xz} + C'_{3321}\cdot\varepsilon'_{yx} + C'_{3322}\cdot\varepsilon'_{yy} + C'_{3323}\cdot\varepsilon'_{yz} \\ &+ C'_{3331}\cdot\varepsilon'_{zx} + C'_{3332}\cdot\varepsilon'_{zy} + C'_{3333}\cdot\varepsilon'_{zz} + S'_{331}u' + S'_{332}v' + S'_{333}w'\end{aligned} \tag{3.36c}$$

$$\begin{aligned}\sigma'_{xy} &= C'_{1211}\cdot\varepsilon'_{xx} + C'_{1212}\cdot\varepsilon'_{xy} + C'_{1213}\cdot\varepsilon'_{xz} + C'_{1221}\cdot\varepsilon'_{yx} + C'_{1222}\cdot\varepsilon'_{yy} + C'_{1223}\cdot\varepsilon'_{yz} \\ &+ C'_{1231}\cdot\varepsilon'_{zx} + C'_{1232}\cdot\varepsilon'_{zy} + C'_{1233}\cdot\varepsilon'_{zz} + S'_{121}u' + S'_{122}v' + S'_{123}w'\end{aligned} \tag{3.36d}$$

$$\begin{aligned}\sigma'_{yx} &= C'_{2111}\cdot\varepsilon'_{xx} + C'_{2112}\cdot\varepsilon'_{xy} + C'_{2113}\cdot\varepsilon'_{xz} + C'_{2121}\cdot\varepsilon'_{yx} + C'_{2122}\cdot\varepsilon'_{yy} + C'_{2123}\cdot\varepsilon'_{yz} \\ &+ C'_{2131}\cdot\varepsilon'_{zx} + C'_{2132}\cdot\varepsilon'_{zy} + C'_{2133}\cdot\varepsilon'_{zz} + S'_{211}u' + S'_{212}v' + S'_{213}w'\end{aligned} \tag{3.36e}$$

$$\begin{aligned}\sigma'_{yz} &= C'_{2311}\cdot\varepsilon'_{xx} + C'_{2312}\cdot\varepsilon'_{xy} + C'_{2313}\cdot\varepsilon'_{xz} + C'_{2321}\cdot\varepsilon'_{yx} + C'_{2322}\cdot\varepsilon'_{yy} + C'_{2323}\cdot\varepsilon'_{yz} \\ &+ C'_{2331}\cdot\varepsilon'_{zx} + C'_{2332}\cdot\varepsilon'_{zy} + C'_{2333}\cdot\varepsilon'_{zz} + S'_{231}u' + S'_{232}v' + S'_{233}w'\end{aligned} \tag{3.36f}$$

$$\begin{aligned}\sigma'_{zy} &= C'_{3211}\cdot\varepsilon'_{xx} + C'_{3212}\cdot\varepsilon'_{xy} + C'_{3213}\cdot\varepsilon'_{xz} + C'_{3221}\cdot\varepsilon'_{yx} + C'_{3222}\cdot\varepsilon'_{yy} + C'_{3223}\cdot\varepsilon'_{yz} \\ &+ C'_{3231}\cdot\varepsilon'_{zx} + C'_{3232}\cdot\varepsilon'_{zy} + C'_{3233}\cdot\varepsilon'_{zz} + S'_{321}u' + S'_{322}v' + S'_{323}w'\end{aligned} \tag{3.36g}$$

$$\begin{aligned}\sigma'_{zx} &= C'_{3111}\cdot\varepsilon'_{xx} + C'_{3112}\cdot\varepsilon'_{xy} + C'_{3113}\cdot\varepsilon'_{xz} + C'_{3121}\cdot\varepsilon'_{yx} + C'_{3122}\cdot\varepsilon'_{yy} + C'_{3123}\cdot\varepsilon'_{yz} \\ &+ C'_{3131}\cdot\varepsilon'_{zx} + C'_{3132}\cdot\varepsilon'_{zy} + C'_{3133}\cdot\varepsilon'_{zz} + S'_{311}u' + S'_{312}v' + S'_{313}w'\end{aligned} \tag{3.36h}$$

$$\begin{aligned}\sigma'_{xz} &= C'_{1311}\cdot\varepsilon'_{xx} + C'_{1312}\cdot\varepsilon'_{xy} + C'_{1313}\cdot\varepsilon'_{xz} + C'_{1321}\cdot\varepsilon'_{yx} + C'_{1322}\cdot\varepsilon'_{yy} + C'_{1323}\cdot\varepsilon'_{yz} \\ &+ C'_{1331}\cdot\varepsilon'_{zx} + C'_{1332}\cdot\varepsilon'_{zy} + C'_{1333}\cdot\varepsilon'_{zz} + S'_{131}u' + S'_{132}v' + S'_{133}w'\end{aligned} \tag{3.36i}$$

and the newly added $\underline{D}'\nabla\bar{u}'$ are expanded as

$$\begin{aligned}D'_x &= D'_{111}\varepsilon'_{xx} + D'_{112}\varepsilon'_{xy} + D'_{113}\varepsilon'_{xz} + D'_{121}\varepsilon'_{yx} + D'_{122}\varepsilon'_{yy} + D'_{123}\varepsilon'_{yz} \\ &+ D'_{131}\varepsilon'_{zx} + D'_{132}\varepsilon'_{zy} + D'_{133}\varepsilon'_{zz}\end{aligned} \tag{3.37a}$$

$$D'_y = D'_{211}\varepsilon'_{xx} + D'_{212}\varepsilon'_{xy} + D'_{213}\varepsilon'_{xz} + D'_{221}\varepsilon'_{yx} + D'_{222}\varepsilon'_{yy} + D'_{223}\varepsilon'_{yz} + D'_{231}\varepsilon'_{zx} + D'_{232}\varepsilon'_{zy} + D'_{233}\varepsilon'_{zz} \tag{3.37b}$$

$$D'_z = D'_{311}\varepsilon'_{xx} + D'_{312}\varepsilon'_{xy} + D'_{313}\varepsilon'_{xz} + D'_{321}\varepsilon'_{yx} + D'_{322}\varepsilon'_{yy} + D'_{323}\varepsilon'_{yz} + D'_{331}\varepsilon'_{zx} + D'_{332}\varepsilon'_{zy} + D'_{333}\varepsilon'_{zz} \tag{3.37c}$$

By using Eq. (3.36) and Eq. (3.37), the weak form of the governing equation in the transformed space is

$$\begin{aligned}
&-\varepsilon'_{xx,test}\sigma'_{xx} - \varepsilon'_{yy,test}\sigma'_{yy} - \varepsilon'_{zz,test}\sigma'_{zz} \\
&-\varepsilon'_{xy,test}\sigma'_{xy} - \varepsilon'_{yx,test}\sigma'_{yx} - \varepsilon'_{yz,test}\sigma'_{yz} - \varepsilon'_{zy,test}\sigma'_{zy} - \varepsilon'_{zx,test}\sigma'_{zx} - \varepsilon'_{xz,test}\sigma'_{xz} \\
&+\omega^2\Big[u'_{test}\cdot\left(\rho'_{xx}u' + \rho'_{xy}v' + \rho'_{xz}w'\right)\ldots \\
&+v'_{test}\cdot\left(\rho'_{yx}u' + \rho'_{yy}v' + \rho'_{yz}w'\right) + w'_{test}\cdot\left(\rho'_{zx}u' + \rho'_{zy}v' + \rho'_{zz}w'\right)\Big] \\
&-u'_{test}\cdot D'_x - v'_{test}\cdot D'_y - w'_{test}\cdot D'_z = 0
\end{aligned} \tag{3.38}$$

The weak form, though practically unrealizable, allows numerical simulations of designed devices for confirming the accuracy of the calculated material properties. The computational results can set the standards of the performances of ideal devices designed by transformation elasticity.

Elastic wave propagation in the cloaking device simulated by COMSOL Multiphysics [54] is shown in Fig. 3.1. The cloaking device has material properties calculated by Eq. (3.22) ~ (3.25) and the weak form Eq. (3.38) is solved. The waves maintain their wave fronts ideally after passing the cloaking device, never to reach the inside of the device. However, it is hard to expect the perfect performance of the device in reality because the material properties $\underline{S}'$ and $\underline{D}'$ cannot be achieved. To preserve the performance as much as possible, the ignored terms should be minimized.

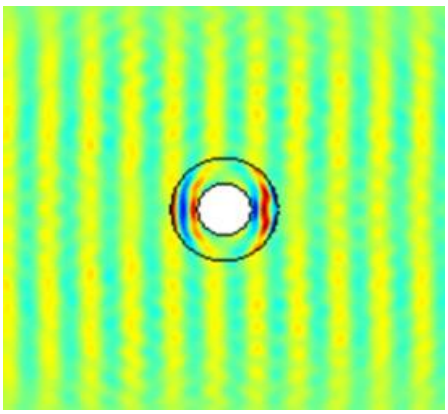

Fig. 3. 1 Simulation for elastic wave propagation in an ideal cloaking device.

3.3 Conformal Transformation

The solution to minimize the extra terms in this thesis is *conformal transformation*. Conformal mapping is a function that preserves an angle between two arbitrary lines after transformation, and a space is transformed by means of complex functions [56].

Conformal mapping is occasionally used for transformation devices. In Ref. [2, 57], an invisibility cloak for electromagnetic and acoustic waves is engineered by using conformal mapping. Practically, the isotropy of density after transformation is verified in transformation acoustics. It is helpful for realization of devices engineered by any transformation methods because anisotropic material property is one of difficulties in realization. A broadband lens for directional emission is realized with the benefit of conformal mapping [58]. Ref. [59-62] are also dedicated to conformal mapping in elastodynamics, but they do not identify the decrease of the extra terms and engineering a

practical use of devices. Other methodology for elastic wave controlling devices by using conformal transformation is suggested in Ref. [63-66]. They applied conformal transformation locally to infinitesimal parts of solid media, so that the extra terms are not concerned. However, the function and the size of designed devices are limited due to the local property.

Here, the contributions of conformal transformation on the simplification of the extra terms in transformation elasticity are presented in detail in addition to derivation of the isotropic properties of solid media. Using the newly introduced features, elastodynamic waves are easily controlled in various devices.

3.3.1 Derivation of Material Properties in conformal transformation

Let us inspect Eq. (3.24) and Eq. (3.25) thoroughly to comprehend the composition of the extra terms and reduce the magnitude of them. By substituting the stiffness tensor expressed with the Lame's constants,

$$C_{ijkl} = \lambda\delta_{ij}\delta_{kl} + \mu(\delta_{ik}\delta_{jl} + \delta_{il}\delta_{jk}) \tag{3.39}$$

the extra terms are re-written as

$$S'_{pqr} = \frac{1}{\det J}\frac{\partial x'_p}{\partial x_i}\frac{\partial x'_q}{\partial x_j}\left[\lambda\delta_{ij}\delta_{kl} + \mu(\delta_{ik}\delta_{jl} + \delta_{il}\delta_{jk})\right]\frac{\partial^2 x'_r}{\partial x_k \partial x_l} \tag{3.40}$$

$$D'_{pqr} = \frac{1}{\det J}\frac{\partial^2 x'_p}{\partial x_i \partial x_j}\left[\lambda\delta_{ij}\delta_{kl} + \mu(\delta_{ik}\delta_{jl} + \delta_{il}\delta_{jk})\right]\frac{\partial x'_q}{\partial x_k}\frac{\partial x'_r}{\partial x_l} \tag{3.41}$$

As can be seen, the extra terms are composed of the Lame's constants and the 1st, 2nd derivatives of a mapping equation. Pentamode materials are to diminish the magnitude of shear modulus so that they work like fluid out of influence of shear deformations. Although they have their shear moduli successfully decreased, their stabilities are threatened instead. Unlike the pentamode materials, application of conformal transformation focuses on the reduction of the magnitude of the 2nd order derivatives. By using the characteristics of conformal transformation, the magnitude of the extra terms are controlled.

The most important feature of conformal transformation is *Cauchy-Riemann condition* which relates the 1st order derivatives of a mapping equation.

$$\frac{\partial x'}{\partial x} = \frac{\partial y'}{\partial y}, \tag{3.42a}$$

$$\frac{\partial x'}{\partial y} = -\frac{\partial y'}{\partial x} \tag{3.42b}$$

Typically x and y are taken to the real and imaginary parts respectively of a coordinate z in the original space, i.e. $z = x + iy$. The corresponding coordinate w in the transformed space is $w = x' + iy' = f(x, y) + ig(x, y) = h(z)$. Then the Caucy-Riemann condition may be written in complex form as

$$i\frac{\partial h}{\partial x} = \frac{\partial h}{\partial y} \tag{3.43}$$

Thank to the condition, the Jacobian matrix is skew-symmetric.

$$J = \begin{bmatrix} \frac{\partial x'}{\partial x} & \frac{\partial x'}{\partial y} \\ \frac{\partial y'}{\partial x} & \frac{\partial y'}{\partial y} \end{bmatrix} = \begin{bmatrix} \alpha & \beta \\ -\beta & \alpha \end{bmatrix} \tag{3.44}$$

In this case, the determinant of the J is $\det J = \alpha^2 + \beta^2$. Since the material properties for transformation elasticity require the 2nd order derivatives of a mapping equation, the relations between them can be drawn from Eq. (3.42). These relations have a decisive effect on the minimization of the extra terms. From Eq. (3.42a),

$$\frac{\partial^2 x'}{\partial x^2} = \frac{\partial^2 y'}{\partial x \partial y}, \tag{3.45a}$$

$$\frac{\partial^2 x'}{\partial x \partial y} = \frac{\partial^2 y'}{\partial y^2} \tag{3.45b}$$

and from Eq. (3.42b),

$$\frac{\partial^2 x'}{\partial x \partial y} = -\frac{\partial^2 y'}{\partial x^2}, \tag{3.46a}$$

$$\frac{\partial^2 x'}{\partial y^2} = -\frac{\partial^2 y'}{\partial x \partial y} \tag{3.46b}$$

By using Eq. (3.42) and Eq. (3.45), a density matrix is simplified to a scalar value, i.e. a density is isotropic and has no off-diagonal terms, and a transformed stiffness tensor is a multiple of the original stiffness tensor. Moreover, the extra terms are dramatically decreased.

Let us consider material properties in the 2D space to apply the Cauchy-Riemann

condition. A density matrix after transformation has generally 4 components in it. Following the notation in Eq. (3.22), the $(1,1)$ component ρ'_{xx} is expanded as

$$\begin{aligned}\rho'_{xx} &= \frac{\rho}{\det J}\frac{\partial x'}{\partial x_i}\frac{\partial x'}{\partial x_i} + \frac{1}{\det J}\frac{1}{(-i\omega)^2}\frac{\partial^2 x'}{\partial x_i \partial x_j} C_{ijkl} \frac{\partial^2 x'}{\partial x_k \partial x_l} \\ &= \frac{\rho}{\det J}\left(\left(\frac{\partial x'}{\partial x}\right)^2 + \left(\frac{\partial x'}{\partial y}\right)^2\right) + \ldots \\ &\quad \frac{1}{\det J}\frac{1}{(i\omega)^2}\left(C_{1111}\left(\frac{\partial^2 x'}{\partial x^2}\right)^2 + C_{2222}\left(\frac{\partial^2 x'}{\partial y^2}\right)^2 + 2C_{1122}\frac{\partial^2 x'}{\partial x^2}\frac{\partial^2 x'}{\partial y^2} + 4C_{1212}\left(\frac{\partial^2 x'}{\partial x \partial y}\right)^2\right)\end{aligned} \tag{3.47}$$

Some terms are associated according to the major and minor symmetry of a stiffness tensor shown in Eq. (3.7) and Eq. (3.8). By substituting the relations of the 1st, 2nd derivatives and the Lame's constant of an isotropic stiffness tensor, it is simplified as

$$
\begin{aligned}
\rho'_{xx} &= \frac{\rho}{\det J}\left(\alpha^2+\beta^2\right)-\ldots \\
&\frac{1}{\det J}\frac{1}{\omega^2}\left(\left(\lambda+2\mu\right)\left(\left(\frac{\partial^2 x'}{\partial x^2}\right)^2+\left(\frac{\partial^2 x'}{\partial y^2}\right)^2\right)+2\lambda\frac{\partial^2 x'}{\partial x^2}\frac{\partial^2 x'}{\partial y^2}+4\mu\left(\frac{\partial^2 x'}{\partial x\partial y}\right)^2\right) \\
&= \frac{\rho}{\det J}\cdot\det J-\ldots \\
&\frac{1}{\det J}\frac{1}{\omega^2}\left(\left(\lambda+2\mu\right)\left(\left(\frac{\partial^2 y'}{\partial x\partial y}\right)^2+\left(\frac{\partial^2 y'}{\partial x\partial y}\right)^2\right)-2\lambda\left(\frac{\partial^2 y'}{\partial x\partial y}\right)^2+4\mu\left(\frac{\partial^2 x'}{\partial x\partial y}\right)^2\right) \\
&= \rho-\frac{1}{\det J}\frac{1}{\omega^2}\left(\left(\lambda+2\mu\right)\left(\left(\frac{\partial^2 y'}{\partial x\partial y}\right)^2+\left(\frac{\partial^2 y'}{\partial x\partial y}\right)^2\right)-2\lambda\left(\frac{\partial^2 y'}{\partial x\partial y}\right)^2+4\mu\left(\frac{\partial^2 x'}{\partial x\partial y}\right)^2\right) \\
&= \rho-\frac{1}{\det J}\frac{1}{\omega^2}\left(2\left(\lambda+2\mu\right)\left(\frac{\partial^2 y'}{\partial x\partial y}\right)^2-2\lambda\left(\frac{\partial^2 y'}{\partial x\partial y}\right)^2+4\mu\left(\frac{\partial^2 x'}{\partial x\partial y}\right)^2\right) \\
&= \rho-\frac{1}{\det J}\frac{1}{\omega^2}\left(4\mu\left(\frac{\partial^2 y'}{\partial x\partial y}\right)^2+4\mu\left(\frac{\partial^2 x'}{\partial x\partial y}\right)^2\right) \\
&= \rho-\frac{4\mu}{\det J}\frac{1}{\omega^2}\left(\left(\frac{\partial^2 x'}{\partial x\partial y}\right)^2+\left(\frac{\partial^2 y'}{\partial x\partial y}\right)^2\right)
\end{aligned}
\tag{3.48}
$$

The terms including λ are cancelled with each other by proper swaps of the 2nd order derivatives. The resulting terms are composed of the original density, shear modulus μ and the geometric variables. The $(2,2)$ component ρ'_{yy} is also expanded as following.

$$
\begin{aligned}
\rho_{22}' &= \frac{\rho}{\det J}\frac{\partial y'}{\partial x_i}\frac{\partial y'}{\partial x_i} + \frac{1}{\det J}\frac{1}{(-i\omega)^2}\frac{\partial^2 y'}{\partial x_i \partial x_j} C_{ijkl}\frac{\partial^2 y'}{\partial x_k \partial x_l} \\
&= \frac{\rho}{\det J}\left(\left(\frac{\partial y'}{\partial x}\right)^2 + \left(\frac{\partial y'}{\partial y}\right)^2\right) - \ldots \\
&\quad \frac{1}{\det J}\frac{1}{\omega^2}\left(C_{1111}\left(\frac{\partial^2 y'}{\partial x^2}\right)^2 + C_{2222}\left(\frac{\partial^2 y'}{\partial y^2}\right)^2 + 2C_{1122}\frac{\partial^2 y'}{\partial x^2}\frac{\partial^2 y'}{\partial y^2} + 4C_{1212}\left(\frac{\partial^2 y'}{\partial x \partial y}\right)^2\right) \\
&= \frac{\rho}{\det J}\left(\alpha^2 + \beta^2\right) - \ldots \\
&\quad \frac{1}{\det J}\frac{1}{\omega^2}\left((\lambda + 2\mu)\left(\left(\frac{\partial^2 y'}{\partial x^2}\right)^2 + \left(\frac{\partial^2 y'}{\partial y^2}\right)^2\right) + 2\lambda\frac{\partial^2 y'}{\partial x^2}\frac{\partial^2 y'}{\partial y^2} + 4\mu\left(\frac{\partial^2 y'}{\partial x \partial y}\right)^2\right) \\
&= \rho - \frac{1}{\det J}\frac{1}{\omega^2}\left((\lambda + 2\mu)\left(\left(\frac{\partial^2 x'}{\partial x \partial y}\right)^2 + \left(\frac{\partial^2 x'}{\partial x \partial y}\right)^2\right) - 2\lambda\left(\frac{\partial^2 x'}{\partial x \partial y}\right)^2 + 4\mu\left(\frac{\partial^2 x'}{\partial x \partial y}\right)^2\right) \\
&= \rho - \frac{4\mu}{\det J}\frac{1}{\omega^2}\left(\left(\frac{\partial^2 x'}{\partial x \partial y}\right)^2 + \left(\frac{\partial^2 y'}{\partial x \partial y}\right)^2\right) = \rho_{11}'
\end{aligned}
\tag{3.49}
$$

This component has the same value with the first diagonal component, whereas the off-diagonal terms have another remarkable characteristic due to conformal transformation. The $(1,2)$ component is expanded as

$$
\begin{aligned}
\rho'_{xy} &= \frac{\rho}{\det J}\frac{\partial x'}{\partial x_i}\frac{\partial y'}{\partial x_i} + \frac{1}{\det J}\frac{1}{(-i\omega)^2}\frac{\partial^2 x'}{\partial x_i \partial x_j} C_{ijkl} \frac{\partial^2 y'}{\partial x_k \partial x_l} \\
&= \frac{\rho}{\det J}\left(\frac{\partial x'}{\partial x}\frac{\partial y'}{\partial x} + \frac{\partial x'}{\partial y}\frac{\partial y'}{\partial y}\right) - \ldots \\
&\frac{1}{\det J}\frac{1}{\omega^2}\left(C_{1111}\frac{\partial^2 x'}{\partial x^2}\frac{\partial^2 y'}{\partial x^2} + C_{2222}\frac{\partial^2 x'}{\partial y^2}\frac{\partial^2 y'}{\partial y^2} + \ldots\right. \\
&\left. C_{1122}\frac{\partial^2 x'}{\partial x^2}\frac{\partial^2 y'}{\partial y^2} + C_{2211}\frac{\partial^2 y'}{\partial x^2}\frac{\partial^2 x'}{\partial y^2} + 4C_{1212}\frac{\partial^2 x'}{\partial x \partial y}\frac{\partial^2 y'}{\partial x \partial y}\right) \\
&= \frac{\rho}{\det J}(\alpha\beta - \alpha\beta) - \ldots \\
&\frac{1}{\det J}\frac{1}{\omega^2}\left[(\lambda + 2\mu)\left(\frac{\partial^2 x'}{\partial x^2}\frac{\partial^2 y'}{\partial x^2} + \frac{\partial^2 x'}{\partial y^2}\frac{\partial^2 y'}{\partial y^2}\right) + \ldots\right. \\
&\left.\lambda\left(\frac{\partial^2 x'}{\partial x^2}\frac{\partial^2 y'}{\partial y^2} + \frac{\partial^2 y'}{\partial x^2}\frac{\partial^2 x'}{\partial y^2}\right) + 4\mu\frac{\partial^2 x'}{\partial x \partial y}\frac{\partial^2 y'}{\partial x \partial y}\right] \\
&= -\frac{1}{\det J}\frac{1}{\omega^2}\left[(\lambda + 2\mu)\left(\frac{\partial^2 y'}{\partial x \partial y}\cdot\left(-\frac{\partial^2 x'}{\partial x \partial y}\right) + \left(-\frac{\partial^2 y'}{\partial x \partial y}\right)\cdot\frac{\partial^2 x'}{\partial x \partial y}\right) + \ldots\right. \\
&\left.\lambda\left(\frac{\partial^2 y'}{\partial x \partial y}\frac{\partial^2 x'}{\partial x \partial y} + \left(-\frac{\partial^2 y'}{\partial x \partial y}\right)\cdot\left(-\frac{\partial^2 x'}{\partial x \partial y}\right)\right) + 4\mu\frac{\partial^2 x'}{\partial x \partial y}\frac{\partial^2 y'}{\partial x \partial y}\right] \qquad (3.50) \\
&= -\frac{1}{\det J}\frac{1}{\omega^2}\left[-2(\lambda + 2\mu)\frac{\partial^2 x'}{\partial x \partial y}\frac{\partial^2 y'}{\partial x \partial y} + 2\lambda\frac{\partial^2 y'}{\partial x \partial y}\frac{\partial^2 x'}{\partial x \partial y} + 4\mu\frac{\partial^2 x'}{\partial x \partial y}\frac{\partial^2 y'}{\partial x \partial y}\right] \\
&= \frac{1}{\det J}\frac{1}{(i\omega)^2}\left(-2(\lambda + 2\mu) + 2\lambda + 4\mu\right)\frac{\partial^2 x'}{\partial x \partial y}\frac{\partial^2 y'}{\partial x \partial y} = 0
\end{aligned}
$$

The (2.1) component is expanded in the same manner and turns to be zero. As can be seen, all the 1st and the 2nd derivatives of a conformal mapping equation are cancelled and the off-diagonal terms have a value of zero.

From Eq. (3.48) ~ (3.50), the density matrix in the transformed space is simply expressed

as

$$\underline{\rho}' = \begin{bmatrix} \rho'_{xx} & \rho'_{xy} \\ \rho'_{yx} & \rho'_{yy} \end{bmatrix} = \begin{bmatrix} \rho'_{xx} & 0 \\ 0 & \rho'_{xx} \end{bmatrix} = \rho'_{xx}$$
$$= \rho - \frac{4\mu}{\det J}\frac{1}{\omega^2}\left(\left(\frac{\partial^2 x'}{\partial x \partial y}\right)^2 + \left(\frac{\partial^2 y'}{\partial x \partial y}\right)^2\right) \tag{3.51}$$

Generally a density in the transformed space is in the tensor form, but it can be treated as a scalar when using conformal transformation. Since the density has no off-diagonal terms and is of a unit value, the material composing the device is isotropic in density. It is a big advantage in the process of realization.

Transformation of a stiffness tensor also takes advantage of the properties of conformal transformation. The component of $i, j, k, l = 1$ or 2 are dealt here because the 2D space is transformed in this case. Let us examine it to begin with the component C'_{1111}. According to Eq. (3.23) and considering the components of an isotropic stiffness tensor before transformation,

$$C'_{1111} = \frac{1}{\det J}\frac{\partial x'}{\partial x_i}\frac{\partial x'}{\partial x_j}C_{ijkl}\frac{\partial x'}{\partial x_k}\frac{\partial x'}{\partial x_l}$$
$$= \frac{1}{\det J}\left[C_{1111}\left\{\left(\frac{\partial x'}{\partial x}\right)^4 + \left(\frac{\partial x'}{\partial y}\right)^4\right\} + 2C_{1122}\left(\frac{\partial x'}{\partial x}\right)^2\left(\frac{\partial x'}{\partial y}\right)^2 + 4C_{1212}\left(\frac{\partial x'}{\partial x}\right)^2\left(\frac{\partial x'}{\partial y}\right)^2\right] \tag{3.52}$$

By substituting Eq. (3.44) and the Lame's constants,

$$
\begin{aligned}
C'_{1111} &= \frac{1}{\det J}\left[C_{1111}\left(\alpha^4+\beta^4\right)+2C_{1122}\alpha^2\beta^2+4C_{1212}\alpha^2\beta^2\right] \\
&= \frac{1}{\det J}\left[\left(\lambda+2\mu\right)\left(\alpha^4+\beta^4\right)+2\lambda\alpha^2\beta^2+4\mu\alpha^2\beta^2\right] \\
&= \frac{1}{\det J}\left[\lambda\left(\alpha^4+2\alpha^2\beta^2+\beta^4\right)+2\mu\left(\alpha^4+2\alpha^2\beta^2+\beta^4\right)\right] \\
&= \frac{1}{\det J}\left(\lambda+2\mu\right)\left(\alpha^2+\beta^2\right)^2 = \frac{1}{\det J}\left(\lambda+2\mu\right)\left(\det J\right)^2 \\
&= \det J\cdot\left(\lambda+2\mu\right) = \det J\cdot C_{1111}
\end{aligned}
\tag{3.53}
$$

The first component in the transformed stiffness tensor is simply a $\det J$ multiple of the original counterpart. Other components are expanded and simplified in the same way.

$$
\begin{aligned}
C'_{2222} &= \frac{1}{\det J}\left[C_{1111}\left\{\left(\frac{\partial y'}{\partial x}\right)^4+\left(\frac{\partial y'}{\partial y}\right)^4\right\}+2C_{1122}\left(\frac{\partial y'}{\partial x}\right)^2\left(\frac{\partial y'}{\partial y}\right)^2+4C_{1212}\left(\frac{\partial y'}{\partial x}\right)^2\left(\frac{\partial y'}{\partial y}\right)^2\right] \\
&= \frac{1}{\det J}\left[C_{1111}\left(\alpha^4+\beta^4\right)+2C_{1122}\alpha^2\beta^2+4C_{1212}\alpha^2\beta^2\right] = C_{1111}'
\end{aligned}
\tag{3.54}
$$

C'_{2222} has the same value with C'_{1111} as it does in the original stiffness tensor.

$$
\begin{aligned}
C'_{1122} &= \frac{1}{\det J}\left[C_{1111}\left\{\left(\frac{\partial x'}{\partial x}\right)^2\left(\frac{\partial y'}{\partial x}\right)^2+\left(\frac{\partial x'}{\partial y}\right)^2\left(\frac{\partial y'}{\partial y}\right)^2\right\}+\ldots\right. \\
&\quad C_{1122}\left\{\left(\frac{\partial x'}{\partial x}\right)^2\left(\frac{\partial y'}{\partial y}\right)^2+\left(\frac{\partial x'}{\partial y}\right)^2\left(\frac{\partial y'}{\partial x}\right)^2\right\}+\ldots \\
&\quad \left.C_{1212}\left(\frac{\partial x'}{\partial x}\frac{\partial x'}{\partial y}\frac{\partial y'}{\partial x}\frac{\partial y'}{\partial y}+\frac{\partial x'}{\partial x}\frac{\partial x'}{\partial y}\frac{\partial y'}{\partial y}\frac{\partial y'}{\partial x}+\frac{\partial x'}{\partial y}\frac{\partial x'}{\partial x}\frac{\partial y'}{\partial x}\frac{\partial y'}{\partial y}+\frac{\partial x'}{\partial y}\frac{\partial x'}{\partial x}\frac{\partial y'}{\partial y}\frac{\partial y'}{\partial x}\right)\right] \\
&= \frac{1}{\det J}\left[2\left(\lambda+2\mu\right)\alpha^2\beta^2+\lambda\left(\alpha^4+\beta^4\right)-4\mu\alpha^2\beta^2\right] \\
&= \frac{1}{\det J}\left[2\lambda\alpha^2\beta^2+\lambda\left(\alpha^4+\beta^4\right)\right] = \frac{1}{\det J}\lambda\left(\alpha^4+2\alpha^2\beta^2+\beta^4\right) \\
&= \frac{1}{\det J}\lambda\cdot\left(\det J\right)^2 = \det J\cdot\lambda = \det J\cdot C_{1122}
\end{aligned}
\tag{3.55}
$$

C'_{1122} is likewise a $\det J$ multiple of the original one and C'_{2211} has the same

property. A shear modulus C'_{1212} is

$$
\begin{aligned}
C'_{1212} &= \frac{1}{\det J}\left[C_{1111}\cdot 2\alpha^2\beta^2 - C_{1122}\cdot 2\alpha^2\beta^2 + C_{1212}\left(\alpha^4 - 2\alpha^2\beta^2 + \beta^4\right)\right] \\
&= \frac{1}{\det J}\left[2\left(\lambda+2\mu\right)\alpha^2\beta^2 - 2\lambda\alpha^2\beta^2 + \mu\left(\alpha^4 - 2\alpha^2\beta^2 + \beta^4\right)\right] \\
&= \frac{1}{\det J}\cdot\mu\left(\alpha^4 + 2\alpha^2\beta^2 + \beta^4\right) \\
&= \frac{1}{\det J}\cdot\mu\left(\alpha^2+\beta^2\right)^2 = \frac{1}{\det J}\cdot\mu\left(\det J\right)^2 \\
&= \det J\cdot\mu = \det J\cdot C_{1212}
\end{aligned}
\tag{3.56}
$$

and $C'_{1212} = C'_{1221} = C'_{2112} = C'_{2121}$ is also valid. The other components that were zero in the original isotropic stiffness tensor remain zero after the transformation. The expansion of C'_{1112} is presented as an example.

$$
\begin{aligned}
C'_{1112} = \frac{1}{\det J}\Bigg[& C_{1111}\left\{\left(\frac{\partial x'}{\partial x}\right)^3\frac{\partial y'}{\partial x} + \left(\frac{\partial x'}{\partial y}\right)^3\frac{\partial y'}{\partial y}\right\} + \ldots \\
& C_{1122}\left\{\left(\frac{\partial x'}{\partial x}\right)^2\frac{\partial x'}{\partial y}\frac{\partial y'}{\partial y} + \left(\frac{\partial x'}{\partial y}\right)^2\frac{\partial x'}{\partial x}\frac{\partial y'}{\partial x}\right\} + \ldots \\
& C_{1212}\left(\frac{\partial x'}{\partial x}\frac{\partial x'}{\partial y}\frac{\partial x'}{\partial x}\frac{\partial y'}{\partial y} + \frac{\partial x'}{\partial x}\frac{\partial x'}{\partial y}\frac{\partial x'}{\partial y}\frac{\partial y'}{\partial x} + \frac{\partial x'}{\partial y}\frac{\partial x'}{\partial x}\frac{\partial x'}{\partial x}\frac{\partial y'}{\partial y} + \frac{\partial x'}{\partial y}\frac{\partial x'}{\partial x}\frac{\partial x'}{\partial y}\frac{\partial y'}{\partial x}\right)\Bigg] \\
= \frac{1}{\det J}\Big[& C_{1111}\left\{\alpha^3\cdot(-\beta) + \beta^3\alpha\right\} + C_{1122}\left\{\alpha^2\beta\alpha + \beta^2\alpha\cdot(-\beta)\right\} + C_{1212}\left(2\alpha^3\beta - 2\alpha\beta^3\right)\Big] \\
= \frac{1}{\det J}\Big[& -\left(\lambda+2\mu\right)\alpha\beta\left(\alpha^2-\beta^2\right) + \lambda\alpha\beta\left(\alpha^2-\beta^2\right) + 2\mu\alpha\beta\left(\alpha^2-\beta^2\right)\Big] = 0
\end{aligned}
\tag{3.57}
$$

From Eq. (3.53) ~ (3.56), the following is concluded.

$$
\underline{C}' = \det J\cdot\underline{C} \tag{3.58}
$$

This relation is quite advantageous for realization in that the calculation of the wave velocity in a device is simple and clear.

Next is the minimization of the extra terms by the relations Eq. (3.42), Eq. (3.45) and Eq. (3.46). The components of $\underline{S}'$ in the 2D space is

$$\underline{S}' = \begin{bmatrix} s'_{111} & s'_{112} \\ s'_{121} & s'_{122} \\ s'_{211} & s'_{212} \\ s'_{221} & s'_{222} \end{bmatrix} \tag{3.59}$$

The $(1,1)$ term s'_{111} is

$$\begin{aligned}
s'_{111} &= \frac{1}{\det J}\frac{\partial x'}{\partial x_i}\frac{\partial x'}{\partial x_j}C_{ijkl}\frac{\partial^2 x'}{\partial x_k \partial x_l} \\
&= \frac{1}{\det J}\left[C_{1111}\left(\left(\frac{\partial x'}{\partial x}\right)^2\frac{\partial^2 x'}{\partial x^2}+\left(\frac{\partial x'}{\partial y}\right)^2\frac{\partial^2 x'}{\partial y^2}\right)+\ldots\right. \\
&\quad \left. C_{1122}\left(\left(\frac{\partial x'}{\partial x}\right)^2\frac{\partial^2 x'}{\partial y^2}+\left(\frac{\partial x'}{\partial y}\right)^2\frac{\partial^2 x'}{\partial x^2}\right)+4C_{1212}\frac{\partial x'}{\partial x}\frac{\partial x'}{\partial y}\frac{\partial^2 x'}{\partial x \partial y}\right] \\
&= \frac{1}{\det J}\left[(\lambda+2\mu)\left(\alpha^2\frac{\partial^2 x'}{\partial x^2}+\beta^2\frac{\partial^2 x'}{\partial y^2}\right)+\lambda\left(\alpha^2\frac{\partial^2 x'}{\partial y^2}+\beta^2\frac{\partial^2 x'}{\partial x^2}\right)+4\mu\alpha\beta\frac{\partial^2 x'}{\partial x \partial y}\right] \\
&= \frac{1}{\det J}\left[(\lambda+2\mu)\left(\alpha^2\frac{\partial^2 y'}{\partial x \partial y}-\beta^2\frac{\partial^2 y'}{\partial x \partial y}\right)+\lambda\left(-\alpha^2\frac{\partial^2 y'}{\partial x \partial y}+\beta^2\frac{\partial^2 y'}{\partial x \partial y}\right)+4\mu\alpha\beta\frac{\partial^2 x'}{\partial x \partial y}\right] \\
&= \frac{1}{\det J}\left[(\lambda+2\mu)\left(\alpha^2-\beta^2\right)\frac{\partial^2 y'}{\partial x \partial y}-\lambda\left(\alpha^2-\beta^2\right)\frac{\partial^2 y'}{\partial x \partial y}+4\mu\alpha\beta\frac{\partial^2 x'}{\partial x \partial Y}\right]y \\
&= \frac{1}{\det J}\left[2\mu\left(\alpha^2-\beta^2\right)\frac{\partial^2 y'}{\partial x \partial y}+4\mu\alpha\beta\frac{\partial^2 x'}{\partial x \partial y}\right] \\
&= \frac{2\mu}{\det J}\left[\left(\alpha^2-\beta^2\right)\frac{\partial^2 x'}{\partial x^2}+2\alpha\beta\frac{\partial^2 y'}{\partial y^2}\right]
\end{aligned} \tag{3.60}$$

and the $(1,2)$ term is

$$s'_{112} = \frac{2\mu}{\det J}\left[2\alpha\beta\frac{\partial^2 x'}{\partial x^2}-\left(\alpha^2-\beta^2\right)\frac{\partial^2 y'}{\partial y^2}\right] \tag{3.61}$$

The rest terms in the $\underline{S}'$ matrix of conformal transformation are expressed only with s'_{111} and s'_{112} as

$$s'_{111} = s'_{122} = s'_{212} = -s'_{221} \tag{3.62a}$$

$$s'_{112} = -s'_{121} = -s'_{211} = -s'_{222} \tag{3.62b}$$

The relation between $\underline{S}'$ and $\underline{D}'$ presented in Eq. (3.25) is valid for all mapping equations. Thus, the extra terms shown in conformal transformation are governed only by two terms, s'_{111} and s'_{112}. Therefore, the reduction of s'_{111} and s'_{112} is directly connected to the decrease of the extra terms.

Similar to the transformed density, s'_{111} and s'_{112} consist of a shear modulus μ and geometric variables, with λ terms cancelled with each other due to the characteristics of conformal transformation. For general transformation equations, Eq. (3.42), Eq. (3.45) and Eq. (3.46) are invalid; the 1st and the 2nd derivatives are regarded as arbitrary and λ terms generally remain. When using conformal transformation, on the other hand, the terms including λ in the extra terms are cancelled, diminishing the magnitude of the components in $\underline{S}'$ and $\underline{D}'$. Since λ tends to be larger than μ for most of materials, the extra terms might be considerably decreased. Consequently, transformation of a space by using a conformal mapping equation results in small extra terms, which is significant for realization of transformation devices.

3.3.2 Proportion of Extra Terms

To check the findings in conformal transformation, the quantification of the influence of the extra terms are presented here. Through 3 examples in each of which two devices having the same function are designed by a general transformation and a conformal transformation, the distributions of the portion of the extra terms are visualized and numerical indications are given to show how the extra terms should be small enough to be ignored in the realization. Finally, wave propagations in the wave control devices designed with or without the extra terms are numerically simulated and compared.

3.3.2.1 Proportional Index and Distributions

A procedure to confirm the proportion of the extra terms when using conformal transformation is required. Thus, an index is established here to indicate how much portion the extra terms charge. On account of the relation between $\underline{S}'$ and $\underline{D}'$ presented in Eq. (3.25), the investigation on the proportion of $\underline{S}'$ tensor might be sufficient. For the 2D space, there are 4 components in the stress tensor shown in Eq. (3.35). The shear stress σ'_{xy} and σ'_{yx} are the same, i.e. the stress tensor is symmetric because the coordinate and the displacement are transformed by the same Jacobian tensor. Finally, the components to be inspected are

$$\sigma'_{xx} = C'_{1111}\cdot\varepsilon'_{xx} + C'_{1112}\cdot\varepsilon'_{xy} + C'_{1121}\cdot\varepsilon'_{yx} + C'_{1122}\cdot\varepsilon'_{yy} + S'_{111}u' + S'_{112}v' \quad (3.63a)$$

$$\sigma'_{yy} = C'_{2211}\cdot\varepsilon'_{xx} + C'_{2212}\cdot\varepsilon'_{xy} + C'_{2221}\cdot\varepsilon'_{yx} + C'_{2222}\cdot\varepsilon'_{yy} + S'_{221}u' + S'_{222}v' \quad (3.63b)$$

$$\sigma'_{xy} = C'_{1211}\cdot\varepsilon'_{xx} + C'_{1212}\cdot\varepsilon'_{xy} + C'_{1221}\cdot\varepsilon'_{yx} + C'_{1222}\cdot\varepsilon'_{yy} + S'_{121}u' + S'_{122}v' \quad (3.63c)$$

As more dominant the first four terms including the C'_{ijkl} s, it is easy to ignore the extra terms. If the C'_{ijkl} terms are sufficiently larger than the extra term, Eq. (3.21) can be treated

$$\nabla' \cdot \left(\underline{C}'(x') \nabla' \bar{u}' \right) = -\omega^2 \underline{\rho}'(x') \bar{u}' \tag{3.64}$$

where the extra terms are eliminated and the transformed governing equation has the same form with Eq. (3.14). To check this point, the following indices are established as

$$I_{s,xx} = \left[\frac{S'u'}{C'\nabla'u'} \right]_{xx} = \frac{S'_{111}u' + S'_{112}v'}{C'_{1111} \cdot \varepsilon'_{xx} + C'_{1112} \cdot \varepsilon'_{xy} + C'_{1121} \cdot \varepsilon'_{yx} + C'_{1122} \cdot \varepsilon'_{yy}} \tag{3.65a}$$

$$I_{s,xy} = \left[\frac{S'u'}{C'\nabla'u'} \right]_{xy} = \frac{S'_{121}u' + S'_{122}v'}{C'_{1211} \cdot \varepsilon'_{xx} + C'_{1212} \cdot \varepsilon'_{xy} + C'_{1221} \cdot \varepsilon'_{yx} + C'_{1222} \cdot \varepsilon'_{yy}} \tag{3.65b}$$

$$I_{s,yy} = \left[\frac{S'u'}{C'\nabla'u'} \right]_{yy} = \frac{S'_{221}u' + S'_{222}v'}{C'_{2211} \cdot \varepsilon'_{xx} + C'_{2212} \cdot \varepsilon'_{xy} + C'_{2221} \cdot \varepsilon'_{yx} + C'_{2222} \cdot \varepsilon'_{yy}} \tag{3.65c}$$

Each index shows the ratio of the extra terms to the pure stiffness terms inside the designed device. The indices are affected not only by the magnitude of the stiffness tensor and the extra $\underline{S}'$-related terms, but also by displacement and strain fields. Therefore, the main purpose of a device is important because it determines the mode and the direction of elastic waves and further, displacement and strain fields. To keep the performance of a device intact when ignoring the extra terms, the indices presented in Eq. (3.65) preferably have small values.

3.3.2.2 Example 1 : Cloakings

The first example to examine the distribution of the suggested indices is a cloaking. An elastic cloaking can prevent elastic waves from getting inside of it. The internal space of an ideal cloaking is then stress-free. There are numerous mapping equations to achieve this kind of devices. Among them, two mapping equations are chosen in order to compare the distribution of the indices; one is a general mapping equation and the other is a conformal one. By two different mappings, the original space shown in Fig. 3.2(a) is transformed to Fig. 3.2(b) and (c), respectively. A general mapping equation for the transformation to Fig. 3.2(b) is suggested in the cylindrical coordinate as Eq. (A.1), while a conformal one for the transformation to Fig. 3.2(c) is, using the complex coordinate z and w,

$$w = \frac{1}{2}\left(z \pm \sqrt{z^2 - 4a^2}\right) \tag{3.66}$$

where a decides the inner radius of the cloaking device. Unlike that Eq. (A.1) transforms the region of $r' < R_2$, Eq. (3.66) targets the entire space during the transformation. Therefore, the design domain should be limited to the same dimension as that of the general transformation. The outside area of the design domain in Fig. 3.2(c) is distorted, but the degree of deformation is quite small. Thus, the medium of the outside area can be regarded as the same as the original material.

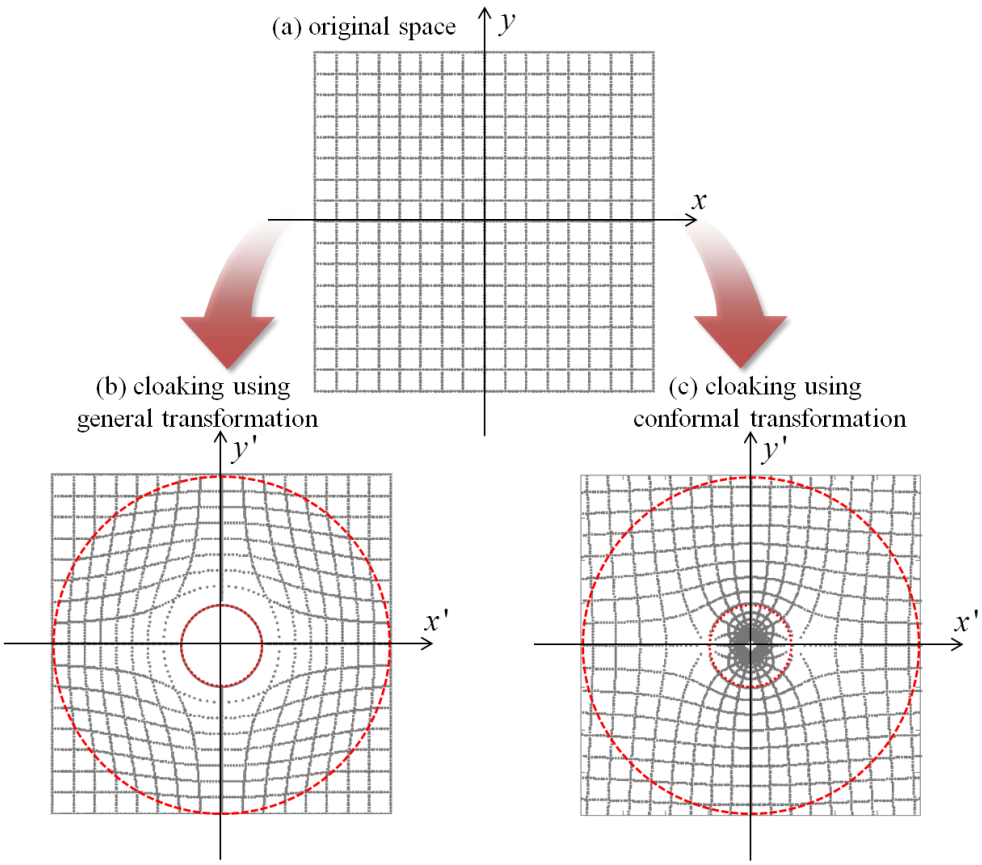

Fig. 3. 2 Two kinds of transformation for cloakings. (a) An original space is transformed by (b) a general transformation and (c) a conformal transformation for a cloaking device engineering. Waves in the x' direction propagate the same way in two different spaces.

Since waves propagate along the transformed line, the cloaking devices designed by the different mapping equations have the same function for the waves incident in the x' direction. The regions bounded by the inner and the outer circles in Fig. 3.2(b) and (c) are designated as the design domain of the devices. Their material properties like density

tensors, stiffness tensors, $\underline{S}'$ and $\underline{D}'$ tensors are calculated by Eq. (3.22) ~ Eq. (3.25) using each mapping equation. For these two devices, the distributions of the indices suggested in Eq. (3.65) are visualized in Fig. 3.3.

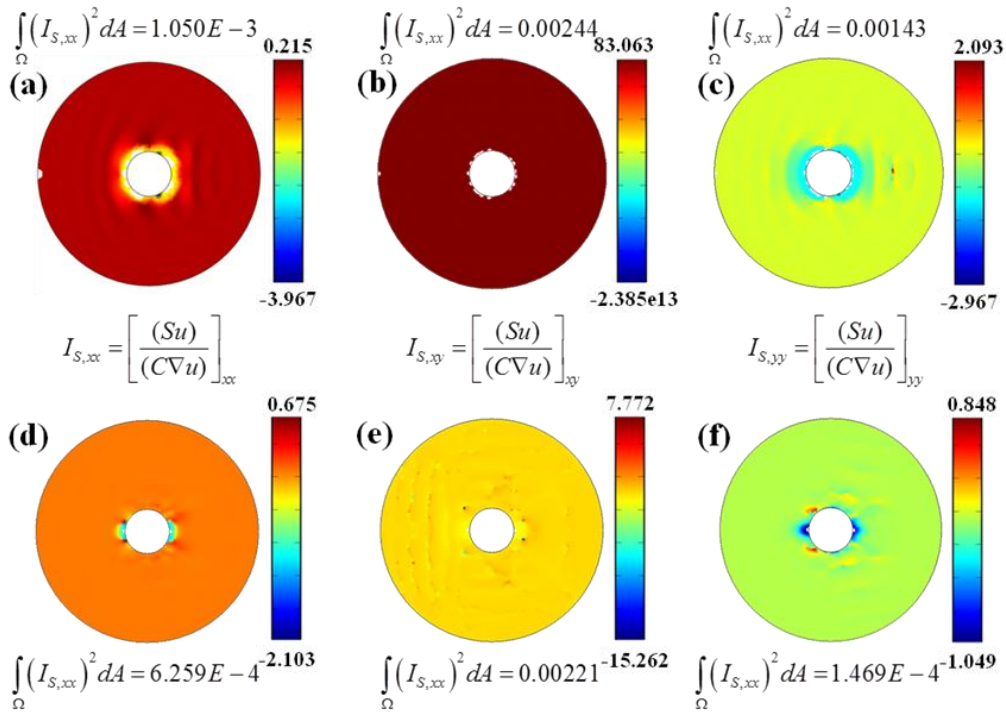

Fig. 3. 3 The distributions of $I_{S,xx}$, $I_{S,xy}$ and $I_{S,yy}$ in the cloaking designed by using (a, b, c) the general transformation and (d, e, f) the conformal transformation. The integrals of the square of each index are smaller in the conformal cloaking.

The maximum values of three indices are larger in the general transformation than the conformal transformation. Since the area of larger index within the design domain is also important, the integral of the square of each index are presented in Fig. 3.3. The integral

of each is also larger in the general transformation. It means that the extra terms of the general transformation are more difficult to ignore. In addition, it also means that the performances of the device engineered by the general transformation are more degraded when the extra terms are ignored. Therefore, conformal transformation is more advantageous for designing a cloaking device with the extra terms excluded.

The simulation results for elastic wave propagations in two kinds of cloakings are presented in Fig. 3.4. The original medium is aluminum in the 2D space. The inner and the outer radius of the cloakings are 0.02 m and 0.1 m, respectively. Therefore, a in Eq. (3.66) is 0.02 m. The material properties of the cloakings are calculated by using Eq. (3.22) ~ (3.25) based on the properties of aluminum. The 150 kHz dilatational plane waves which propagating direction is the same with the direction of particle movement are incident toward the cloaking. Figure 3.4(a) and (b) are the cloakings designed by using the general transformation with and without the extra terms, respectively. As can be seen, the wave fronts in Fig. 3.4(a) remain relatively intact after passing the cloaking, while the cloaking in Fig. 3.4(b) noticeably weakens the central part of the elastic waves. Compared with the ideal conformal cloaking designed including the extra terms shown in Fig. 3.4(c), on the other hand, the conformal cloaking designed without the extra terms keeps the wave fronts relatively undamaged after passing the cloaking as Fig. 3.4(d). These results are visualized through graphs in Fig. 3.4(e) and (f). Along the cross section $\overline{AB}$, the distributions of the displacements in the x' direction of Fig. 3.4(a) and (c) are plotted as blue and red dotted lines respectively in Fig. 3.4(e). The wave front of the

general cloaking without the extra terms is rather uneven relative to that with the extra terms. The distribution of (b) is similar to the case in which no cloaking is applied. In contrast, from Fig. 3.4(f) where the distributions of the displacements along $\overline{AB}$ of Fig. 3.4(b) and (d) are plotted, the performance of the conformal cloaking has no change even if the extra terms are excluded. Although there are the peaks near the outer radius of the cloaking, the distribution of the conformal cloaking is more even than the general one. Therefore, it is possible to detect a wave of a considerable amplitude anywhere right behind the conformal cloaking.

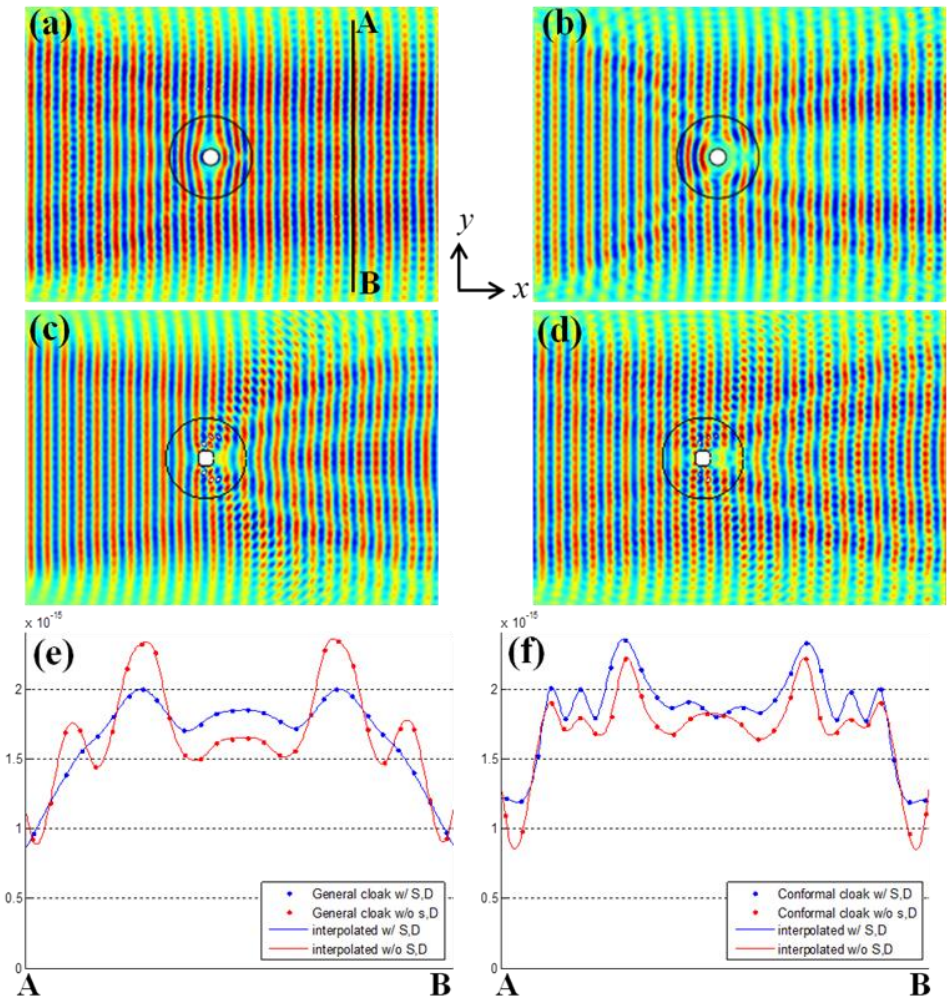

Fig. 3. 4 Wave propagation in (a, b) the general cloaking and (c, d) the conformal cloaking. (a) and (c) include the extra terms, while (b) and (d) are simulated without the extra terms. The distributions of the x' displacements on $\overline{AB}$ are presented for (e) the general cloaking and (f) the conformal cloaking.

3.3.2.3 Example 2 : Wave Collimators

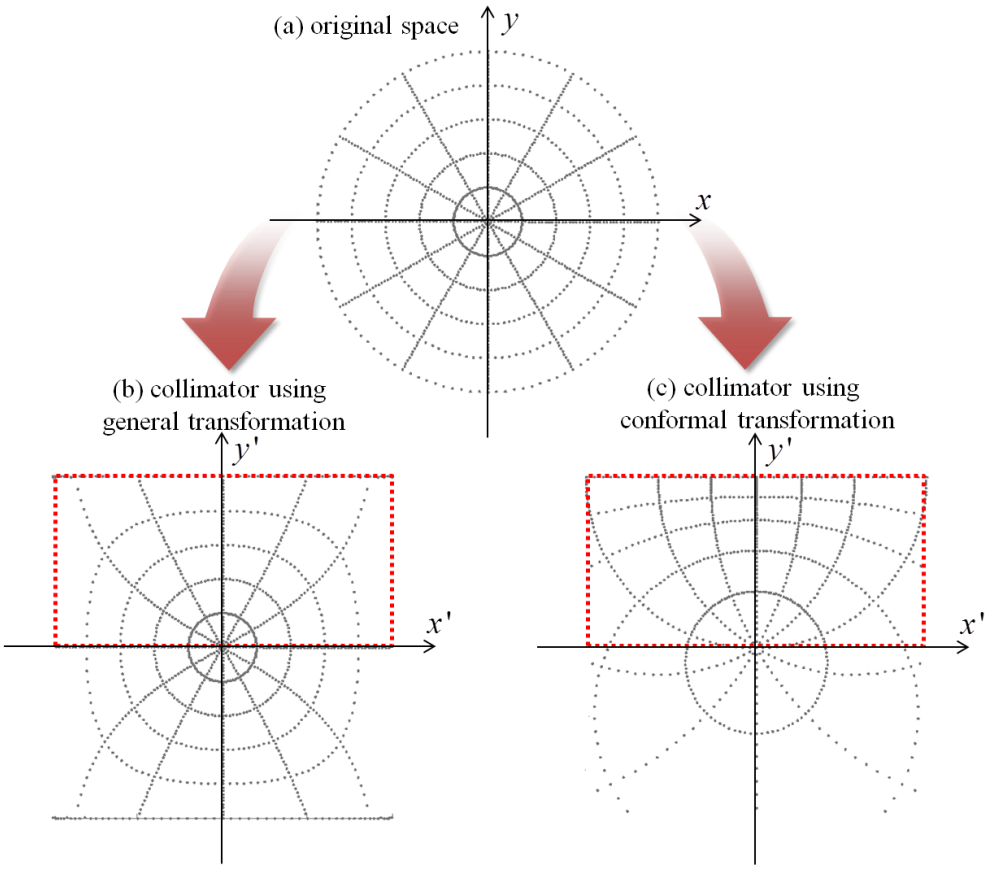

Fig. 3. 5 Two kinds of transformation for wave collimators. (a) An original space in the cylindrical coordinate system is transformed to the design domains for wave collimators by (b) a general transformation and (c) a conformal transformation. The curvilinear wave fronts of the waves incident from the point source at the origin are flattened when escaping from the devices.

The next example to prove the superiority of conformal transformation in ignoring the

extra terms in transformation elasticity is a wave collimator. A wave collimator means a device that makes the directions of waves become more aligned in a specific direction, especially parallel in this case. Two different ways of transformation for wave collimators are shown in Fig. 3.5. The general mapping equation for the transformation from Fig. 3.5(a) to Fig. 3.5(b) is

$$x' = \frac{w}{a} x, \qquad y' = \frac{ly}{\sqrt{a^2 - x^2}} \tag{3.67}$$

where a, w and l are the radius of the design domain in the original space, half the width and half the height of the design domain in the transformed space. This mapping has been used earlier in Ref. [33]. Of the transformed design domain, the upper half rectangular region is used for the actual device domain, which size is $2w \times l$ and $a = w = l = 1$. Meanwhile, the conformal mapping equation for the transformation to Fig. 3.5(c) is

$$w = ip \frac{z - ip}{z + ip} \tag{3.68}$$

where p is a scale parameter for determining the geometry and has a value of 1 in this case so that Eq. (3.68) results in the design domain of the similar dimension with Eq. (3.67). The same region with Fig. 3.5(b) is selectively used for the device. By using the devices, the waves occurred at the origin point with circular wave fronts are gradually flattened as progressing toward the top of the devices.

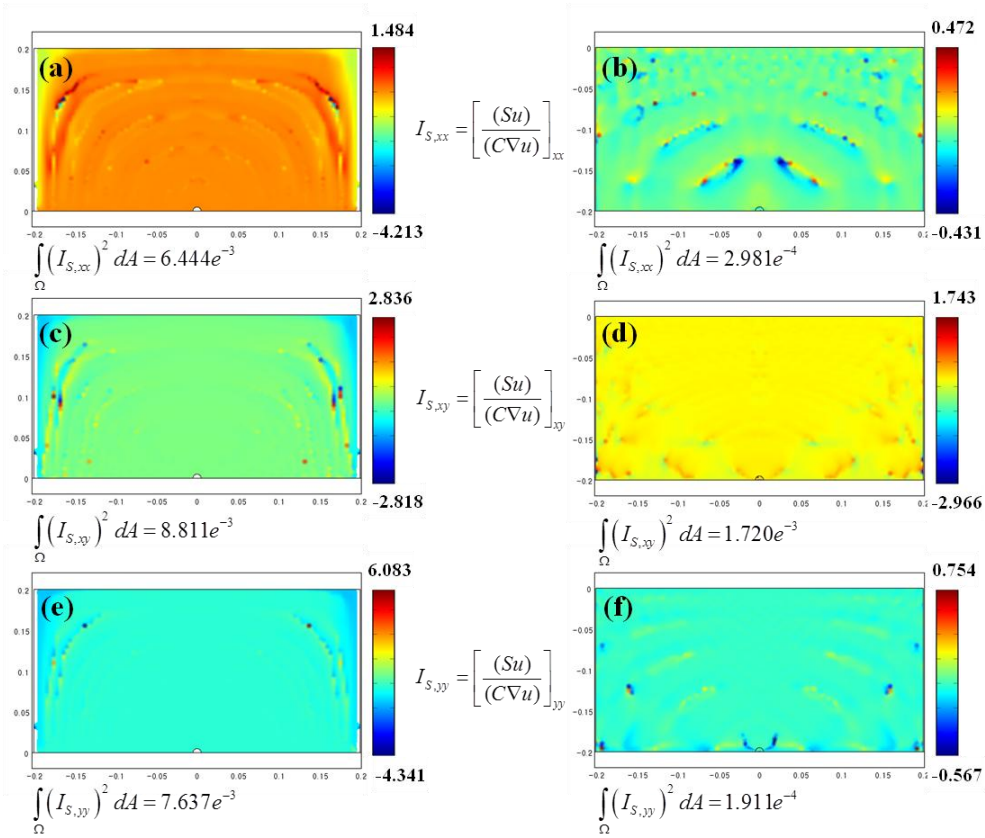

Fig. 3. 6 The distributions of $I_{S,xx}$, $I_{S,xy}$ and $I_{S,yy}$ in the wave collimators designed by (a, c, e) the general transformation and (b, d, f) the conformal transformation. The integrals of the square of each index are smaller in the conformal collimator.

Just as in the cloaking example, the distributions of three indices are plotted in Fig. 3.6. In these cases, 150 kHz dilatational harmonic waves are incident from the point source at the bottom center of the devices. Aluminum is used as an original medium. There are some non-uniform points due to the maximum and the minimum amplitudes of the

harmonic waves, but the tendency are similar at any phase in a cycle. The integrals of the square of each index have larger values in the case of the general transformation. It can be seen also in this example that the proportions of the extra terms are higher when using the general transformation.

Figure 3.7 shows wave propagations in the wave collimators. The displacements in the y' direction in the collimator designed by using the general transformation with and without the extra terms are plotted in Fig. 3.7(a) and (c), respectively. According to the Fig. 3.7(e) where the displacements in the general collimators are plotted along the cross section $\overline{AB}$, there is a slight difference between the distributions of the collimators with and without $\underline{S}'$ and $\underline{D}'$. In the case of the collimator transformed by the conformal mapping equation, one with the extra terms in Fig. 3.7(b) and the other without the extra terms in Fig. 3.7(d) looks the same. The comparison of the distributions of the displacements in Fig. 3.7(f) proves that they match perfectly with each other. In other words, the extra terms have little impact on the performances of the conformal devices.

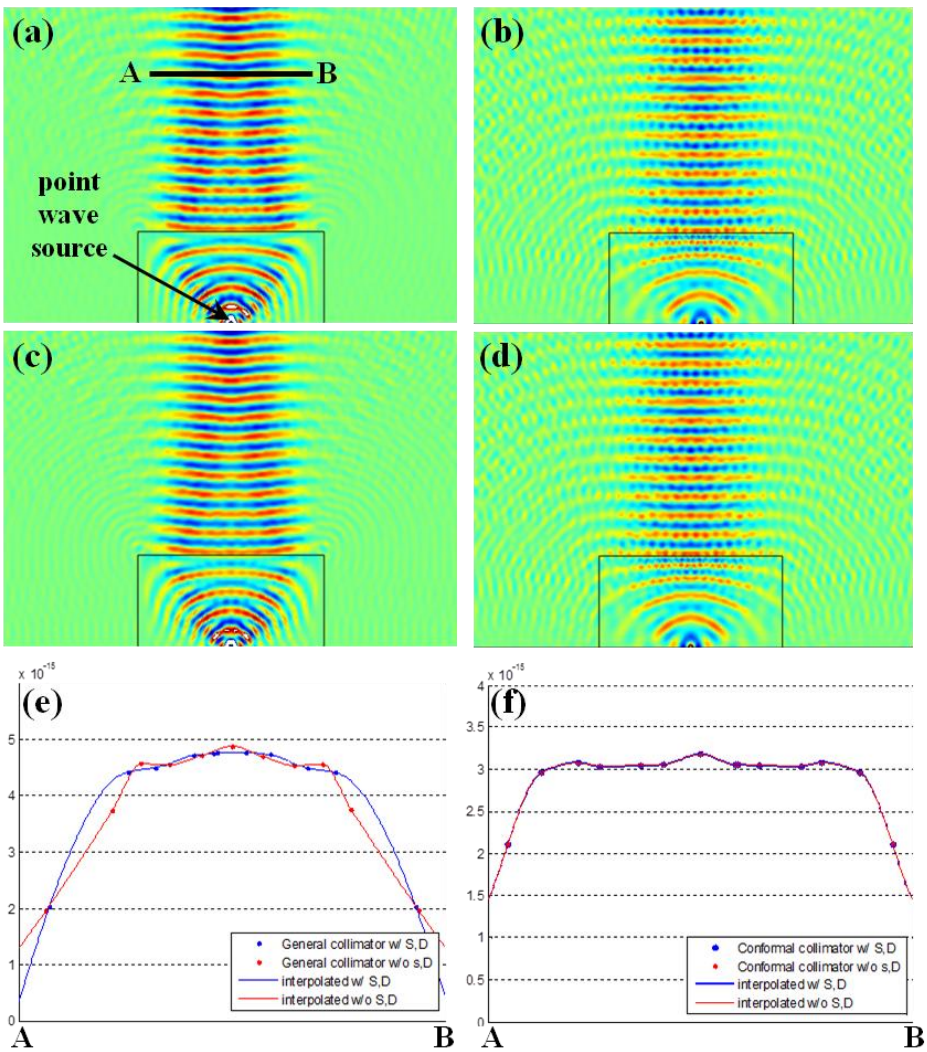

Fig. 3. 7 Wave propagation in the collimators designed by using (a, c) the general transformation and (b, d) the conformal transformation. (a) and (b) includes the extra terms while (c) and (d) do not. The distributions of the displacements in the y' direction are plotted for (e) the general one and (b) the conformal one.

3.3.2.4 Example 3 : Wave Bend Guiders

The last example is wave bend guiders which changes the direction of wave propagations, especially rotates the direction of path by 90° counter-clockwise in this example. By using these devices, waves incident downwards to the top of the device are bent by 90° and propagate horizontally after passing the device and vice versa.

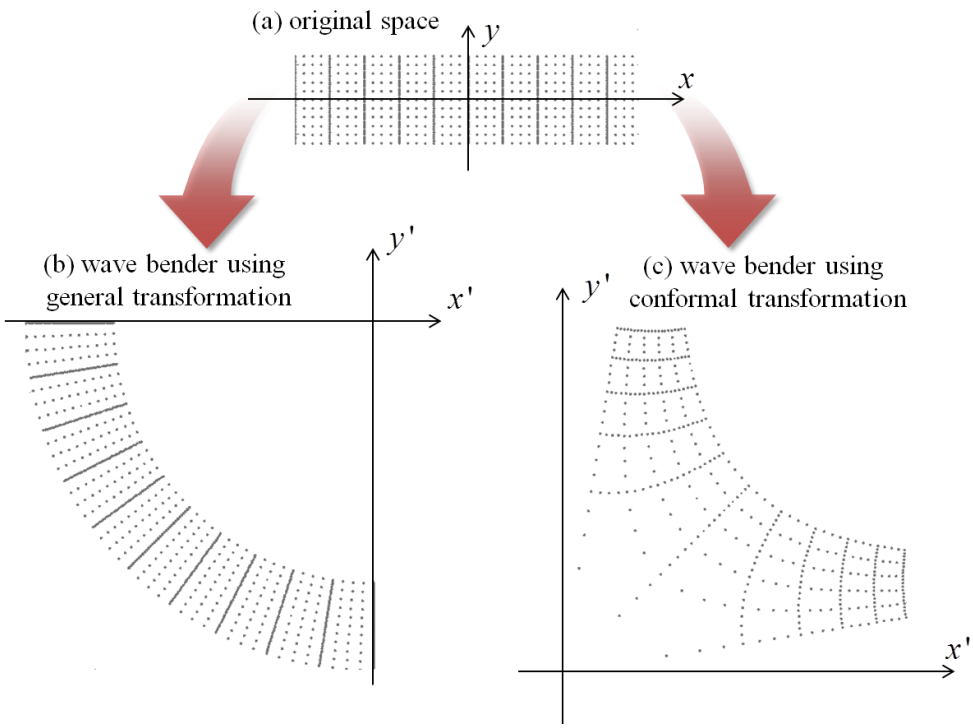

Fig. 3. 8 Two kinds of transformation for wave bend guiders. (a) An original space in a rectangular form is transformed to a curvilinear space in which waves propagate along the curvilinear path by (a) a general mapping equation and (b) a conformal mapping equation.

The design domain in the original space in Fig. 3.8(a) are the area of $-1 \le x \le 1$ and $-0.25 \le y \le 0.25$. In this space, waves propagate along the x direction. By the general mapping equation

$$\begin{aligned} r' &= -\frac{1}{2}y + 0.875 \\ \theta' &= \frac{\pi}{4}x + \frac{5\pi}{4} \end{aligned} \tag{3.69}$$

the design domain is transformed to a quarter of a perfect circle in Fig. 3.8(b). The inner and the outer radius of the transformed design domain are 0.75 and 1, respectively. On the other hand, the conformal mapping equation for Fig. 3.8(c) is

$$w = \exp\left(i\frac{\pi}{20}\right)z^{0.4} \tag{3.70}$$

The exponents of Eq. (3.70) determine the form and the angle of the wave bend guider. Of many conformal mapping equations to make a wave bend guider, Eq. (3.70) is chosen because it results in the design domain of a similar size Fig. 3.8(b) and proper performances. Due to the characteristic of conformal transformation, the inlet and the outlet of the wave bend guider are not perfectly flat unlike the counterpart of the general transofrmation. However, the bend guider engineered by Eq. (3.70) is fully functional as much as the counterpart designed by Eq. (3.69).

The distributions of three indices of each wave bend guider and the integrals of the square of indices are presented in Fig. 3.9. Like the previous examples, the device designed by the conformal transformation has larger integral values than the general one.

Nevertheless, the integrals of both wave bend guiders have significantly small dimensions compared with the previous examples. Thus, considerable performances are expected for both devices even if the extra terms are excluded.

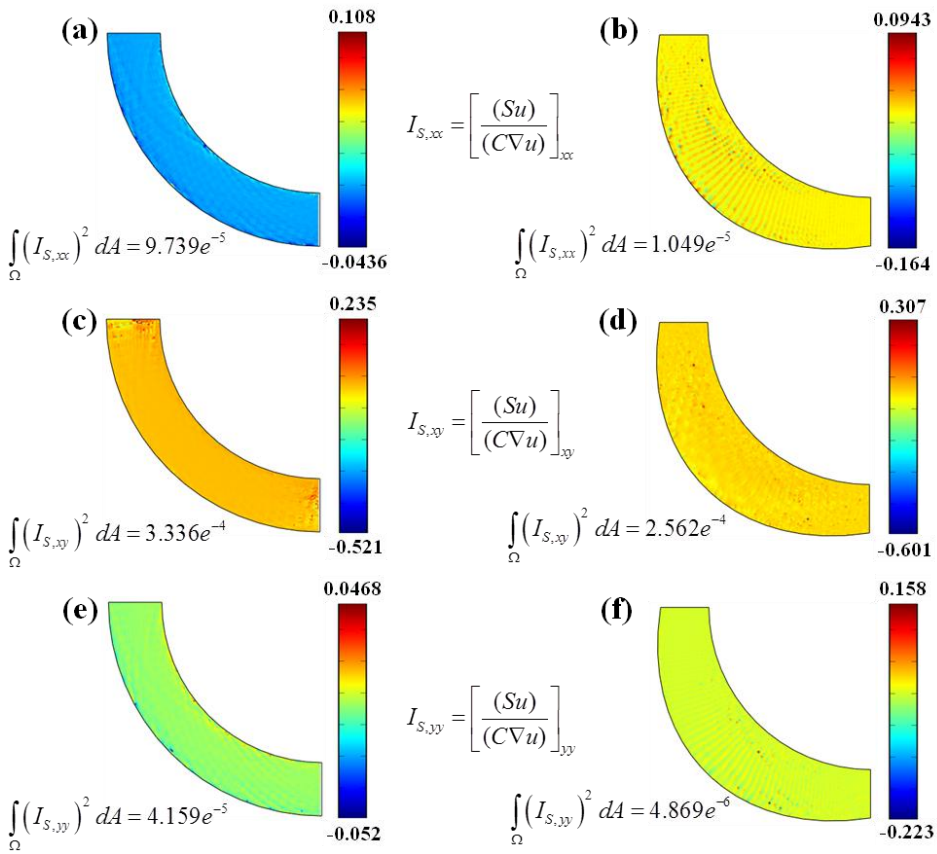

Fig. 3. 9 The distributions of $I_{S,xx}$, $I_{S,xy}$ and $I_{S,yy}$ in the wave bend guider designed by (a, c, e) the general transformation and (b, d, f) the conformal transformation. The integrals of the square of each index in both cases are small enough to be ignored in the realization process.

According to Fig. 3.10, there is no difference in elastic wave propagation in the wave bend guiders between the cases with or without the extra terms. Therefore, the extra terms are considered not to affect the performance of the wave bend guiders designed by both transformations.

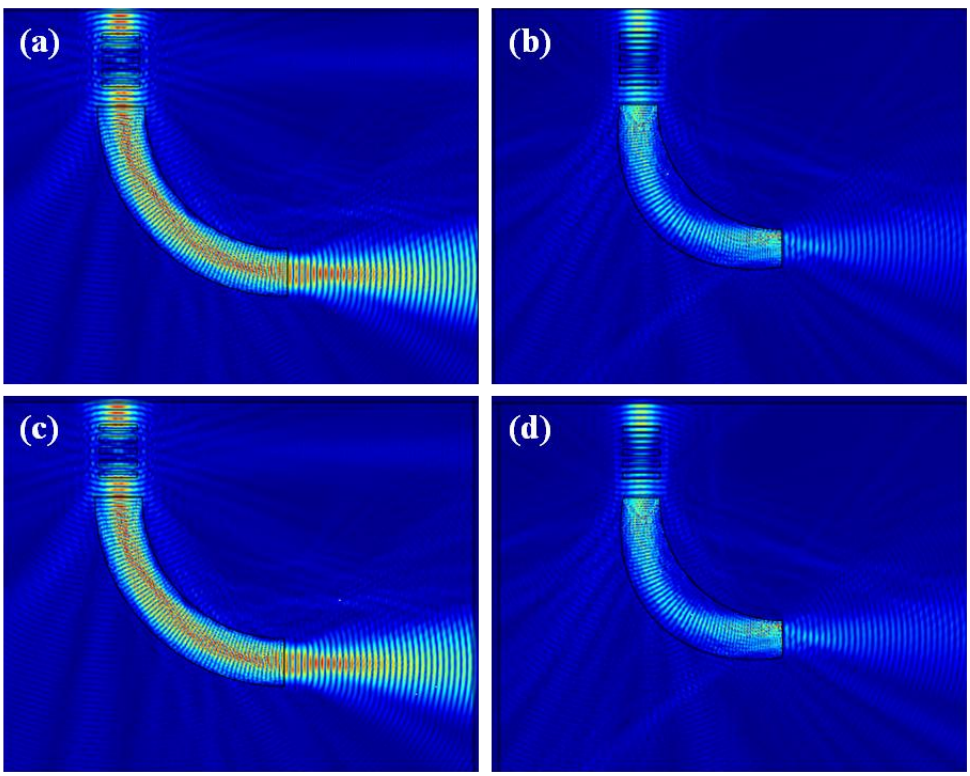

Fig. 3. 10 Wave propagation in the wave bend guiders designed by (a) the general mapping equation including $\underline{S}'$ and $\underline{D}'$ (b) the conformal mapping equation including $\underline{S}'$ and $\underline{D}'$ (c) the general mapping equation excluding $\underline{S}'$ and $\underline{D}'$ (b) the conformal mapping equation excluding $\underline{S}'$ and $\underline{D}'$.

3.3.3 Zero extra terms

How much the extra terms $\underline{S}'$ and $\underline{D}'$ in transformation elasticity affect in the governing equations and how to reduce them are discussed so far. Especially in conformal transformation, the extra terms are governed only by two components as presented in Eq. (3.60) and Eq. (3.61). Although they contribute to reduction of the proportion of unrealizable terms, it is practically ideal for them to be zero. Then the governing equation is free from the extra terms and performances of a device in reality are as designed. Therefore, it is quite meaningful to find mapping equations that make extra terms zero.

Two terms s'_{111} and s'_{112} consists of μ and geometric variables derived from a conformal mapping equation. In order to maintain the stability of a structure, it is desirable for μ to have a non-zero value. Then the terms in the brackets in Eq. (3.60) and Eq. (3.61) should be zero.

$$\left(\alpha^2 - \beta^2\right)\frac{\partial^2 x'}{\partial x^2} + 2\alpha\beta\frac{\partial^2 y'}{\partial y^2} = 0 \tag{3.71}$$

$$2\alpha\beta\frac{\partial^2 x'}{\partial x^2} - \left(\alpha^2 - \beta^2\right)\frac{\partial^2 y'}{\partial y^2} = 0 \tag{3.72}$$

There are two solutions to satisfy Eq. (3.71) and Eq. (3.72):

$$\alpha = \pm i\beta \tag{3.73a}$$

$$\frac{\partial^2 x'}{\partial x^2} = \frac{\partial^2 y'}{\partial y^2} = 0 \tag{3.73b}$$

Of two solutions, Eq. (3.73a) is invalid because α and β are set to be real. Thus Eq. (3.73b) should be satisfied in order to make s'_{111} and s'_{112} zero. From the relations Eq. (3.45) and Eq. (3.46), it can be drawn that the 2nd order derivatives of a conformal mapping equation should be zero. Then, for $\frac{\partial x'}{\partial x}$ and $\frac{\partial y'}{\partial y}$ to satisfy the Cauchy-Riemann condition presented in Eq. (3.42a), the following estimations are possible:

$$\frac{\partial x'}{\partial x} = f_1(y) + c_1 = \alpha \tag{3.74a}$$

$$\frac{\partial y'}{\partial y} = f_2(x) + c_2 = \alpha \tag{3.74b}$$

where c_1 and c_2 are constants of integration, and one of the 1st order derivatives α should be constant, not a function of coordinates. Then the following is concluded.

$$f_1(y) = f_2(x) = 0 \tag{3.75a}$$

$$c_1 = c_2 = \alpha \tag{3.75b}$$

A transformed coordinate is expressed with an original coordinate as

$$x' = \alpha x + g_1(y) + c_3 \tag{3.76a}$$

$$y' = \alpha y + g_2(x) + c_4 \tag{3.76b}$$

where c_3 and c_4 are constants of integration. Since Eq. (3.76) should satisfy the Cauchy-Reimann condition shown in Eq. (3.42b),

$$\frac{\partial x'}{\partial y} = g_1'(y) = \beta \tag{3.77a}$$

$$\frac{\partial y'}{\partial x} = g_2'(x) = -\beta \tag{3.77b}$$

and from these,

$$g_1(y) = \beta y \tag{3.78a}$$

$$g_2(x) = -\beta x \tag{3.78b}$$

are drawn. By substituting Eq. (3.78) to Eq. (3.76), the conformal mapping equation is completed as

$$x' = \alpha x + \beta y + c_3 \tag{3.79a}$$

$$y' = \alpha y - \beta x + c_4 \tag{3.79b}$$

To represent the mapping equation in z and w,

$$\begin{aligned} w &= x' + iy' = \alpha x + \beta y + c_3 + i\left(\alpha y - \beta x + c_4\right) \\ &= \alpha\left(x + iy\right) - i\beta\left(x + iy\right) + \left(c_3 + ic_4\right) \\ &= \alpha z - i\beta z + \left(c_3 + ic_4\right) \end{aligned} \tag{3.80}$$

is obtained, where it should be noted that α, β, c_3 and c_4 are constant. Figure 3.11 shows several examples of the derived conformal mapping equation. As can be seen, the transformed spaces allow waves straight paths. This conclusion can be inferred intuitively from the fact that all the 2nd order derivatives of a mapping equation should be zero. This means all distorted grid lines should be linear in the transformed space and thus, waves move along straight paths as it do in the original space. Therefore, wave controlling devices designed by Eq. (3.80) are practically useless. However, it is worth

demonstrating this conclusion by analytically deriving Eq. (3.80) and its transformation results.

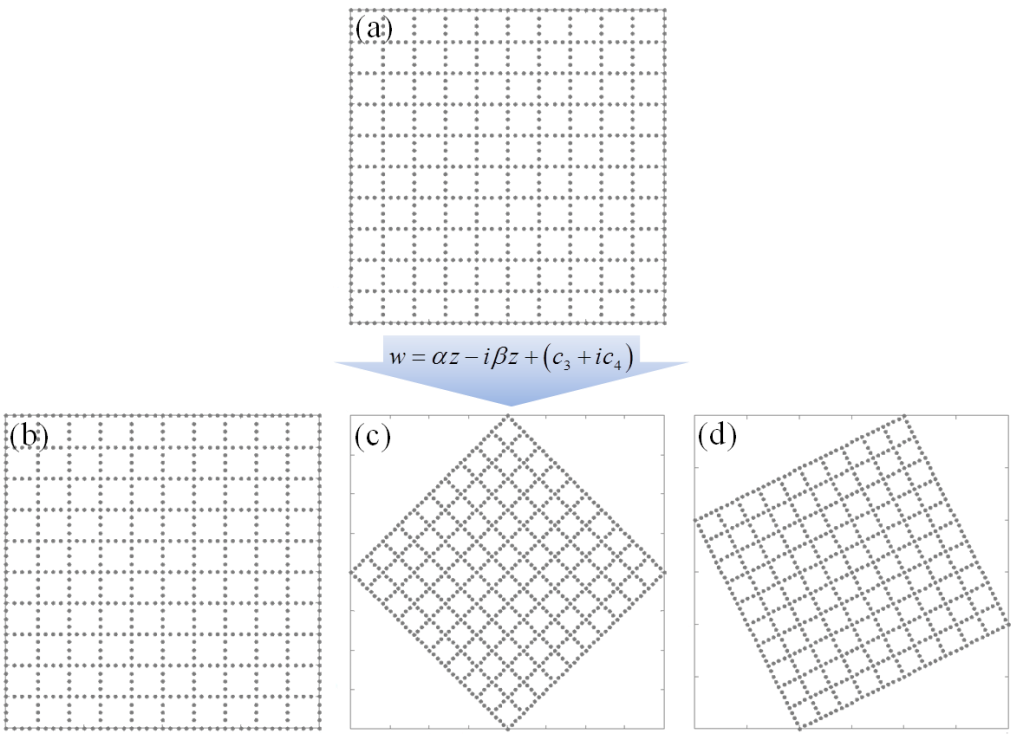

Fig. 3. 11 Examples of conformal transformations having no extra term. (a) An original space where coordinates are denoted by $z = x + iy$ is transformed by a conformal mapping equation $w = \alpha z - i\beta z + (c_3 + ic_4)$ to the transformed space where coordinates are denoted by w (b) $\alpha = 1, \beta = c_3 = c_4 = 0$, (c) $\alpha = 1, \beta = 1, c_3 = c_4 = 0$ and (d) $\alpha = 1, \beta = 2, c_3 = c_4 = 0$

Chapter 4.

Realization of Elastic Cloaking

by Using Conformal Transformation

4.1 Chapter Overview

In this chapter, a specific process to design a conformal elastic cloaking by using Eq. (3.66) is presented based on the previous chapters. The conformal cloaking is designed without the extra terms because they are minimized by using a conformal transformation. Besides, the engineering of the conformal cloaking is easy since the density and the stiffness tensor is further simplified due to the characteristics of conformal transformation. The relationship of material properties before and after the conformal transformation is presented as a design variable. Then, phononic crystal (PCs), an artificially designed material is suggested to control the design variable. A detailed method for designing the conformal cloaking by combining a variety of kinds of PC is presented. Finally, the performances of the cloaking s experimentally confirmed with a set of transducers developed and manufactured by our own laboratory.

4.2 Wave Velocity in Elastic Cloakings

Thanks to the characteristics of conformal transformation and the frequency range used

for elastic waves are ultrasonic (from 20 kHz to 2 MHz), the density is assumed as

$$\rho' = \rho + \frac{4\mu}{\det J}\frac{1}{(i\omega)^2}\left(\left(\frac{\partial^2 x'}{\partial x \partial y}\right)^2 + \left(\frac{\partial^2 y'}{\partial x \partial y}\right)^2\right) \simeq \rho \tag{4.1}$$

and the components of the extra terms are assumed to be ignorable according to 3.3.2.

$$s'_{111} = \frac{2\mu}{\det J}\left[\left(\alpha^2 - \beta^2\right)\frac{\partial^2 x'}{\partial x^2} + 2\alpha\beta\frac{\partial^2 y'}{\partial y^2}\right] \simeq 0 \tag{4.2}$$

$$s'_{112} = \frac{2\mu}{\det J}\left[2\alpha\beta\frac{\partial^2 x'}{\partial x^2} - \left(\alpha^2 - \beta^2\right)\frac{\partial^2 y'}{\partial y^2}\right] \simeq 0 \tag{4.3}$$

Consequently, the elastodynamic governing equation can be regarded as Eq. (3.64). It is in the similar form with the EM/acoustic governing equation in the transformed space, and it can be considered that the form invariance is kept after the transformation. Then the relation between elastic wave speeds in the original space and the transformed space can be obtained as

$$v'(x') = \sqrt{\det J(x')} \cdot v \tag{4.4a}$$

$$\frac{v'(x')}{v} = \sqrt{\det J(x')} \tag{4.4b}$$

where v is the wave speed in an the original isotropic medium. It is necessary to adjust the wave speed within the cloaking device to satisfy this relation.

The distribution of $\sqrt{\det J}$ is presented in Fig. 3.12 when the inner and the outer radii of the cloaking are 0.02 m and 0.1 m, respectively. It has a value close to 1 in most region, but small or extremely large values are distributed near the inner radius. It means

that , since this distribution is identical to the distribution of the ratio of wave speed, elastic waves propagate at the same rate with the original medium at most part of the cloaking, while they change their wave speeds and directions dramatically near the inner radius.

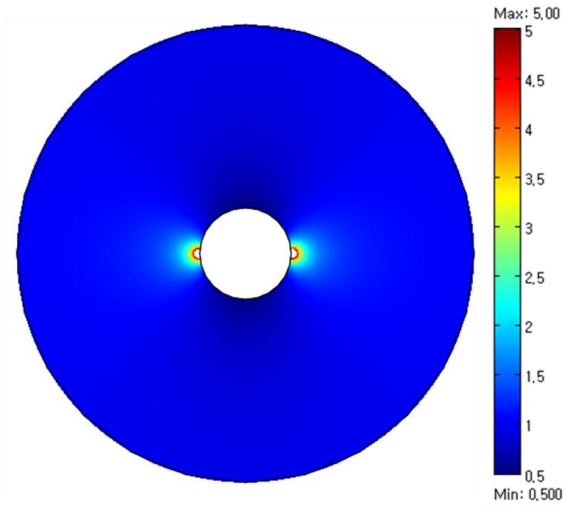

Fig. 4. 1 The distribution of $\sqrt{\det J}$ in the design domain of the conformal cloaking

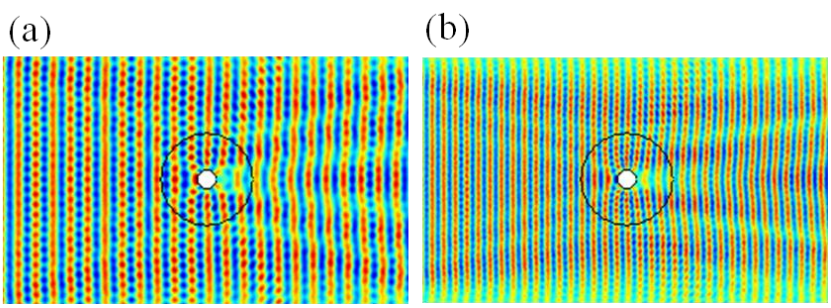

Fig. 4. 2 Wave propagation in a conformal cloaking with material properties controlled only by $\sqrt{\det J}$ at a frequency of (a) 100 kHz and (b) 150 kHz.

Numerical simulations are conducted to examine elastic wave propagation in the conformal cloaking which material properties are controlled only by the distribution of $\sqrt{\det J}$. This conformal cloaking is frequency-independent and broadband because $\sqrt{\det J}$ is not a function of frequency. Figure 4.2 shows that time-harmonic elastic waves maintain their wave front above a certain level after passing the cloaking. In this case, a 3t Cu plate is employed as an original medium and the cloaking is embedded in the plate around the hole.

4.3 Engineering of Elastic Cloaking Composed of Phononic Crystals

Based on the simulation results showing the reliability of the conformal cloaking designed only by the distribution of $\sqrt{\det J}$ in Fig. 4.2, a specific methodology for designing the cloaking is proposed here. PC is used as a key to finely adjusting the wave speed in the Cu plate. PC is an artificial structure that is formed by periodic variation of acoustic/elastic materials [8, 67-76]. The periodic variation is typically an arrangement of hole or other inclusions in a host material such as a periodically drilled aluminum or a set of periodically arranged cylinders made of iron in water. The characteristics of wave propagation in PCs vary depending on the period, the direction, forms and material properties of inclusions.

In this thesis, a 3t Cu plate is chosen as the original material and thus, the host material of PCs is Cu. The specification of the unit cell of PC is shown in Fig. 4.3. Two sides of

the square unit cell are 5 mm as can be seen in Fig. 4.3(a), which is the same as the lattice constant of the square lattice. Copper as the host material guarantees the stability of the cloaking by firmly supporting the structure. Although a pure Cu is isotropic, PCs are generally anisotropic due to the hole or the inclusion. The Brillouin zone corresponding to the unit cell is shown in Fig. 4.3(b) to indicate the behavior of waves depending on the wave number along each direction. Figure 4.3(c) is the band structure of the Cu PC with a hole of radius 0.001 m. It shows the permitted frequency along the boundaries of the Brillouin zone. Each band corresponds to a certain mode of elastic waves and the red line in Fig. 4.3(c) is the band of S0 wave. The band structure changes as the type and the radius of the inclusion change. The group velocity of a wave at a specific frequency is calculated from the band structure using

$$v'_{PC} = \frac{\partial \omega}{\partial k} = 2\pi \frac{\partial f}{\partial k} \tag{4.5}$$

where ω, f and k indicate the angular frequency, the frequency and the wave number. The wave number is calculated with the lattice constant and the location on the boundaries of the Brillouin zone.

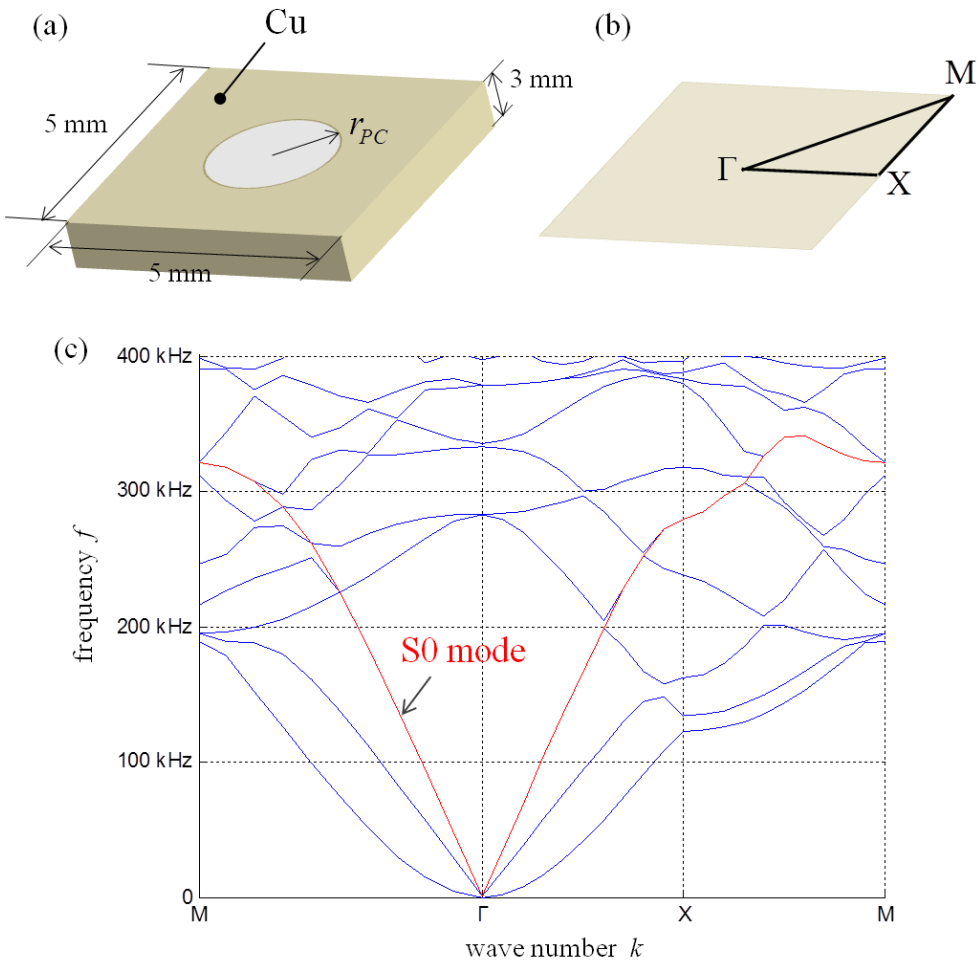

Fig. 4. 3 (a) The unit cell of the Cu PC arranged in the square lattice and (b) the Brillouin zone of a square lattice to present the directions inside the unit cell. (c) the band structure of the Cu unit cell with a hole of radius 0.001m. The red line is for S0 waves.

The wave speed in the unit cell is controlled by the radius of the inclusion r_{PC}. By combining various PCs, a wave in the structure can change its velocity and direction.

This kind of structure is called GRadient-INdex (GRIN) PC [77-80]. The filling fraction of the inclusion in the unit cell is defined as

$$ff = \frac{\text{the area of the inclusion}}{\text{the area of the unit cell}} = \frac{r_{PC}^2 \pi}{0.005^2} \tag{4.6}$$

By changing the inclusion and r_{PC}, it is possible to control the wave speed in the cloaking.

S0 waves are employed, which propagating direction in a guided structure is the same with the direction of particle movement. The S0 wave velocity v in a 3t Cu plate is 3759.4 m/s at the target frequency 100 kHz. According to Fig. 4.1, v' is larger than v in some parts, i.e. $\sqrt{\det J} > 1$, and in the rest, smaller than v. Once the type of the inclusion is determined, the wave speed in the Cu plate monotonously increases or decreases. Therefore, the inclusions for the area of $\sqrt{\det J} > 1$ and $\sqrt{\det J} < 1$ should be different and be designed separately. For this reason, the distributions of $\sqrt{\det J}$ of two parts are separately presented in Fig. 4.4. From this figure, it is possible to know the boundary lines of two parts.

For the region of $\sqrt{\det J} < 1$ shown in Fig. 4.4(a), the inclusion must be selected as a material in which it is hard for elastic waves to propagate. In other words, the inclusions should be able to restrain the wave propagation. Thus, the material used in this region is a drilled Cu PC because it is essentially blocked for elastic waves to propagate in the air in

the hole. As the radius of a hole becomes larger, the wave speed in the cloaking becomes smaller. On the other hand, the region of $\sqrt{\det J} > 1$ shown in Fig. 4.4(b) requires a material capable of promoting the progress of elastic waves. Therefore, silicon is chosen for the inclusion of Cu PCs, in which elastic wave velocity is much higher than v.

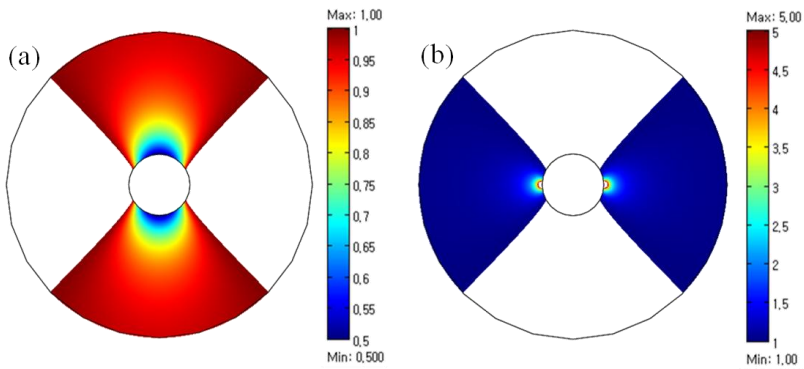

Fig. 4. 4 The distribution of $\sqrt{\det J}$ within the region of (a) $\sqrt{\det J}$ smaller than 1 and (b) larger than 1

To examine how the wave speed in the Cu PCs changes according to the change of r_{PC}, the unit cells of various inclusion sizes are analyzed numerically by COMSOL Multiphysics. The results are shown in Table 4.1 and Table 4.2. Since material properties change depending on the direction, as mentioned before, wave speeds are obtained in two different directions, ΓX and ΓM. The effective wave speed of a certain PC, v'_{eff} is calculated as an average value of two speeds [79]. By using the averaged wave speed, the ratio of v'_{PC} and v are found, which means $\sqrt{\det J}$.

Table 4. 1 S0 wave velocity in drilled PCs in Cu plates at 100 kHz

r_{PC} (ff)	$v'_{\Gamma X}$	$v'_{\Gamma M}$	v'_{eff}	v'_{eff}/v_{Cu}
0.1 mm (0.13%)	3755.0	3752.6	3753.80	0.9985
0.2 mm (0.50%)	3741.4	3738.9	3740.15	0.9949
0.3 mm (1.13%)	3718.4	3715.4	3716.90	0.9887
0.4 mm (2.01%)	3686.1	3681.7	3683.90	0.9799
0.5 mm (3.14%)	3645.1	3637.5	3641.30	0.9686
0.6 mm (4.52%)	3595.8	3582.6	3589.20	0.9547
0.7 mm (6.16%)	3539.6	3517.8	3528.70	0.9386
0.8 mm (8.04%)	3477.6	3443.6	3460.60	0.9205
0.9 mm (10.18%)	3411.2	3361.4	3386.30	0.9008
1.0 mm (12.57%)	3341.8	3272.8	3307.30	0.8797
1.1 mm (15.21%)	3270.3	3179.1	3224.70	0.8578
1.2 mm (18.10%)	3197.6	3081.7	3139.65	0.8351
1.3 mm (21.24%)	3124.4	2981.8	3053.10	0.8121
1.4 mm (24.63%)	3051.1	2880.4	2965.75	0.7889
1.5 mm (28.27%)	2977.6	2777.8	2877.70	0.7655
1.6 mm (32.17%)	2903.6	2671.0	2787.30	0.7414
1.7 mm (36.32%)	2828.3	2562.6	2695.45	0.7170
1.8 mm (40.72%)	2750.3	2452.1	2601.20	0.6919
1.9 mm (45.36%)	2664.0	2337.6	2500.80	0.6652
2.0 mm (50.27%)	2567.0	2215.8	2391.40	0.6361
2.1 mm (55.44%)	2453.4	2080.6	2267.00	0.6030
2.2 mm (60.84%)	2309.4	1920.8	2115.10	0.5626
2.3 mm (66.50%)	2100.2	1699.8	1900.00	0.5054
2.4 mm (50.27%)	2567.0	2215.8	2391.40	0.6361

Table 4. 2 S0 wave velocity in Si-included PCs in Cu plates at 100 kHz

r_{PC} (ff)	$v'_{\Gamma X}$	$v'_{\Gamma M}$	v'_{eff}	v'_{eff}/v_{Cu}
0.1 mm (0.13%)	3761.6	3759.2	3759.20	0.9999
0.2 mm (0.50%)	3768.0	3765.5	3766.75	1.0020
0.3 mm (1.13%)	3778.5	3776.1	3777.30	1.0048
0.4 mm (2.01%)	3793.3	3790.8	3792.05	1.0087
0.5 mm (3.14%)	3812.1	3809.6	3810.85	1.0137
0.6 mm (4.52%)	3835.3	3832.7	3834.00	1.0198
0.7 mm (6.16%)	3862.9	3860.2	3861.55	1.0272
0.8 mm (8.04%)	3895.1	3892.3	3893.70	1.0357
0.9 mm (10.18%)	3932.2	3929.4	3930.80	1.0456
1.0 mm (12.57%)	3974.7	3971.7	3973.20	1.0569
1.1 mm (15.21%)	4022.5	4019.9	4021.20	1.0696
1.2 mm (18.10%)	4076.5	4074.4	4075.45	1.0841
1.3 mm (21.24%)	4137.5	4135.9	4136.70	1.1004
1.4 mm (24.63%)	4206.3	4205.4	4205.85	1.1188
1.5 mm (28.27%)	4283.9	4283.9	4283.90	1.1395
1.6 mm (32.17%)	4371.7	4372.6	4372.15	1.1630
1.7 mm (36.32%)	4471.0	4473.2	4472.10	1.1896
1.8 mm (40.72%)	4583.9	4587.4	4585.65	1.2198
1.9 mm (45.36%)	4712.5	4717.1	4714.80	1.2541
2.0 mm (50.27%)	4859.9	4863.3	4861.60	1.2932
2.1 mm(55.42%)	5029.6	5031.5	5030.55	1.3381
2.2 mm(60.82%)	5226.3	5226.3	5226.30	1.3902
2.3 mm(66.48%)	5456.2	5453.9	5455.05	1.4510
2.4 mm(72.38%)	5727.4	5722.3	5724.85	1.5228

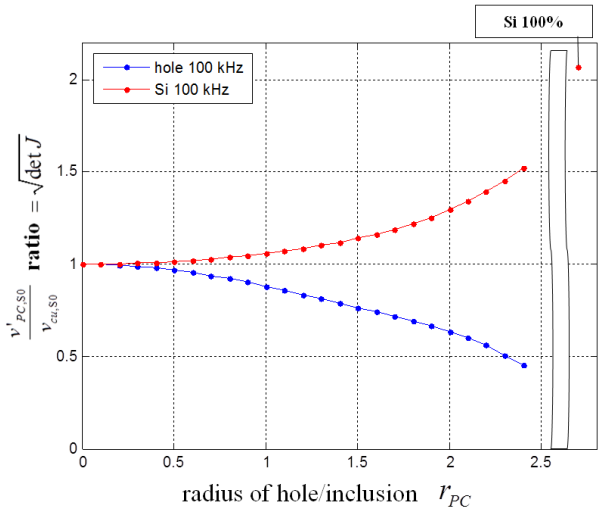

Fig. 4. 5 The v'_{PC}/v ratio as a function of r_{PC}

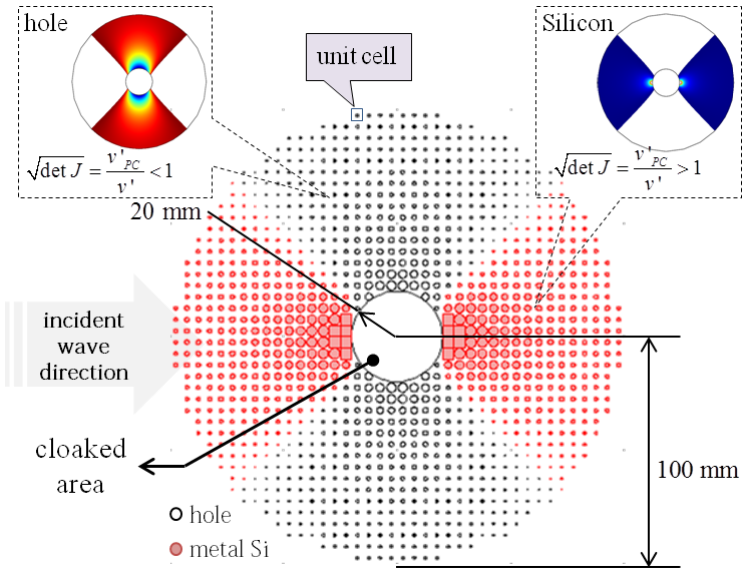

Fig. 4. 6 The cloaking designed by using GRIN PC. The design domain is divided into two parts: (ⅰ) drilled PCs are used for lower wave speed and (ⅱ) PCs with Si inclusions are used for higher wave speed.

The detailed specification of the arrangement and the sizes of holes/inclusions are presented in Fig. 4.7. Since the arrangements are symmetric to two axes, the first quadrant of the cloaking design domain is shown. As mentioned before, the radii of the holes/inclusions are getting larger as closer to the cloaked region for radical change of wave speed and direction.

For a drilled PC, the wave speed gradually decreases as r_{PC} of the hole increases, while the wave speed in a Si-included PC increases as r_{PC} of the inclusion increases. The graph of v'_{PC}/v ratio as a function of r_{PC} is plotted in Fig. 4.5. According to Fig. 4.4(b), there is a region of $v'_{PC}/v = \sqrt{\det J} \geq 1.5$ which cannot be cover with a Si-included PC, but the area of this region is very small. A Silicon cube in the same form with the unit cell is supposed to make up for that region sufficiently, in which S0 wave speed at 100 kHz is 7778.3 m/s.

The next step is to compart the design domain into unit cells and find the $\sqrt{\det J}$ for each cell referring to Fig. 4.4 Then the type and the radius of each unit cell can be determined referring to Table 4.1, Table 4.2 and Fig. 4.5. A series of this process results in the arrangement of PCs in the cloaking design domain as Fig. 4.6. The region of $\sqrt{\det J} < 1$ is filled with the drilled PCs and the other of $\sqrt{\det J} > 1$ with the Si-included PCs. Since $\sqrt{\det J}$ has extreme value near the inner radius, r_{PC} of the hole or the inclusion is getting larger as closer to the inner hole in order to change the wave

speed dramatically. Especially, pure Si unit cells are used on both sides of the cloaked area for very high speed as mentioned before.

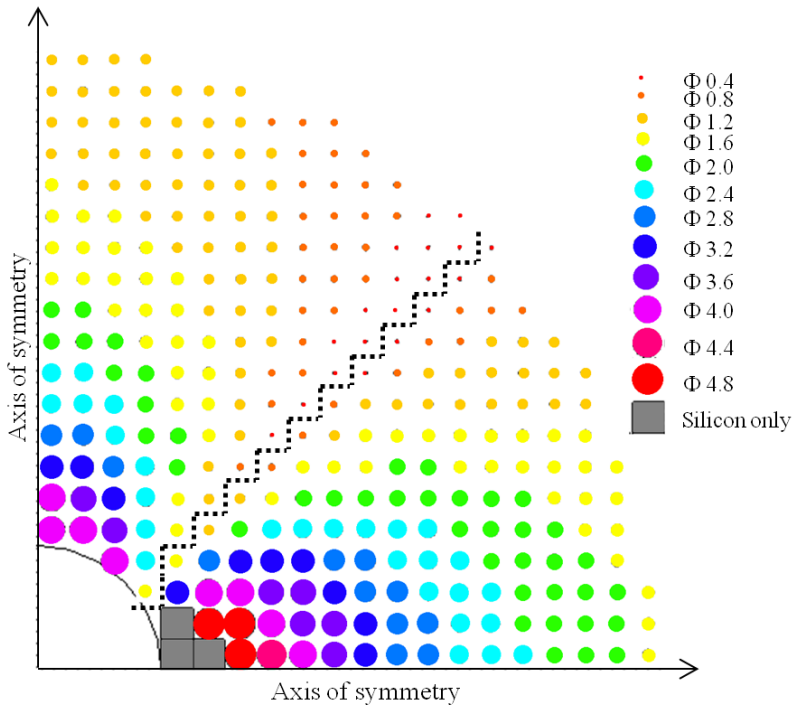

Fig. 4. 7 The arrangement of the holes and Si inclusions in the conformal cloaking with the reduced material properties at 100 kHz. The circles above the dotted line are holes and the rest under the line are Si inclusions.

4.4 Experiments and Results

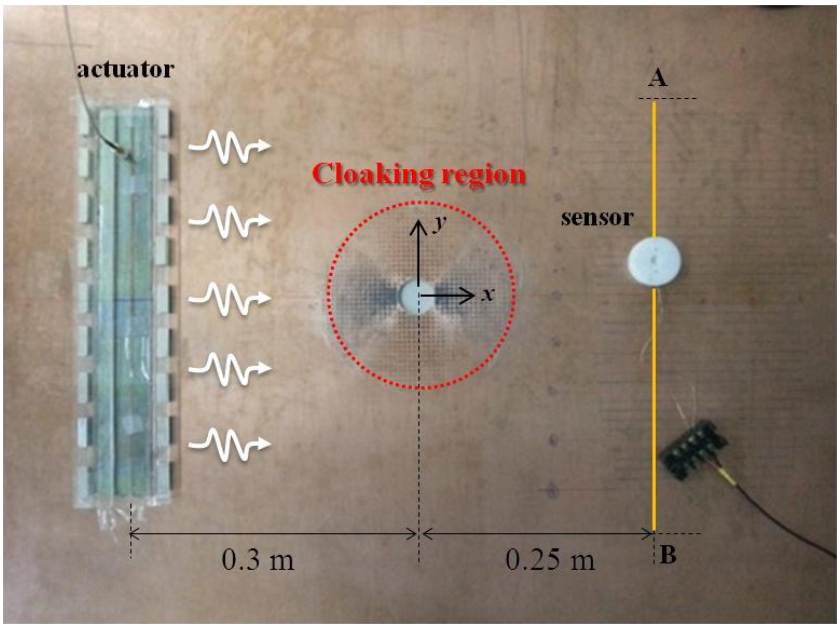

Fig. 4. 8 Experimental set up for evaluation of the conformal cloaking in a 3t Cu plate

The conformal elastic cloaking is experimentally evaluated. The experimental setup is described in Fig. 4.8. The conformal cloaking is fabricated in the 3t Cu plate this way; the plate is drilled at all the places where the holes and Si inclusions are to be located and then the mixture of Si powder and binder is sintered and compressed in the holes where Si inclusions should be filled. Magnetostrictive patch-type transducers are employed to actuate and receive the wave signals. The sensor named OPMT [81, 82] is a transducer that can deliver the strain of a ferromagnetic patch deformed by magnetic fields to a nonferromagnetic solid. By changing the arrangement of a couple of permanent magnets

and coil arrays, various modes of elastic waves can be generated. For S0 wave sensing, the direction of the static magnetic field generated by the permanent magnets is parallel with the direction of dynamic magnetic field generated by the AC current in coils. The actuator is fabricated by borrowing the working principle of PSA-OPMT, another kind of magnetostrictive patch-type transducer suggested in [82, 83] for the generation of plane waves of exact target frequency. A coil array of equal intervals is employed for this transducer and this interval can manipulate wave length and working frequency. A Gaussian pulse of 100 kHz-centered frequency is generated toward the cloaking with a plane wave front. The corresponding wave length is 0.0376 m. For elastic waves to fully develop, the transducer is 0.3 m away to the left from the center of the cloaking and the sensor measures the wave signals on the line $\overline{AB}$ that is 0.25 m away to the right from the center of the cloaking. The signals are measured at intervals of 0.01 m on $\overline{AB}$. At each measuring point, the signals are measured 1000 times and averaged to improve the reliability.

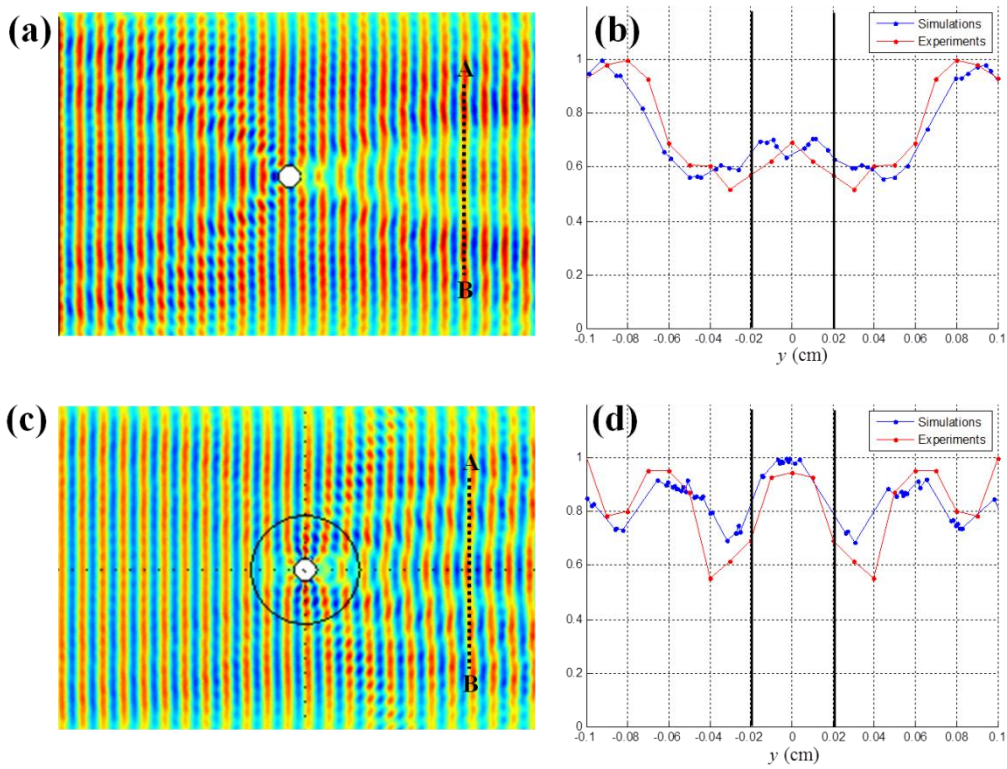

Fig. 4. 9 The comparisons of the strain field in the x' direction. The fields are the simulations of the strain distribution (a) without the cloaking and (b) with the cloaking with the reduced material properties. The cross sectional distributions along $\overline{AB}$ in simulation and experimental results are juxtaposed (c) for the bare plate and (b) for the plate with the embedded cloaking.

The experimental results compared with the simulation results for the cases with and without the elastic cloaking are shown in Fig. 4.9. According to Fig. 4.9(b) and (d), the experimental results and the simulation results are in good agreement with each other. For the distribution of the strain in the x' direction along the cross section in Fig. 4.9(a)

where the elastic cloaking is not applied, the central part of the distribution is weakened. Signals from $x = -0.06\ \mathrm{m}$ to $x = 0.06\ \mathrm{m}$ has about 0.6 times of the maximum value (See Fig. 4.9(b)) because of the shadow zone behind the hole. Though the amplitude of the waves behind the hole is recovered to a certain degree due to wave diffraction, it cannot keep up the magnitude of the incident waves. On the other hand, the dented part is recovered (see Fig. 4.9(d)) when the conformal cloaking with the reduced material properties are applied as Fig. 4.9(c). Although there are some oscillations in the distribution shown in Fig. 4.9(d) occurred by the deficiency of the material properties and the limitation to the outer boundary of the design domain, the distribution of the central parts is rather even on average. Practically, the standard deviation of the equally spaced 100 points of the simulation result in Fig. 4.9(b) is 0.015, while the counterpart in Fig. 4.9(d) is 0.008. In other words, more uniform magnitude of signals can be received behind the hole when the cloaking is embedded. The fact that the standard deviation is almost halved can support the performance of the conformal cloaking. Conclusively, the elastic conformal cloaking having the reduced material properties are feasible and of excellent stability.

Chapter 5.

Cloaking Bandage : Applications of Elastic Cloakings

5.1 Chapter Overview

Here, we introduce one of the available applications of the elastic cloaking other than the cloaking function itself; *stress bandage*. Its concept is stress shielding by the attachment of devices just as you would put an adhesive bandage on the wound. The conformal elastic cloaking can contribute to relieve stress concentration in solid structures by controlling the direction of wave propagation. How the cloaking dissipates the concentrated stress at a certain point is first suggested. The specification of the device to mitigate stress is also presented considering the circumstances and the features of wave propagation. Then the numerical simulations of the stress concentration and the mitigation of stress in a thin plate are shown to prove the efficiency of application of the cloaking.

5.2 Concepts of Stress Bandage

When an infinite homogeneous structure is loaded by a force of uniform intensity, the distribution of stress or strain is identical at any point of the structure. However, the inhomogeneities or the discontinuities of a structure cause stress concentration, and large load may result in the deformation or even the destruction of the structure. For example,

when a thin plate with a hole inside it is loaded at its ends uniformly by a tensile stress, the maximum stress is occurred at both side of the hole in a direction tangent to the hole with a value of three times of the stress. If it exceeds the ultimate tensile strength, fractures are generated in the direction perpendicular to the tensile stress. The continuous loading would cause crack development or even destruction of the structure. To avoid the generation and the growth of cracks, the transformed shape of the elastic cloaking is employed. Since it is impossible to embed the cloaking around cracks in the existing structures, a method to adhere the cloaking devices to the surfaces of the structures with the cracks inside their cavities is adopted; therefore, the attached cloaking device is named *cloaking patch*. Propagating waves can generate the continuous tension and compression to the medium and the cloaking patch is supposed to deconcentrate the tensile or compressive stress by changing the paths of waves.

Stress bandage by the cloaking patch aims two cases: (1) relieving the stress concentration at both sides of a hole under tensile stress, and (2) reducing the tensile stress that develops the existing cracks. It is worthy of evaluation of the tensile stress concentrated at a certain point by propagating elastic waves. Let us look for each case in turn.

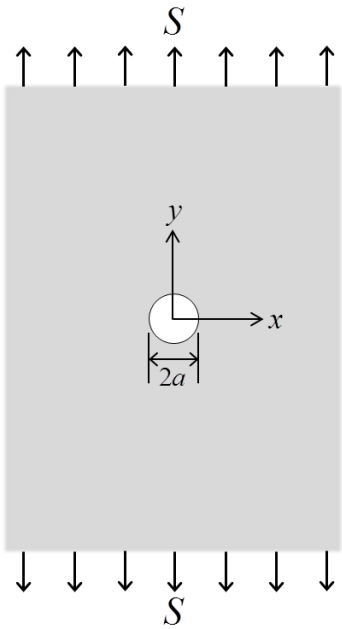

Fig. 5. 1 A thin plate with a small hole of radius a at the center of it is loaded at its ends uniformly by a tensile force intensity S.

The first case is described in Fig. 5.1. A tensile stress intensity S is applied at both ends of a thin plate uniformly. If there is no hole, a uniform stress is loaded to the plate. With the hole at the center in the plate with the infinite width and length, the stresses for the cylindrical coordinate are given as [52, 84]

$$\sigma_{rr} = \frac{S}{2}\left[\left(1-\frac{a^2}{r^2}\right)+\left(-1+4\frac{a^2}{r^2}-3\frac{a^4}{r^4}\right)\cos 2\theta\right] \tag{5.1a}$$

$$\sigma_{\theta\theta} = \frac{S}{2}\left[\left(1+\frac{a^2}{r^2}\right)+\left(1+3\frac{a^4}{r^4}\right)\cos 2\theta\right] \tag{5.1b}$$

$$\sigma_{r\theta} = \frac{S}{2}\left(1 + 2\frac{a^2}{r^2} - 3\frac{a^4}{r^4}\right)\sin 2\theta \tag{5.1c}$$

Then the maximum stress occurs at $(\pm a, 0)$ in a direction tangent to the hole with a value of $3S$ and σ_{rr} decreases exponentially as r increases [84, 85]. In case of the finite dimension of the plate, the stress is concentrated at the same point with a value less than $3S$ as a function of the radius of the hole and the size of the plate [84, 86]. The large stress should be mitigated because it possibly threatens the robustness of the structure. Practically a lot of cracks occur around rivet holes in solid structures such as ships or pipelines. When S0 harmonic waves propagates in the y direction, the maximum tensile stress at the hole occurs when the displacements at the upper half of the hole is in the positive y direction and the counterparts at the lower half of the hole is in the negative y direction. Then, it is plausible for the stress concentration by harmonic waves to occur cracks at the hole.

The second case is the growth of the existing cracks as depicted in Fig. 5.2. If a tensile stress is applied to the crack further, they possibly develop, leading to breakage of the structure. Especially, the infinite stress is applied to the crack tip O in the tangential direction like the first case. The width of the crack is close to 0 and the maximum σ_y generated by elastic waves propagating in the y direction occurs when the direction of displacements at the upper and the lower part of the crack are opposite with each other and the displacements along the x axis are zero.

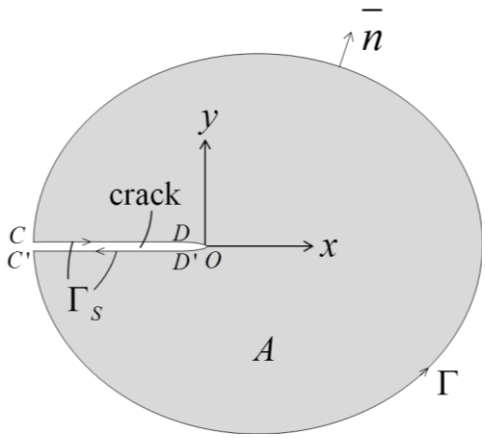

Fig. 5. 2 A crack bounded by an arbitrary path in an elastic body and a set of rectangular coordinate

Let us consider the attachment of the elastic cloaking to the surfaces of the plate with the hole or the crack. It is theoretically impossible to guide S0 waves thoroughly along the cloaking as shown in the previous chapter because the cloaking is not embedded in the plate. However, part of waves - especially near the surfaces of the plate – can be affected by the cloaking. The cloaking patches might serve to relieve the stress concentration at the holes or the crack tips as a result.

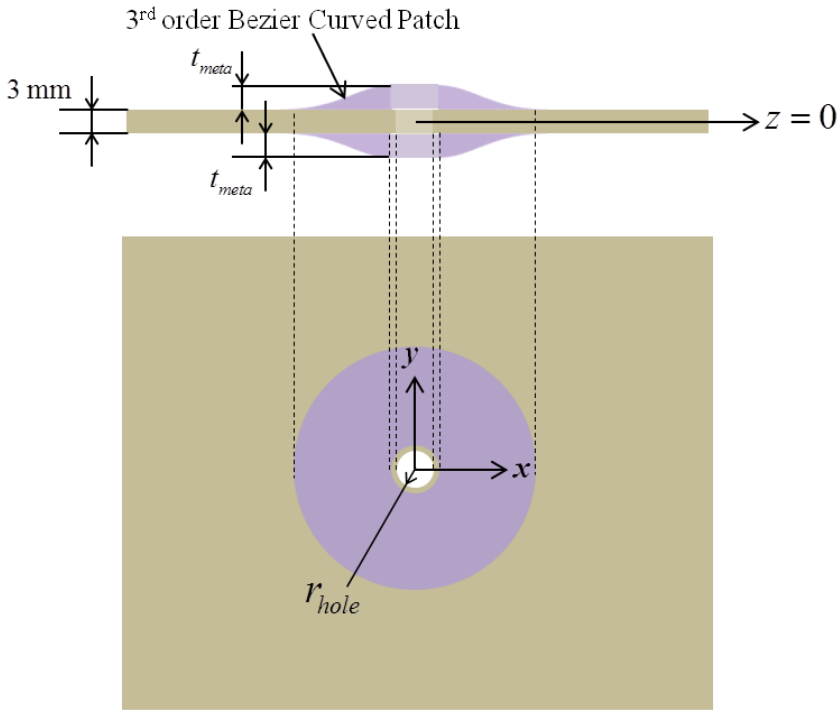

Fig. 5. 3 The shape of the cloaking patches and their applications to the drilled plate.

The attachment of the cloaking patch to the plate with a hole is described in Fig. 5.3. Elastic waves are incident in the x direction. Without the cloaking patch, the maximum stress occurs at $(0, \pm r_{hole})$ in the x direction. The matrix of the cloaking patch is the same with the plate. The thickness of the cloaking patch is gradually changed to avoid the discontinuity between the plate and the cloaking-patched plate. If the cloaking patches have uniform thickness, the profile of the cloaking-patched plate is stepped and the incident waves are reflected at the edge of the cloaking due to impedance mismatch. Therefore, it is important to eliminate impedance mismatch at any point by using gradual thickness change. In this thesis, the profile of the cloaking patch is a 3rd order Bezier

curve so that the slope of the thickness both at the inner and the outer radii of the patch is zero as depicted in Fig. 5.3. In addition, the inner radius of the patch is larger than the radius of hole in order to allow the space that a rivet head or other supporting part occupies. In case of a crack, the crack length is shorter than the inner diameter of the cloaking patch. By applying the cloaking patch to the surfaces of the drilled or cracked plate, the concentrated stress is expected to be relieved. The increased thickness and the change of direction of the wave propagation contribute to the decrease of the maximum stress.

5.3 Effects of Stress Bandage

The influences of the cloaking patches are numerically proved by using COMSOL Multiphysics. For each case, three models are compared: (1) stress concentration at a hole or a crackin the plate is evaluated as a control, (2) the patches made of an isotropic material on the surfaces of the damaged plate and (3) the cloaking patches on the surfaces of the damaged plate are evaluated. The analysis of model (2) is evaluated to determine whether just the increase of the thickness of plate attributes to the mitigation of the concentrated stress. Even though the change in the thickness reduces the stress concentration of course, the employment of the cloaking patches is supposed to be more efficient.

5.3.1 Stress Bandage in a Plate with a Hole

Let us consider the case of elastic wave propagation in a plate with a hole. Figure 5.4 shows the distribution of stress in the x direction generated by harmonic elastic wave propagations in the 3t Cu plates with the hole of radius 0.015 m. The waves are S0 mode of 100 kHz-centered frequency and the wave length is 0.0376 m. The inner and the outer radius of the cloaking patch is 0.02 m and 0.1 m, respectively. If the cloaking patches are not attached to the plate as shown in Fig. 5.4(a), the maximum σ_{xx} occurs at $(0, \pm 0.015)$ when the wave front of the maximum tensile stress is coincident with the y axis, which value is 6.23 Pa.

In case the patches made of Cu as shown in Fig. 5.4(b), they are unable to have a great effect on stress bandage. Since the patches are isotropic, the waves propagate along perfectly horizontal paths in the area covered with the patches. For the waves along $y = \pm 0.02\,\mathrm{m}$, the amplitude decreases in the patch-covered area based on the principle of the conservation of energy. On the other hand, the waves propagating along $y = \pm 0.015\,\mathrm{m}$ have their amplitude decreased within the region covered with the patches. However, they recover their amplitude within the cavity of the cloaking patches to the incident level. Instead, part of the waves are reflected at the inner boundary of the cloaking patches due to the discontinuity of the thickness, occurring the reduction of the stress. Therefore, the tensile stress experienced by the points $(0, \pm 0.015)$ slightly

reduces compared with Fig. 5.4(a). The resultant maximum σ_{xx} at $(0, \pm 0.015)$ is 4.72 Pa.

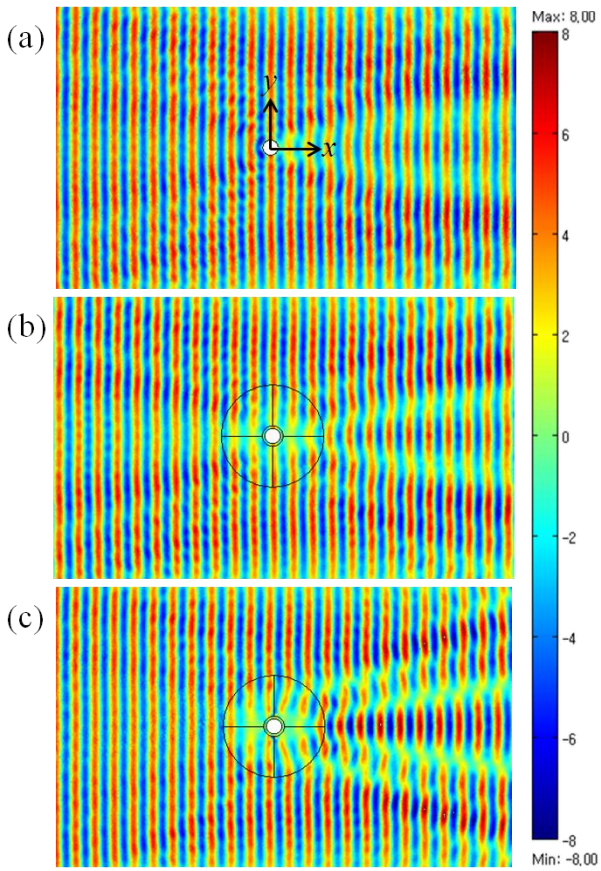

Fig. 5. 4 The distribution of σ_{xx} in the drilled Cu plate (a) without any patches, (b) with the Cu patches and (c) with the cloaking patches attached on two surfaces.

When attaching the cloaking patches on the surfaces of the drilled plate as Fig. 5.4(c), more improved result can be obtained. Since the elastic waves are partially guided along

the curved paths in the cloaking patches, energy delivered to the points $(0, \pm 0.015)$ is fundamentally reduced. According to Fig. 5.4(c), the wave front of maximum σ_{xx} seems to be mismatch with the y axis while the maximum σ_{xx} at $(0, \pm 0.015)$ occurs at this phase. The reason of mismatch is connected with the results in the previous chapter. Due to the characteristics of the cloaking, the waves within the cloaking-patched region are slightly delayed, causing the non-straight wave fronts. Focused on the distribution of σ_{xx} near the hole, it is found that the maximum σ_{xx} at $(0, \pm 0.015)$ is 1.93 Pa. It is clearly shown that, when the cloaking patches are installed to the plate, the maximum σ_{xx} experienced by the hole decreases by about 70 %. Consequently, the cloaking patches are expected to make a great contribution to prevention of cracks around the hole.

5.3.2 Stress Bandage in a Cracked Plate

The cloaking patches contribute to stress bandage when a plate is already cracked. According to 5.3.1, cracks are generated along the direction perpendicular to the wave propagation and the width of the cracks is close to zero. Based on these points, the simulation modeling is presented in Fig. 5.5(a). Elastic waves propagate the x direction like the previous cases, and the crack lying along the y direction completely penetrate the 3t Cu plate. In this case, a theoretically infinite stress σ_{xx} loads at the crack tips, which is the most troublesome features in analyzing the total amount of the stress. To

mitigate the infinite tensile stress, the cloaking patches are attached on and under the cracked plate.

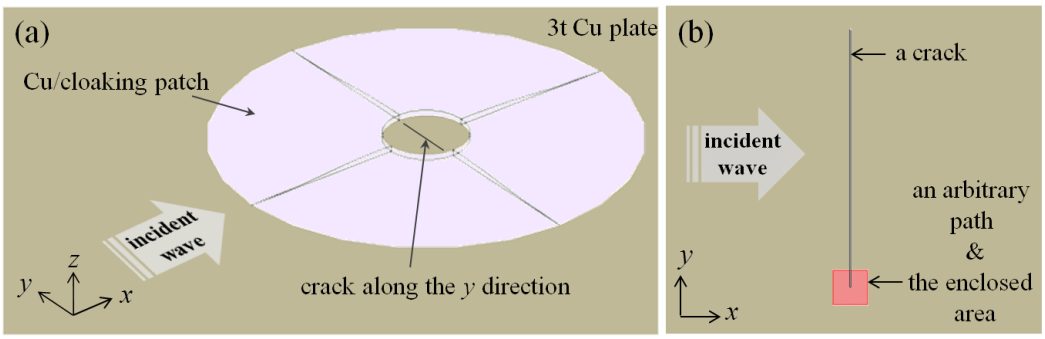

Fig. 5. 5 A cracked plate with the cloaking patches on it. (a) The patches relieve the stress concentration at the tips of the crack aligned in the y direction when elastic waves are incident in the x direction. (b) An arbitrary path surrounding the crack tip and the enclosed area are defined for stress analysis

In order to resolve the difficulty in the analysis, an analyzing method named *J*-integral was suggested [87-89], where the strain energy release rate for a crack in a solid structure subject to monotonous loading is calculated by contour path integral along an arbitrary path. If a time-independent force intensity is applied to the solid body shown in Fig. 5.2, the strain energy release rate is calculated as

$$J_k = \int_{\Gamma+\Gamma_S} \left[W_e n_k - T_i u_{i,k} \right] d\Gamma \qquad (k = x, y) \tag{5.2}$$

where Γ, Γ_S, W_e, n_k, T_i denote the arbitrary curve surrounding the crack tip, the curves from $C(C')$ to $D(D')$ along the crack surfaces, the strain energy density, the

normal vector component and the traction: $T_i = \sigma_{ij} n_j$ [89]. The strain energy density is calculated as $W_e = \frac{1}{2}\sigma_{ij}\varepsilon_{ij}$.

In this thesis, however, the dynamic terms should be added since the loading is time-varying. According to Ref. [90-93], the strain energy release rate of the crack tip loaded by the time-varying force intensity is

$$J_k = \int_{\Gamma+\Gamma_S} \left[W_e n_k - T_i u_{i,k} \right] d\Gamma + \iint_A \left(\rho \ddot{u}_i - F_i \right) u_{i,k} \, dA \qquad (k = x, y) \tag{5.3}$$

where ρ, $\ddot{u}_i$ and F_i are the density of the medium, the acceleration and the body force. Assuming the body force is zero and expressing the second integral in Eq. (5.3) as

$$\rho \ddot{u}_i u_{i,k} = \frac{\partial}{\partial t}\left(\rho \dot{u}_i u_{i,k} \right) - \frac{\partial}{\partial x_k}\left(\frac{1}{2}\rho \dot{u}_i^2 \right) \tag{5.4}$$

Equation (5.3) changes its form as

$$J_k = \int_{\Gamma+\Gamma_S} \left[W_e n_k - T_i u_{i,k} \right] d\Gamma + \frac{\partial}{\partial t}\iint_A \left(\rho \dot{u}_i u_{i,k} \right) dA - \iint_A \frac{\partial}{\partial x_k}\left(\frac{1}{2}\rho \dot{u}_i^2 \right) dA \tag{5.5}$$

Then applying the divergence theorem to the last domain integral, it can be rewritten as

$$\begin{aligned} J_k &= \int_{\Gamma+\Gamma_S} \left[\left(W_e - \frac{1}{2}\rho \dot{u}_i^2 \right) n_k - T_i u_{i,k} \right] d\Gamma + \frac{\partial}{\partial t}\iint_A \left(\rho \dot{u}_i u_{i,k} \right) dA \\ &= \int_{\Gamma+\Gamma_S} \left[\left(W_e - K \right) n_k - T_i u_{i,k} \right] d\Gamma + \frac{\partial}{\partial t}\iint_A \left(\rho \dot{u}_i u_{i,k} \right) dA \end{aligned} \tag{5.6}$$

where $K = \frac{1}{2}\rho \dot{u}_i^2$ is the kinetic energy density.

While Ref. [90-93] deal the problems of continuously stretched structures though the force intensity is time-varying, the structures presented in this thesis experience the repeated tension and compression by time-harmonic elastic waves. Therefore, Eq. (5.6) should be time-averaged over a cycle [94]. Let $\langle\ \rangle$ indicate the time-averaged value, then the time-averaged strain energy release rate is defined as

$$\overline{J_k} = \int_{\Gamma+\Gamma_S} \left\langle \left(W_e - K\right) n_k - T_i u_{i,k} \right\rangle d\Gamma \tag{5.7}$$

The last term in Eq. (5.6) vanishes because the time-averaged value of the time derivative of periodic quantity is zero. The exact strain energy release rate at a crack tip under a harmonic stress can be calculated by Eq. (5.7), and from the rate, the dynamic stress intensity factors can be evaluated. The factor for the opening mode K_I in Fig. 5.5(b) is related to the strain energy release rate as

$$\overline{J_y} = \frac{\kappa+1}{8\mu} K_I^2 \tag{5.8}$$

where κ is defined as following

$$\kappa = \begin{cases} 3-4\nu & \text{: plane strain} \\ \left(3-\nu\right)/\left(1+\nu\right) & \text{: plane stress} \end{cases} \tag{5.9}$$

and μ and ν denote the shear modulus and the Poisson's ratio, respectively. Since the cracked plate is discussed here, κ for plane stress is used.

The numerical calculations are conducted along the arbitrary path that embraces the crack tip shown in Fig. 5.5(b). The distributions of σ_{xx} near the crack tips are presented

in Fig. 5.6. As can be seen in Fig. 5.6(a), a large stress is exerted to the crack tips when no patch is attached. Although the Cu patches are attached to the plated embracing the crack inside them as Fig. 5.6(b), the stress exerted to the crack tips does not seem to be mitigated. On the contrary, the stress at the crack tips considerably decreases when the cloaking patches are attached to the plate as Fig. 5.6(c). Though a relatively large stress is exerted to the crack tips even when the cloaking patches are applied, the magnitude of the stress the cracks experience is much reduced because the distribution of tensile stress near the crack tips decreases on the whole.

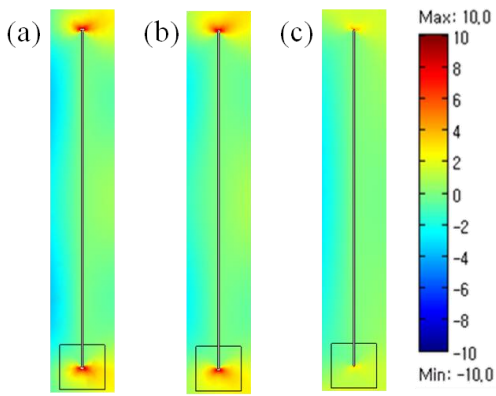

Fig. 5. 6 The distribution of σ_{xx} near the crack tips (a) in a cracked plate, (b) in a cracked plate with the Cu patches attached on it and(c) in a cracked plate with the cloaking patches attached on it. The scale of colorbar is fixed.

To quantify the stress by using K_I, J_y depending on the phase and its time-averaged value is evaluated for each case (see Table 5.1). The values for the phase from $180°$ to

Table 5. 1 The strain energy release rates J_y and the dynamic stress intensity factor K_I of three cases

phase	crack	copper patch	cloaking patch
0°	7.92253E-14	1.97273E-14	9.30956E-15
10°	8.74673E-14	2.93403E-14	8.56177E-15
20°	9.06663E-14	4.05597E-14	7.67083E-15
30°	8.84364E-14	5.20321E-14	6.74421E-15
40°	8.10464E-14	6.23738E-14	5.89367E-15
50°	6.93879E-14	7.03376E-14	5.22180E-15
60°	5.48669E-14	7.49628E-14	4.80963E-15
70°	3.92350E-14	7.56916E-14	4.70688E-15
80°	2.43775E-14	7.24360E-14	4.92594E-15
90°	1.20865E-14	6.55888E-14	5.44039E-15
100°	3.84440E-15	5.59758E-14	6.18818E-15
110°	6.45423E-16	4.47564E-14	7.07912E-15
120°	2.87537E-15	3.32840E-14	8.00574E-15
130°	1.02653E-14	2.29422E-14	8.85628E-15
140°	2.19238E-14	1.49785E-14	9.50282E-15
150°	3.64448E-14	1.03533E-14	9.94032E-15
160°	5.20768E-14	9.62453E-14	1.00431E-14
170°	6.69343E-14	1.28801E-14	9.82401E-15
$\overline{J}_y$	4.56559E-14	4.74703E-14	7.37357E-15
K_I	7.08671E-02	7.22616E-02	2.84797E-02

$350°$ are exactly the same with those from $0°$ to $170°$. The time-averaged strain energy release rate $\overline{J_y}$ and the corresponding K_I are calculated. K_I of the cracked plate without patch or with the Cu patches is over $7E-02$, while that of the cracked plate with the cloaking patches is under $3E-02$. Since the failure of the structure is more likely to happen as the value of K_I is larger, the cloaking patches contribute to the improvement of the robustness of the structure by guiding the S0 waves partially along the designated paths in them. In other words, the cracks that have suffered from the tensile stress exerted by the S0 waves are partially free from the influence of them by the attachment of the cloaking patches on the surfaces of the cracked plate.

5.4 Experiments on Stress Bandage

5.4.1 Fabrication and Experimental Setup

Based on the simulation results, we try to verify experimentally the effect of stress bandage. Measurement of the stress at hole is targeted because it is hard to measure the exact stress concentrated at a crack tip. The specification of the cloaking patch is the same as that used in the cloaking experiment except the change of the thickness. The fabricated cloaking patch is shown in Fig. 5.7. To taper the thickness of the patch, the disc-shaped cloaking device is grinded.

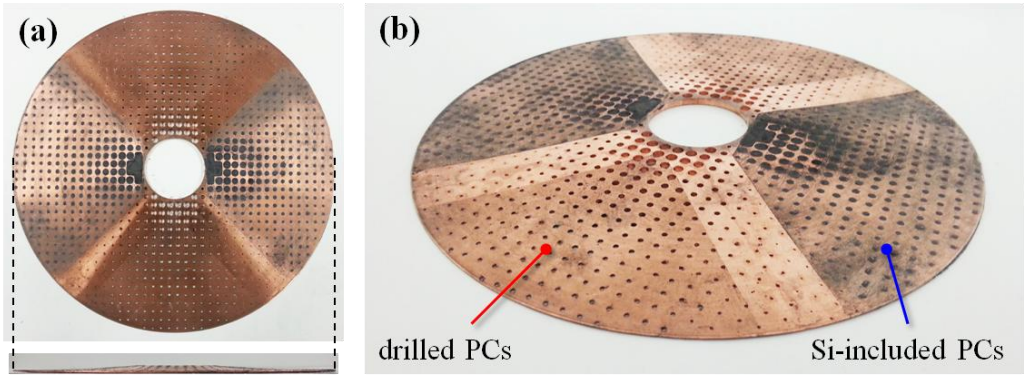

Fig. 5. 7 The cloaking patch composed of PCs. (a) The front view and the side view of the cloaking patch are shown. The thickness of the patch changes gradually. (b) The cloaking patch is composed of two sections: the drilled PC area and the Si-included PC area.

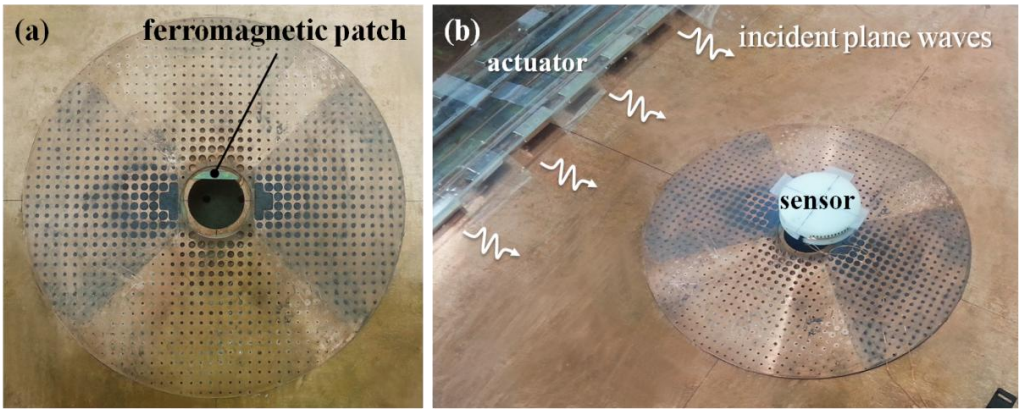

Fig. 5. 8 Attachment of the cloaking patch to the plate with the hole. (a) the arrangement of the cloaking patch and the ferromagnetic patch used for sensing and (b) non-contacting measurement of the wave signals with OPMT located on the cloaking patch.

After fabrication, it is attached to the surface of a Cu plate which is 3 mm thick and contains a hole of radius 15 mm as depicted in Fig. 5.8. Epoxy is used as adhesive to make the plate and the cloaking patch move integrally. The ferromagnetic patch is in the form of arch as shown in Fig. 5.8(b) because it should cover a narrow area around the hole and it is now overlapped with the cloaking patch. Like the cloaking experiments, OPMT is used as a sensor. In this case, the sensor is away from the patch by 3 mm since the maximum thickness of the cloaking patch is 3 mm. In spite of the offset, the wave signal can be measured because OPMT senses the electric field generated by the deformation of the ferromagnetic patch. The wave signals with/without the cloaking patch attachment are received to demonstrate the reduction of the stress concentrated near the hole. The generated voltage is proportional to the strain, and the stress can be regarded to be directly proportional to the strain because the stress and the strain in the x direction are dominant in this case. In order to maintain the measuring condition, the sensor is placed 3 mm off the plate even when the cloaking patch is not applied.

5.4.2 Experimental Results

The received signals are processed with STFT (Short-Time Fourier Transformation) to extract the magnitude of the signals over time and frequency [99]. The results are shown in Fig. 5.9. Since the distance between the actuator and the ferromagnetic patch is 0.2 m and the wave velocity is 3759.4 m/s, the estimated travel time is $5.32e^{-5}$ s, and the target frequency is 100 kHz.

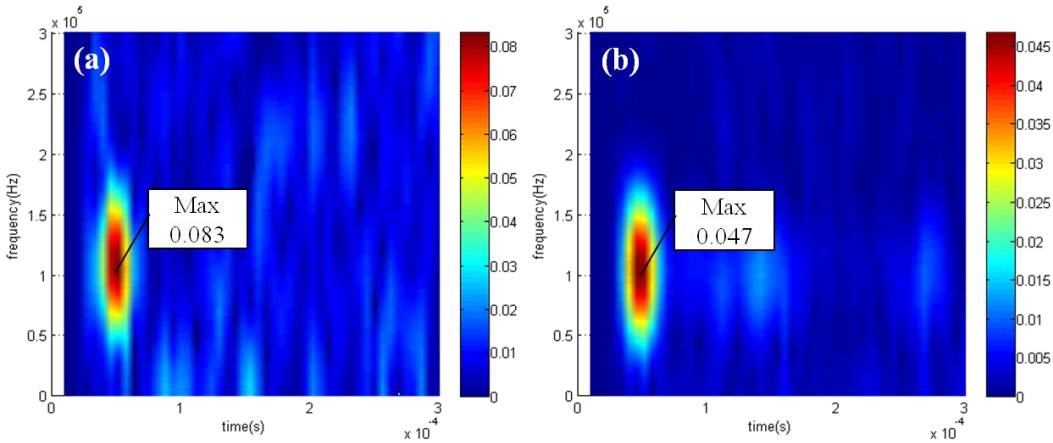

Fig. 5. 9 The signals processed through STFT. (a) the maximum magnitude of the signals is 0.828 when the stress is concentrated near the hole while (b) it is 0.477 when the stress bandage is applied around the hole.

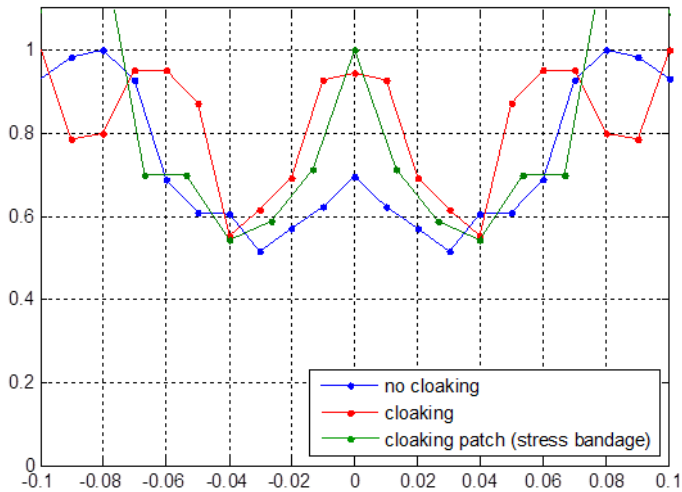

Fig. 5. 10 The comparisons of the stress fields in the x direction.

As can be seen from Fig 5.9, the maximum magnitude of the signal is 0.083 when the

stress bandage is not applied and the stress is concentrated at both sides of the hole. On the other hand, it is decreased to 0.047 when the cloaking patch is attached to a single side of the plate. The experimental decrease rate is 42.4 % while the computational decrease rate in the simulation results is 59 %. The degradation of the decrease rate is due to (ⅰ) inaccurate material properties of the cloaking composed of GRIN PCs of discrete sizes, (ⅱ) deteriorated material properties of Si inclusions by using binder, and (ⅲ) the use of epoxy in attaching the cloaking patch to the Cu plate. If another cloaking patch is attached to the other side of the plate, the stress is expected to reduce much more as shown in 5.3.1.

Another remark in this experiment is that the cloaking patch attached on the surface works as if it is a cloaking embedded in the plate like Fig. 4.8. This is an important function of a cloaking patch because it the maintenance of displacement field or stress field prevent secondary stress concentration or unexpected stress at other parts of the structure. To confirm this point experimentally, we received wave signals along a line on the cloaking patch-attached plate as Fig. 4.8. The result is juxtaposed with the previous results in Fig. 5.10.

As can be seen from Fig. 5.10, the experimental distribution of the x stress without any cloaking device (blue dotted line) is dented at the middle part, while that with the embedded cloaking (red dotted line) is recovered, which are already shown in 4.4.

Although the attachment of the cloaking patch is unable to catch up to the performance of the original embedded cloaking, it contributes to the restoration of the central part of the distribution and the similar tendency with the cloaking. It is confirmed from the green dotted line in Fig. 5.10. Therefore, it is concluded that the mechanical fields are partially maintained only with the attachment of the cloaking patch as if the cloaking is embedded around the hole, so that another stress concentration is prevented.

From these results, it is verified that the cloaking patch works as a mitigator to the stress concentrated at a certain part of a structure by controlling wave propagation. At the same time, the cloaking patch can be considered as a semi-cloaking because the uneven stress distribution near a hole are restored as if an elastic cloaking is installed around the hole.

Chapter 6.

Conclusions

In this study, cloakings are designed by employing transformation methods. Transformation methods are powerful means of controlling electromagnetic, acoustic and elastic waves thank to their features of distributing the gradually changing material properties such as permeability, permittivity, density or modulii. Since the previous methodologies for controlling waves are unable to change propagating directions of waves within a single part of a device, transformation methods can be a breakthrough in wave manipulation. By using transformation methods, various devices like cloakings, cloaking carpets, wave rotators or collimators can be engineered. Of those devices, engineering of cloaking and its application for stress bandage are the main objectives of the thesis.

First, the governing equations under transformation are derived and the characteristics of waves in the transformed space are demonstrated through transformation acoustics. Based on the comprehension of the process and the attribute of transformation acoustics, an elastic cloaking is engineered. Although engineering of devices by transformation elasticity is quite difficult due to the form-variance of the governing equations and resultant terms that do not exist in nature, conformal mapping capacitates the realization of the elastic cloaking. The extra terms generated during the coordinate transformation of an elastic medium are minimized by virtue of the Cauchy-Riemann condition and its

extended relations of conformal mapping equations. It is numerically proved that the proportion of the extra terms is considerably small compared with that of general transformation and the elastic devices with the reduced material properties work well.

On the basis of these results, the elastic cloaking is manufactured with gradient-index phononic crystals, which are composed of various sizes of holes or Si inclusions in the Cu matrix. The performance of the embedded cloaking in the Cu plate is evaluated experimentally by means of the magnetostrictive patch-type transducers developed on our own. The distribution of stres exerted to the plate by the S0 waves after passing the hole and the cloaking is in good agreement with the simulation result. From the experimental and simulation results, it is verified that the elastic cloaking plays an important role in the uniformity and the increase of the magnitude of the elastic waves within the prescribed range when the waves are passing the hole.

As an application of the elastic cloaking, it is employed for stress bandage in the modified form. The cloakings in the form of patch are attached to the damaged plate to partially guide the propagating waves along the designated paths. Consequently the concentrated stress near the hole or the crack tips is relieved the stability of the damaged plate is improved. It is also verified through experiment that the stress concentrated near a hole in the plate is mitigated when stress bandage is applied. Finally, the cloaking patches are expected to contribute to the promotion of the stability of the structures against fracture or failure.

Appendix A.

Acoustic Cloaking in the Cylindrical Coordinate System

Here, the material properties of an acoustic cloaking are derived in the cylindrical coordinate. The properties shown in Chap.2 are calculated rather easily when the transformation equation is based on the Cartesian coordinate. However, the transformation in the cylindrical coordinate system is quite complicated. The transformation for a cloaking, one of the most typical transformations is usually expressed in the cylindrical coordinate system. The distribution of the density and the bulk modulus can be derived as follow.

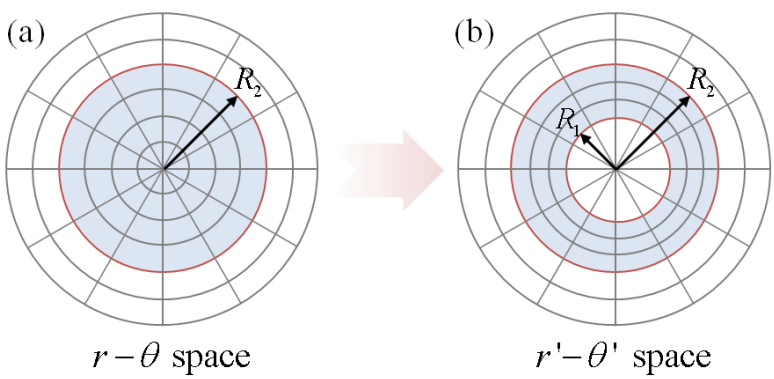

Fig. A. 1 Transformation used for a cloaking (a) a circle in the original space which radius is R_2 (b) a torus in the transformed space where inner and outer radius is R_1 and R_2, respectively.

To achieve this transformation, the mapping equation is as follow.

$$\begin{aligned} r' &= R_1 + r(R_2 - R_1)/R_2, \\ \theta' &= \theta \end{aligned} \tag{A.1}$$

The Jacobian matrix of this mapping equation is

$$J_{r',r} = \frac{\partial(r',\theta')}{\partial(r,\theta)} = diag\left(\frac{R_2 - R_1}{R_2}, 1\right) \triangleq diag(\alpha, 1) \tag{A.2}$$

It does not mean the Jacobian matrix in the cylindrical coordinates because the material properties including J are usually defined by covariant vectors, i.e. all vectors used for material properties are in the form of

$$\overline{E} = [E_1 \ E_2]^T = E_1 \overline{a}^1 + E_2 \overline{a}^2 \tag{A.3}$$

Since vectors defined in the cylindrical coordinate system, however, use its own unit vector, covariant vectors should be transformed to unit vectors in cylindrical coordinates systems by calculating scale factor related to metric tensors [95].

The relations between a covariant vector and a unit vector in the orthogonal coordinate systems expressed by (x, y, z) are

$$\overline{F} = f^i \overline{a}_i = f_i \overline{a}^i \tag{A.4}$$

$$\overline{F} = F^i \hat{e}_i \tag{A.5}$$

where f^i, f_i and F^i are coefficients in each defined vector, and the relations between vectors shown in Eq. (A.4) and Eq. (A.5) are

$$\overline{a}_i = h_i^2 \overline{a}^i = h_i \hat{e}_i \tag{A.6}$$

where h_i is a scale factor. Then the relations between the coefficients are

$$f_i = h_i^2 f^i = h_i F^i \tag{A.7}$$

The scale factors in the cylindrical coordinate system expressed by (r, θ, z) is obtained as

$$h_i = \sqrt{g_{ii}} = \sqrt{\left|\bar{a}_i \cdot \bar{a}_i\right|} = \sqrt{\sum_{j=1}^{2} \frac{\partial x^j}{\partial r^i} \frac{\partial x^j}{\partial r^i}} \tag{A.8}$$

$$\begin{aligned} h_1 &= \sqrt{\cos^2\theta + \sin^2\theta + 0} = 1, \\ h_2 &= \sqrt{r^2\cos^2\theta + r^2\sin^2\theta + 0} = r, \end{aligned} \tag{A.9}$$

Using these results to Eq. (A.7), an arbitrary vector $\bar{E}$ is re-written as

$$\bar{E} = \frac{E_1}{h_1} e_1 + \frac{E_2}{h_2} e_2 = E_1 e_r + \frac{E_2}{r} e_\theta = E_r e_r + E_\theta e_\theta \tag{A.10}$$

and from this, the relation between E_1, E_2, E_3 and E_r, E_θ, E_z is

$$\begin{bmatrix} E_1 \\ E_2 \end{bmatrix} = \begin{bmatrix} 1 & 0 \\ 0 & r \end{bmatrix} \begin{bmatrix} E_r \\ E_\theta \end{bmatrix} \tag{A.11}$$

The Jacobian matrix defined by the unit vectors in the cylindrical coordinate system is then,

$$\begin{bmatrix} E_1 \\ E_2 \end{bmatrix} = \begin{bmatrix} \alpha & 0 \\ 0 & 1 \end{bmatrix} \begin{bmatrix} E_1' \\ E_2' \end{bmatrix} \tag{A.12}$$

$$\begin{bmatrix} 1 & 0 \\ 0 & r \end{bmatrix} \begin{bmatrix} E_r \\ E_\theta \end{bmatrix} = \begin{bmatrix} \alpha & 0 \\ 0 & 1 \end{bmatrix} \begin{bmatrix} 1 & 0 \\ 0 & r' \end{bmatrix} \begin{bmatrix} E_r' \\ E_\theta' \end{bmatrix} \tag{A.13}$$

$$\begin{bmatrix} E_r \\ E_\theta \end{bmatrix} = \begin{bmatrix} \alpha & 0 \\ 0 & \dfrac{r'}{r} \end{bmatrix} \begin{bmatrix} E_r' \\ E_\theta' \\ E_z' \end{bmatrix} \triangleq \overline{J_{c',c}} \cdot \begin{bmatrix} E_r' \\ E_\theta' \end{bmatrix} \tag{A.14}$$

Then the Jacobian matrix of Eq. (A.1) in the cylindrical coordinate system is

$$\overline{J_{c',c}} = \begin{bmatrix} \alpha & 0 \\ 0 & \dfrac{r'}{r} \end{bmatrix} = \begin{bmatrix} \alpha & 0 \\ 0 & \alpha \dfrac{r'}{r' - R_1} \end{bmatrix} \triangleq \begin{bmatrix} \alpha & 0 \\ 0 & \beta \end{bmatrix}, \tag{A.15}$$

which is now used as the Jacobian matrix in Eq. (2.21) and Eq. (2.22). The reciprocal density matrix is

$$\begin{bmatrix} \dfrac{1}{\rho'(x')} \end{bmatrix} = \frac{1}{\rho(x)} \begin{bmatrix} \dfrac{\alpha}{\beta} & 0 \\ 0 & \dfrac{\beta}{\alpha} \end{bmatrix} = \frac{1}{\rho_0} \begin{bmatrix} \dfrac{r' - R_1}{r'} & 0 \\ 0 & \dfrac{r'}{r' - R_1} \end{bmatrix} \tag{A.16}$$

and the bulk modulus is

$$\kappa' = \left(\frac{R_2 - R_1}{R_2} \right)^2 \frac{r}{r - R_1} \kappa \tag{A.17}$$

These properties are in good agreement of the results in Ref. [13, 96]. If the torus device shown in Fig. 2.3(b) has the distribution of material properties like Eq. (A.16) and Eq. (A.17), waves incident outside the device cannot reach the inside circular space. Since the medium properties is unrelated to wave frequency, the devices designed by transformation electromagnetics/acoustics theoretically work for any frequency. Wave propagations in the cloaking device having the calculated material properties are shown in Fig. 2.4. They are computed by using commercial finite element analysis tool COMSOL Multiphysics [54]. Waves generated outside the device propagate around the

circular space inside the device and maintain their wave front after completely getting out of the device.

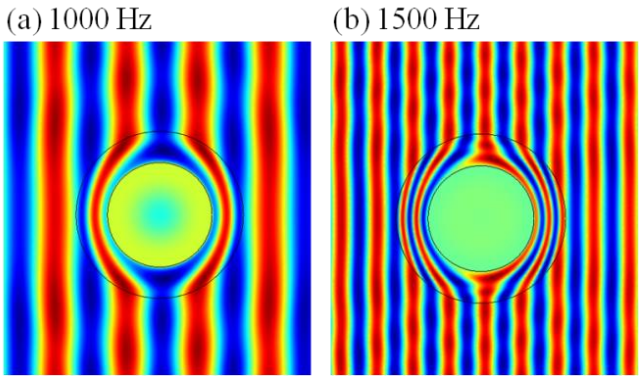

Fig. A. 2 Pressure field by acoustic wave propagation in the cloaking device. Time-harmonic incident waves of (a) 1000 Hz and (b) 1500 Hz are used.

Appendix B.

Engineering of Directional Cloaking by Transformation Acoustics

B.1 Motivation

The acoustic cloaking shown in Appendix A bends all incoming waves so that objects inside the cloaking are transparent in any directions and consequently no one can recognize the inside of the cloak even when the necessity arises. One inside a cloak is likewise unable to perceive waves outside the cloaking since the interior of the cloak is completely separated from the exterior. Thus, this cloaking device is unable to be used flexibly as the occasion demands. One of the main applications of cloaking devices might be of military purpose, where exceptionless isolation of both sides of cloaking is not recommendable. Therefore, we are motivated to add cloaking devices a function of revealing the cloaked objects in some selective directions.

Before introducing the mapping equations for the devices, it is worth reviewing the relevant previous studies. Mei *et al*. [97] and Vasic *et al*. [98] employed inhomogeneous isotropic materials by changing the refractive index distribution for directional cloakings. These devices prevent waves incident in certain directions from entering the cloaked area. However, they have not been proved to reflect waves incoming from other directions. Thus, a new device that makes waves in some directions detour around itself and allows waves in other directions to get into itself, is proposed. This device is beyond the limit of

the previous cloakings by permitting waves in the selective directions.

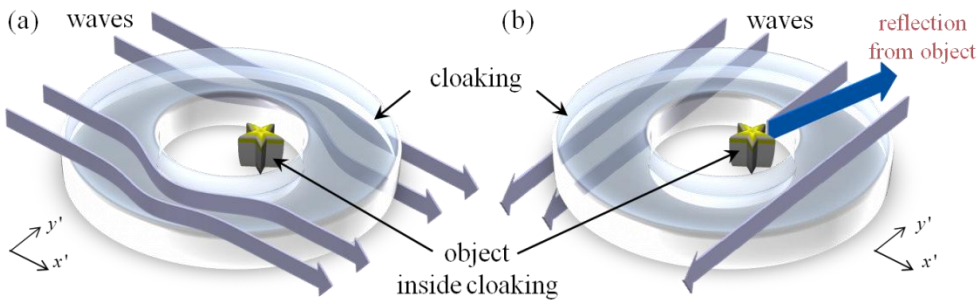

Fig. B. 1 Schematic description of the directional properties of a cloaking device. The device is (a) cloaking an object against plane waves incident along the x direction and (b) reflecting waves incident along the y direction by an object placed inside the device.

The mechanism of the suggested device is depicted in Fig. 2.5; according to Fig. B.1(a), waves incident along the x direction are bent around the cloaked area, not reaching the inside object, while waves along the y direction in Fig. B.1(b) penetrate into the cloaking device. These waves can be reflected when they meet an object having different impedance with medium. This device can be versatile by selectively blocking or allowing ultrasonic waves from sonars. Material distributions of the device described in Fig. B.1 are derived in the next chapter. The formula Eq. (2.21) and Eq. (2.22) are used in the Cartesian coordinate system.

B.2 Mapping Equations and Material Properties

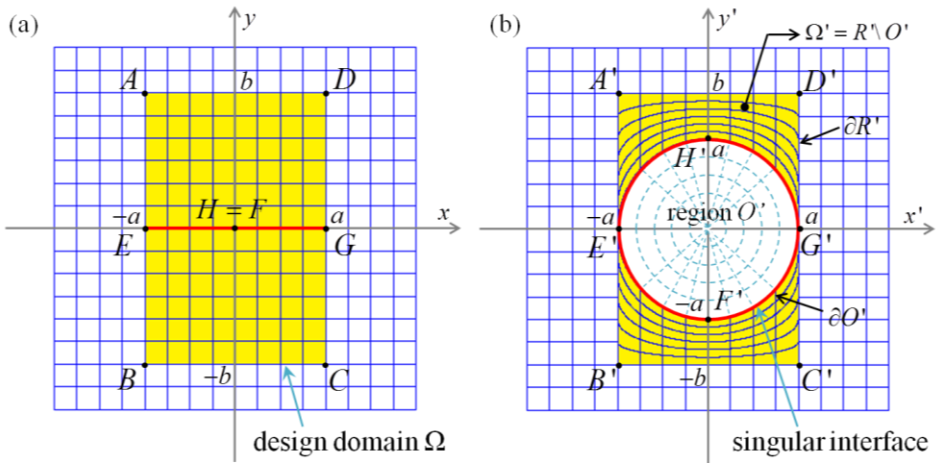

Fig. B. 2 Mapping of the directional cloaking from (a) a rectangular domain with a slit defined in the original space into (b) a rectangular domain with an inside circular cavity defined in the physical space.

Figure B.2 depicts the original and the physical space denoted by $x-y$ and $x'-y'$ coordinates. According to Fig. B.2, a rectangular region $\Omega(2a\times 2b)$ with a slit connecting the points $E(-a,0)$ and $G(a,0)$ in the original space is mapped to another region Ω' bounded by the outside rectangle R' and the inner circle region O' which diameter is the same as the width of R' in the transformed space. The previous cloaking shown in Fig. A.1 is achieved by transforming a circle into a torus, where the central point of the circle in the original space is mapped to the inner circle of the torus in the transformed space. The new cloaking proposed here is based on the

extended idea of the previous cloaking in that a slit line traversing the original design domain is mapped to a circle in the transformed domain.

There are several conditions that a set of the mapping equation should satisfy to realize the directional cloaking properties of a device shown in Fig. B.2 as following :

1. The outer rectangular boundary of the original space is mapped to the outer rectangular boundary $\partial R'$ of the same dimension in the transformed space.
2. The slit in the original space is doubly mapped into two semi-circles above and below the x' axis to make a complete circle of radius a.
3. The horizontal grid lines lying outside of Ω' should be continuously connected to the bent grid lines inside Ω'.
4. The vertical grid lines entering Ω' remain to be vertical all the way towards the inner circular boundary $\partial O'$.
5. At least, the normal impedance of the cloaking at E and G should be infinite while the normal impedance at H and F is the same as those of the medium (air in the present case) filling O'.

Among an infinite number of equations that meet the requirements, the following equation is selected :

$$x' = x,$$

$$y' = \begin{cases} \dfrac{b-\sqrt{a^2-x^2}}{b} y + \sqrt{a^2-x^2}, & 0 \le y \le b, \\ \dfrac{b-\sqrt{a^2-x^2}}{b} y - \sqrt{a^2-x^2}, & -b \le y \le 0, \end{cases} \tag{B.1}$$

This mapping equation is in accordance with all the above mentioned conditions. Condition 1 is for impedance matching when waves move from air to the cloaking device. The impedances at the interface between air and the cloaking material are identical when the dimension of outer boundary is kept. Thank to this condition, waves smoothly propagate into the cloaking device with small reflection. Condition 2, 3 and 4 are for the directional function of the cloaking device. The slit $\overline{EG}$ in Fig. B.2(a) and $E'F'G'H'$ in Fig. B.2(b) are singular, like the central point of the circle in the original space and the inner circle of the transformed space in the previous cloaking. Therefore, grid lines orthogonal to $\overline{EG}$ in the original space are cut by $E'F'G'H'$ in the transformed space. By these conditions, waves incident in the y' direction can enter the inner space O' which is theoretically void, but waves are able to pass through this space if it is assumed to be filled with the air, the same media outside of the cloaking.

Using Eq. (2.21) and Eq. (2.22), the distributions of the reciprocal density and the bulk modulus in the transformed design domain are calculated. For the upper half part of the cloaking device,

$$\left[\frac{1}{\rho'(x')}\right]=\frac{b}{\rho_{air}\left(b-\sqrt{a^2-x'^2}\right)}\begin{bmatrix}1 & -\left(1-\frac{y'-\sqrt{a^2-x'^2}}{b-\sqrt{a^2-x'^2}}\right)\frac{x'}{\sqrt{a^2-x'^2}} \\ sym & \left(1-\frac{y'-\sqrt{a^2-x'^2}}{b-\sqrt{a^2-x'^2}}\right)^2\frac{x'^2}{a^2-x'^2}+\left(\frac{b-\sqrt{a^2-x'^2}}{b}\right)^2\end{bmatrix} \tag{B.2}$$

$$\kappa'(x')=\frac{b-\sqrt{a^2-x'^2}}{b}\kappa_{air} \tag{B.3}$$

are obtained, where ρ_{air} and κ_{air} are the density and the bulk modulus of air. The properties of the lower half part are symmetric for the x' axis.

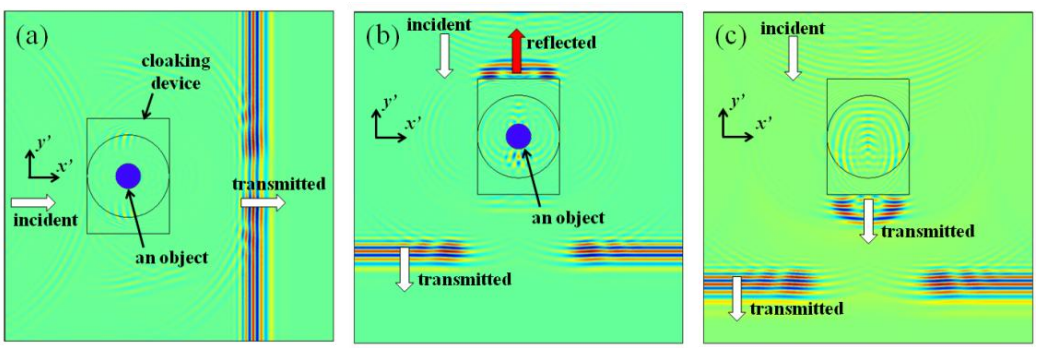

Fig. B. 3 Simulation results for the proposed device using time-harmonic plane waves of the 50 kHz-centered Gaussian pulse. (a, b) The results for waves incident along the x and y directions, respectively when an object is inserted inside the circular cavity of the cloaking. (c) The result for a wave incident along the y direction when there is no object lying inside the cavity.

As an evaluation of the cloaking having the material properties of Eq. (B.2) and Eq. (B.3),

the simulation results are shown in Fig. B.3 by using a time-transient incident plane waves of a Gaussian pulses centered at 50 kHz. Here, a and b are set to be $0.05\,\mathrm{m}$ and $0.07\,\mathrm{m}$, respectively. When a wave is incident along the x' direction (see Fig. B.3(a)), the wave fronts are virtually planar after it passes the cloaking device even though an object (blue circle) exists inside the device. Thus, the object lying can be effectively cloaked against an incoming plane wave along the x' direction. On the other hand, Fig. B.3(b) shows that a wave incident in the y' direction is partially reflected when the object is inside the circular area surrounded by the cloaking. Therefore, the presence of the object can be identified by analyzing the wave reflected back towards the wave source. Meanwhile, Fig. B.3(c) proves that there is no reflection if nothing is inside the device. Finally, Fig. b.3 shows that a cloaking device having the material properties calculated in (B.2) and (B.3) works well in accordance with the research motivation.

B.3 Results and Discussions

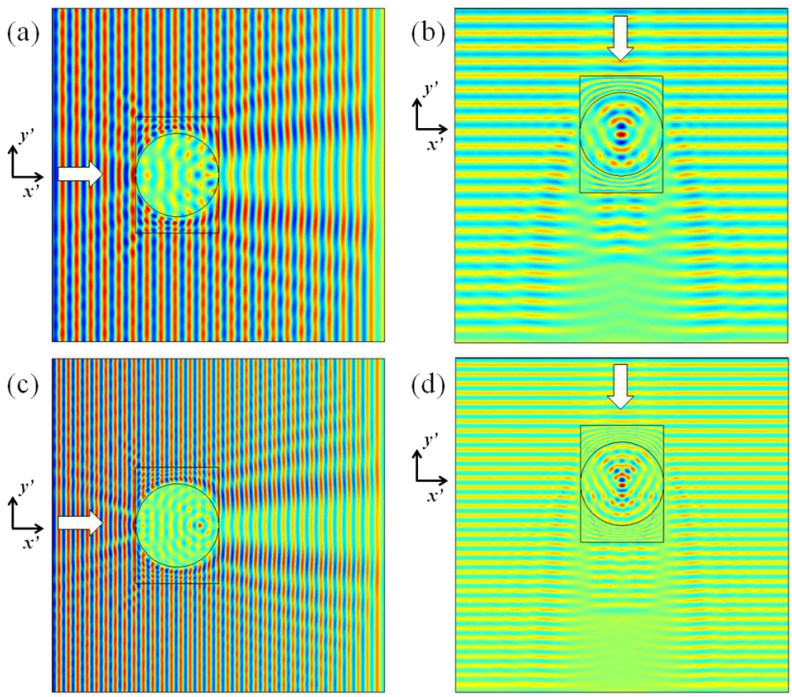

Fig. B. 4 Simulations of time-harmonic wave propagation when no object is inserted inside the cavity. Wave incidences at 20 kHz and 30kHz (a,c) along the cloaking x direction and (b,d) the y direction orthogonal to the cloaking direction.

The features of the directional cloaking are figured out when time-harmonic waves are applied to the cloaking devices as shown in Fig. B.4. Figure B.4 (a) and (b) are the cases of 20 kHz- center frequency waves and Fig. B.4(c) and (d) are of 30 kHz. The following two observations are noticed: (1) there is a slight wave leakage into the cloaked region

O' when the plane wave is incident horizontally, although its wave fronts remain almost planar after passing the cloaking device. It implies that the cloaking function of the device for the horizontal incident waves is not ideally perfect, and (2) a portion of the vertically incident wave that entered O' has a finite time delay when it exits O', compared with the other portion of the incident wave that propagates in the air outside the cloaking device (see Fig. B.4 (b) and (d)). The causes of the findings can be explained in terms of acoustic impedance $Z = \rho c$. For the subsequent investigations on the findings, the polar coordinate system (r', θ') will be introduced in addition to the Cartesian coordinate system (x', y'), the origin of which is located at the center of the region O as the inset of Fig. B.5. Then the points on the boundary of the cloaked area $\partial O'$ are defined as

$$\begin{aligned} x' &= a \sin\theta', \\ y' &= a \cos\theta' \end{aligned} \tag{B.4}$$

To find the density and the acoustic impedances in the notation of (r', θ'), Eq. (B.2) should be rotated by $-\theta$ and the coordinates are substituted by Eq. (B.4) as following. The rotation tensor R is

$$R = \begin{bmatrix} \cos\theta' & -\sin\theta' \\ \sin\theta' & \cos\theta' \end{bmatrix} \tag{B.5}$$

and the reciprocal density tensor in the polar coordinate system can be drawn as

$$\begin{bmatrix} 1/\rho_{nn}' & 1/\rho_{n\theta}' \\ 1/\rho_{n\theta}' & 1/\rho_{\theta\theta}' \end{bmatrix} = R\left[\frac{1}{\rho'}\right]R^T \tag{B.6}$$

The density tensor in the polar coordinate system is

$$\begin{bmatrix} \rho_{nn}' & \rho_{n\theta}' \\ \rho_{n\theta}' & \rho_{\theta\theta}' \end{bmatrix} = \begin{bmatrix} 1/\rho_{nn}' & 1/\rho_{n\theta}' \\ 1/\rho_{n\theta}' & 1/\rho_{\theta\theta}' \end{bmatrix}^{-1} = R\left[\frac{1}{\rho'}\right]^{-1} R^T \tag{B.7}$$

because $R^{-1} = R^T$ for the rotation tensor.

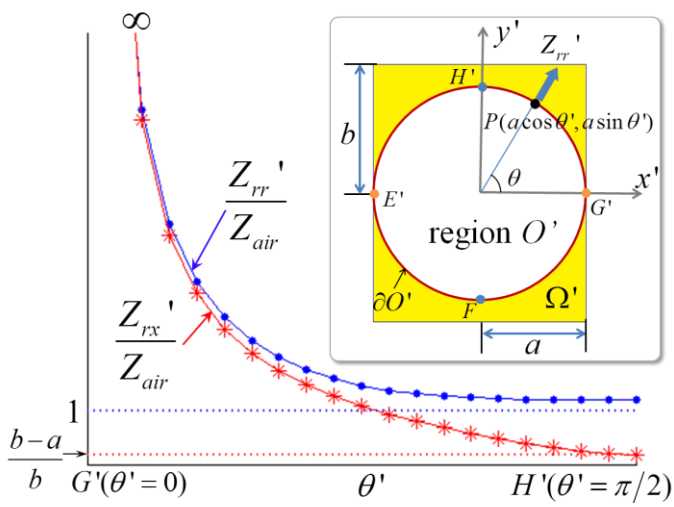

Fig. B. 5 The acoustic impedance components Z_{rr}' and Z_{rx}' as a function of θ', respectively. (inset) Coordinate system used to investigate the acoustic impedance along the boundary $\partial O'$ of the inside cavity O' of the cloaking device. Z_{air} is the impedance of air.

Let us examine the causes of the above mentioned findings. For the wave leakage phenomena for horizontally incident waves, the impedance component Z_{rx} is needed. Acoustic impedance of the perfect cloaking normal to the singular interface can be calculated from the (1,1) component of Eq. (A.16) and Eq. (A.17) as following.

$$Z_{rr}\big|_{r=R_1} = \rho_{rr} c\big|_{r=R_1} = \rho_{rr}\sqrt{\frac{\kappa}{\rho_{rr}}}\Bigg|_{r=R_1} = \sqrt{\rho_{rr}\kappa}\Big|_{r=R_1} \propto \frac{r}{r-R_1}\Bigg|_{r=R_1} \to \infty \qquad \text{(B.8)}$$

As calculated above, acoustic impedance in the radial direction is infinite at the interface between the cloaking and the inner area. Thus, waves in the previous cloaking cannot enter the inner space but flow around it. In case of the directional cloaking, however, acoustic impedance normal to the singular interface changes along the interface. When a plane wave is incident to the cloaking along the x' direction, its wave fronts are vertically straight inside the cloaking. It is because Eq. (B.1) maps the $EFG = EHG$ into $E'H'G' = E'F'G$, air particles at the vertical interface $\overline{A'E'B'}$ follows the curvilinear paths inside Ω'. These air particles are forbidden to the inner boundary $\partial O'$ if the impedance component Z_{rx} along $\partial O'$ is infinite. According to the plot of Z_{rx} along $\partial O'$ as a function of θ' shown in Fig. B.5, Z_{rx} is infinite only at E. Therefore, incident waves can slightly leak into the region O'. However, the leakage seems to be insignificant because $Z_{rx} \gg Z_{air}$ for a wide range of θ.

Next, let us consider the case of time delay phenomena for the vertically incident waves. The key is the fact that waves can pass the inner space which do not exist theoretically in

the initial space. When an incident plane waves enter the upper side of the domain Ω', the horizontal wave fronts become curvilinear as induced from Fig. B.2. It becomes top half circular when it meets $E'H'G'$ of $\partial O'$. The wave fronts is converged at the center point of O' and then diverges to be bottom half of a circle when it exits at $\partial O'$. This means that the travelling wave path is radial inside O'; see Fig. B.4(b) and (d). Compared with the waves travelling outside the cloaking device Ω', the counterparts that have reached O' should propagates along an additional radial path of length $2a$. Consequently, the additional path experienced by the propagating wave inside O' results in the delay in time as can be seen in Fig. B.3 and Fig B.4 since the wave speed inside O' is the same with that in air. Although there is a delay in time between two kinds of transmitted waves, it does not practically matter for the presence purpose of the cloaking device because signal analysis can be carried out only by the reflected waves.

Another issue about the vertically incident waves is the transmission inside O', which is also related to acoustic impedance. If the normal impedance of the cloaking device everywhere along the interface $\partial O'$ is the same with the air, the incident wave would be transmitted perfectly. To calculate the normal impedance of the device, the normal density ρ_{nn} is calculated as

$$\rho_{nn}' = \frac{\rho_{air} b}{\left(b - a\sin\theta'\right)}\left[\left\{\frac{\cos^2\theta'}{\sin^2\theta'} + \left(\frac{b - a\sin\theta'}{b}\right)^2\right\}\cos^2\theta' + 1\right] \tag{B.9}$$

and the normal impedance Z_{nn} is

$$Z_{nn}' = \sqrt{\rho_{nn}'\kappa'} = \sqrt{\rho_{air}\kappa_{air}\left[\left\{\frac{\cos^2\theta'}{\sin^2\theta'} + \left(\frac{b - a\sin\theta'}{b}\right)^2\right\}\cos^2\theta' + 1\right]}$$
$$= Z_{air}\sqrt{\left[\left\{\frac{\cos^2\theta'}{\sin^2\theta'} + \left(\frac{b - a\sin\theta'}{b}\right)^2\right\}\cos^2\theta' + 1\right]}. \quad \text{(B.10)}$$

where ρ_{air} and κ_{air} are the density and bulk modulus of air, respectively. As can be seen in Fig. B.5, the estimated normal impedance component Z_{rr} is the same as Z_{air} only at H ($\theta = \pi / 2$). However, the value of Z_{rr}'/Z_{air} is near 1 for a wide range of θ'. Therefore, most of the incident waves along the *y* direction could be transmitted into the cloaked area O'.

For study further on the performances of the suggested cloaking device, the simulation results are shown in Fig. B.6 in which an object inside O' is off-centered and 30 kHz-centered harmonic plane waves are incident. Wherever the object is located inside O', it is cloaked to the waves incident in the x'. On the other hand, for the waves incident in the y' direction, the patterns of reflected waves are depending on the locations of the object. More precise identification of the existence, the location and the shape of objects inside the cloaked area might be possible by the help of high level signal processing techniques.

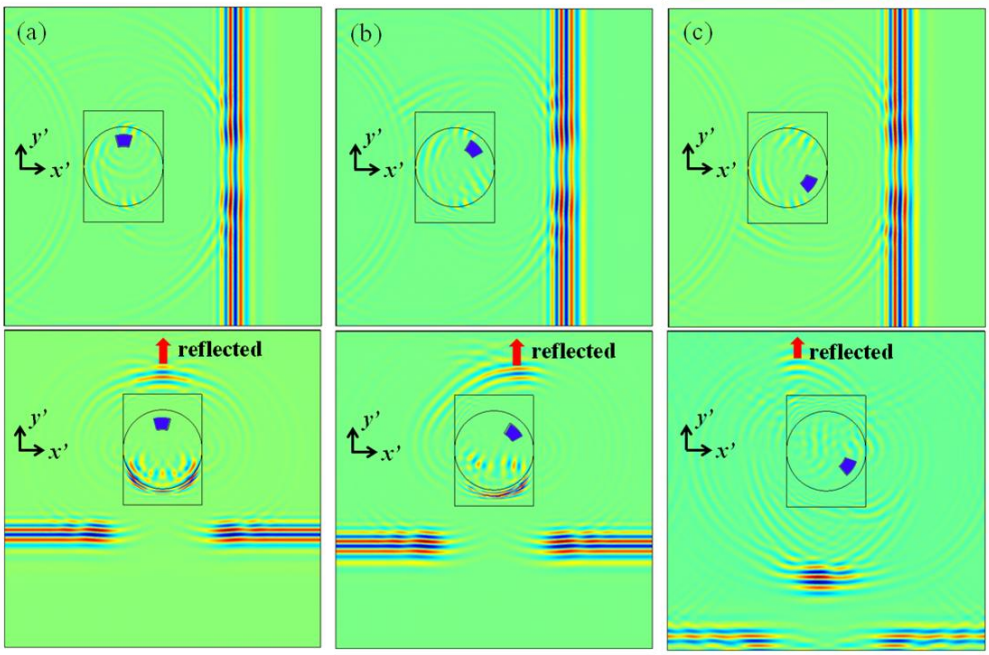

Fig. B. 6 The reflected wave patterns depending on the locations of an object inside the proposed cloaking device. The simulations were conducted for time-harmonic plane waves of the 30 kHz Gaussian pulse.

In conclusion, transformation acoustics was used to design a device with which one can selectively hide or display objects. For the suggested function, a rectangular region was transformed to another rectangle with an inside circular cavity. A mapping equation made horizontal grid lines continuously curvilinear, while vertical grid lines cut by the circular singular interface. The waves incident in the horizontal direction behave as if nothing is inside the device because the waves are bent to flow around the cavity as they do in the perfect cloaking. A slight leakage phenomenon of waves was explained in terms of acoustic impedance. On the contrary, the waves incident in the vertical direction can

penetrate into the inner space of the cloaking device, being reflected towards the incident wave source when there is an inside object. Time delay of waves in this case is due to introduction of new space inside the cavity in the transformed space. Consequently, the suggestion of the transformation equation and the directional cloaking property give a substantial amount of insight and flexibility for engineering wave control devices such as sonars or other armaments Furthermore, in the process of comparing the suggested cloaking device with the previous cloaking shown in Appendix A, the choice of a mapping equation would have a great influence on the functionality and material property distributions of a device.

References

[1] J. B. Pendry, D. Schurig and D. R. Smith, Controlling Electromagnetic Field, Science **312**, 1780-1782 (2006)

[2] U. Leonhardt, Optical Conformal Mapping, Science **312**, 1777-1780 (2006)

[3] D. Schurig, J. J. Mock, B. J. Justice, S. A. Cummer, J. B. Pendry, A. F. Starr and D. R. Smith, Metamaterial Electromagnetic Cloak at Microwave Frequencies, Science **314**, 977-980 (2006)

[4] S. A. Cummer, B.-I. Popa, D. Schurig and D. R. Smith, Full-wave simulations of electromagnetic cloaking structures, Phys. Rev. E **74**, 036621 (2006)

[5] N. Kundtz, D. Gaultney and D. R. Smith, Scattering cross-section of a transformation optics-based metamaterial cloak, New J. Phys. **12**, 043039 (2010)

[6] H. Chen and C. T. Chan, Acoustic cloaking in three dimensions using acoustic metamaterials, Appl. Phys. Lett. **91,** 183518 (2007)

[7] G. W. Milton, M. Briane and J. R. Willis, On cloaking for elasticity and physical equations with a transformation invariant form, New J Phys. **8**, 248 (2006)

[8] M. K. Lee, P. S. Ma, I. K. Lee, H. W. Kim and Y. Y. Kim, Negative refraction experiments with guided shear-horizontal waves in thin phononic crystal plates, Appl. Phys. Lett. **98**, 011909 (2011)

[9] M. K. Lee and Y. Y. Kim, Horizontal cloaking and vertical reflection by transformation acoustics, AIP Advances **3**, 052114 (2013)

[10] M. Wegener and S. Linden, Shaping optical space with metamaterials, Physics Today, 32-36, October 2010

[11] H. Chen, C. T. Chan and P. Sheng, Transformation optics and metamaterials. Nat. Mater. **9**, 387-396 (2010)

[12] Y. Cheng, F. Yang, J. Y. Xu and X. J. Liu, A multilayer structured acoustic cloak with homogeneous isotropic materials, Appl. Phys. Lett. 92, 151913 (2008)

[13] S. A. Cummer and D. Schurig, One path to acoustic cloaking, New J. Phys. **9**, 45 (2007)

[14] D. Torrent and J. Sanchez-Dehesa, Anisotropic mass density by two-dimensional acoustic metamaterials, New J. Phys. **10**, 023004 (2008)

[15] D. Torrent and J. Sanchez-Dehesa, Acoustic cloaking in two dimensions : a feasible approach, New J. Phys. **10**, 063015 (2008)

[16] D. Torrent and J. Sanchez-Dehesa, Broadband acoustic cloaks based on the homogenization of layered materials, Wave Motion **48**, 497-504 (2011)

[17] S. Zhang, C. Xia and N. Fang, Broadband acoustic cloak for ultrasound waves, Phys. Rev. Lett. **106**, 024301 (2011)

[18] M. Farhat, S. Enoch, S. Guenneau and A. B. Movchan, Broadband cylindrical acoustic cloak for linear surface waves in a fluid, Phys. Rev. Lett. **101**, 134501 (2008)

[19] D. Torrent and J. Sanchez-Dehesa, Anisotropic mass density by radially periodic fluid structures, Phys. Rev. Lett. **105**, 174301 (201)

[20] I. Spiousas, D. Torrent and J. Sanchez-Dehesa, Experimental realization of broadband tunable resonators based on anisotropic metafluid, Appl. Phys. Lett. **98**, 244102 (2011)

[21] H. Chen and C. T. Chan, Transformation media that rotate electromagnetic field, Appl. Phys. Lett. **90**, 241105 (2007)

[22] H. Chen, B. Hou, S. Chen, X. Ao, W. Wen and C. T. Chan, Design and experimental realization of a broadband transformation media field rotator at microwave frequencies, Phys. Rev. Lett. **102**, 183903 (2009)

[23] X. Zang and C. Jiang, A rotatable and amplifying optical transformation device, J. Opt. Soc. Am. B **28**, No. 5 (2011)

[24] A. Diatta, G. Dupont, S. Guenneau and S. Enoch, Broadband cloaking and mirages with flying carpets, Opt. Exp. **18** No. 11, 11537 (2010)

[25] T. Ergin, J. Fischer and M. Wegener, Optical phase cloaking of 700 nm light waves in the far field by a three-dimensional carpet cloak, Phys. Rev. Lett. **107**, 173901 (2011)

[26] N. Kundtz and D. R. Smith, Extreme-angle broadband metamaterial lens, Nat. Mater. **9**, 129-132 (2010)

[27] Z. Liang and J. Li, Bending a periodically layered structure for transformation acoustics, Appl. Phys. Lett. **98**, 241914 (2011)

[28] R. Liu, C. Ji, J. J. Mock, J. Y. Chin, T. J. Cui and D. R. Smith, Broadband ground-plane cloak, Science **323**, 366-369 (2009)

[29] B.-I. Popa and S. A. Cummer, Homogeneous and compact acoustic ground cloaks, Phys. Rev. B **83**, 224304 (2011)

[30] B.-I. Popa, L. Zigoneanu and S. A. Cummer, Experimental acoustic ground cloak in air, Phys. Rev. Lett. **106**, 253901 (2011)

[31] D. Shin, Y. Urzhumor, Y. Jung, G. Kang, S. Baek, M. Choi, H. Park, K. Kim and D. R. Smith, Broadband electromagnetic cloaking with smart metamaterials, Nat. Commun. **2219** (2012)

[32] B. Zhang, Y. Luo, X. Liu and G. Barbastathis, Macroscopic invisibility cloak for visible light, Phys. Rev. Lett. **106**, 033901 (2011)

[33]D.-H. Kwon and D. H. Werner, Transformation optical designs for wave collimators, flat lenses and right-angle bends, New J. Phys. **10**, 115023 (2008)

[34] Q. Deng, J. Hu, Z. Chang, X. Zhou and G. Hu, Theory and experiment of isotropic electromagnetic beam bender made of dielectric materials, Adv. Mat. Res. **150-151**, 1508-1516 (2011)

[35] B. Donderici and F. L. Teixeira, Metamaterial blueprints for reflectionless waveguide bends, IEEE Microw. Wirele. Co. **18** No. 4, 233-235 (2008)

[36] X.-Y. He, C. Yang, B. Li, Q. Chen, B.-H. Zhou and C.-X. Tang, Experimental verification of the bending of electromagnetic waves using metamaterials, Appl. Phys. Lett. **98**, 204105 (2011)

[37] J. Luo, P. Xu, H. Chen, B. Hou and L. Gao, Realizing almost perfect bending waveguides with anisotropic epsilon-near-zero metamaterials, Appl. Phys. Lett. **100**, 221903 (2012)

[38] M. Rahm, D. A. Roberts, J. B. Pendry and D. R. Smith, Transformation-optical design of adaptive beam bends and beam expanders, Opt. Exp. **16**, No. 15 (2008)

[39] W. X. Jiang, T. J. Cui, H. F. Ma, X. Y. Zhou and Q. Cheng, Cylindrical-to-plane-wave conversion via embedded optical transformation, Appl. Phys. Lett. **92**, 261903 (2008)

[40] M. Kadic, T. Buckmann, R. Schittny and M. Wegener, Metamaterials beyond electromagnetism, Rep. Prog. Phys. **75**, 126501 (2013)

[41] M. Brun, S. Guenneau and A. B. Movchan, Achieving control of in-plane elastic waves, Appl. Phys. Lett. **94**, 061903 (2009)

[42] M. Farhat, S. Guenneau, S. Enoch and A. B. Movchan, Cloaking bending waves

propagating in thin elastic plates, Phys. Rev. B **79**, 033102 (2009)

[43] M. Farhat, S. Guenneau and S. Enoch, Ultrabroadband elastic cloaking in thin plates, Phys. Rev. Lett. **103**, 024301 (2009)

[44] M. Farhat, S. Guenneau and S. Enoch, Broadband cloaking of bending waves via homogenization of multiply perforated radially symmetric and isotropic thin elastic plates, Phys. Rev. B **85**, 020301 (R) (2012)

[45] N. Stenger, M. Wilhelm and M. Wegener, Experiments on elastic cloaking in thin plates, Phys. Rev. Lett. **108**, 014301 (2012)

[46] M. Kadic, T. Buckmann, N. Stenger,, M. Thiel and M. Wegener, On the practicability of pentamode mechanical metamaterials, Appl. Phys. Lett. **100**, 191901 (2012)

[47] A. N. Norris and A. L. Shuvalov, Elastic cloaking theory, Wave Motion **48**, 525-538 (2011)

[48] L. E. Kinsler, A. R. Frey, A. B. Coppens and J. V. Sanders, Fundamentals of Acoustics, John Wiley & Sons, Inc.: New York, NY (1999)

[49] H. Kuttruff, Ultrasonics : Fundamentals and Applications, Elsevier Science Publishers Ltd., Essex, : England, UK (1991)

[50] D.-H. Kwon and D. H. Werner, Transformation electromagnetic : an overview of the theory and applications, IEEE ANTENN PROPAG. M. **52**, No. 1, 2446 (2010)

[51] G. W. Milton, The Theory of Composites, Cambridge Univ. Press, Cambridge, (2002)

[52] I. H. Shames and J. M. Pitarresi, Introduction to solid mechanics, 3rd ed., Prentice Hall, Upper Saddle River, NJ (2000)

[53] S. H. Crandall, N. C. Dahl and T. J. Lardner, An introduction to the mechanics of solids, 2nd ed., New York (1978)

[54] COMSOL Multiphysics, COMSOL Multiphysics modeling guide: Version 3.5, COMSOL AB: Stockholm (2008)

[55] F. G. Vasquez, G. W. Milton, D. Onofrei and P. Seppecher, Transformation elastodynamics and active exterior acoustic cloaking, S. Guenneau, R. Craster (Eds.), Acoustic Metamaterials: Negative Refraction, Imaging, Lensing and Cloaking, Canopus Academic Publishing and Springer SBM 289–318 (2012)

[56] R. Schinzinger and P. A. A. Laura, Conformal mapping : methods and applications, Dover Publications,Inc., Mineola, NY (2003)

[57] Y. Urzhumov, N. Landy and D. R. Smith, Isotropic-medium three-dimensional cloaks for acoustic and electromagnetic waves, Appl. Phys. Lett. **111**, 053105 (2012)

[58] C. Gu, K. Yao, W. Lu, Y. Lai, H. Chen, B. Hou and X. Jiang, Experimental realization of a broadband conformal mapping lens for directional emission, Appl. Phys. Lett. **100**, 261907 (2012)

[59] G. D. Manolis, R. P. Shaw and S. P. Pavlou, Elastic waves in nonhomogeneous media under 2D conditions : I. Fundamental solutions, Soil Dyn. Earthq. Eng. **19**, 19-30 (1999)

[60] G. D. Manolis, R. P. Shaw and S. P. Pavlou, Elastic waves in nonhomogeneous media under 2D conditions : II. Numerical implementation, Soil Dyn. Earthq. Eng. **18**, 31-46 (1999)

[61] G. D. Manolis and R. P. Shaw, Fundamental solutions for variable density two-dimensional elastodynamic problems, Eng. Anal. Bound. Elem. **24**, 739-750 (2000)

[62] G. D. Manolis, T. V. Rangelov and R. P. Shaw, Conformal mapping methods for

variable parameter elastodynamics, Wave Motion **36**, 185-202 (2002)

[63] Z. Chang, J. Hu, G. Hu, R. Tao and Y. Wang, Controlling elastic waves with isotropic materials, Appl. Phys. Lett. **98**, 121904 (2011)

[64] J. Hu, Z. Chang and G. Hu, Approximate method for controlling solid elastic waves by transformation media, Phys. Rev. B **84**, 201101(R) (2011)

[65] Z. Chang and G. Hu, Elastic wave omnidirectional absorbers designed by transformation method, Appl. Phys. Lett. **101**, 054102 (2012)

[66] Z. Chang, X. Liu and G. Hu, Transformation ray method : controlling high frequency elastic waves (L), J. Acoust. Soc. Am. **132** (4), 2942-2945 (2012)

[67] A. Khelif, P.A. Deymier, B. Djafari-Rouhani, J. O. Vasseur and L. Dobrzynski, Two-dimensional phononic crystal with tunable narrow pass band: Application to a waveguide with selective frequency, J. Appl. Phys. **94**, No.3, 1308-1311 (2003)

[68] T.-T. Wu, Z.-G. Huang and S. Lin, Surface and bulk acoustic waves in two-dimensional phononic crystal consisting of materials with general anisotropy, Phys. Rev. B **69**, 094301 (2004)

[69] X. Zhang and Z. Liu, Negative refraction of acoustic waves in two-dimensional

phononic crystals, Appl. Phys. Lett. **85**, No.2, 341-343 (2004)

[70] A. S. Phani, J. Woodhouse and N. A. Fleck, Wave propagation in two-dimensional periodic lattices, J. Acoust. Soc. Am. **119**, No. 4, 1995-2005 (2006)

[71] J.-C. Hsu and T.-T. Wu, Efficient formulation for band-structure calculations of two-dimensional phononic-crystals plates, Phys. Rev. B **74**, 144303 (2006)

[72] J. Li, Z. Liu and C. Qiu, Negative refraction imaging of acoustic waves by a two-dimensional three-component phononic crystal, Phys. Rev. B **73**, 054302 (2006)

[73] A.-C. Hladky-Hennion, J. Vasseur, B. Dubus, B. Djafari-Rouhani, D. Ekeom and B. Morvan, Numerical analysis of negative refraction of transverse waves in an elastic material, J.Appl. Phys. **104**, 064906 (2008)

[74] A. Sukhovich, L. Jing and J. H. Page, Negative refraction and focusing of ultrasound in two-dimensional phononic crystals, Phys. Rev. B **77**, 014301 (2008)

[75] J. Li, Z. Liu and C. Qiu, Negative refraction imaging of solid acoustic waves by two-dimensional three-component phononic crystal, Phys. Lett. A **372**, 3861-3867 (2008)

[76] P. S. Ma, H. W. Kim, J. H. Oh and Y. Y. Kim, Mode separation of a single-frequency bi-modal elastic wave pulse by a phononic crystal, Appl. Phys. Lett. **99**, 201906 (2011)

[77] E. Centeno, D. Cassagne and J.-P. Albert, Mirage and superbending effect in two-dimensional graded photonic crystals, Phys. Rev. B **73**, 235119 (2006)

[78] H. Kurt, E. Colak, O. Cakmak, H. Caglayan and E. Ozbay, The focusing effect of graded index photonic crystals, Appl. Phys. Lett. **93**, 171108 (2008)

[79] S.-C. S. Lin and T. J. Huang, Gradient-index phononic crystals, Phys. Rev. B **79**, 094302 (2009)

[80] S.-C. S. Lin, B. R. Tittmann, J.-H. Sun, T.-T. Wu and T. J. Huang, Acoustic beamwidth compressor using gradient-index phononic crystals, J. Phys. D: Appl. Phys. **42**, 185502 (2009)

[81] S. H. Cho, J. S. Lee and Y. Y. Kim, Guided wave transduction experiment using a circular magnetostrictive patch and a figure-of-eight coil in nonferromagnetic plates, Appl. Phys. Lett. **88**, 224101 (2006)

[82] J. S. Lee, S. H. Cho and Y. Y. Kim, Radiation patter of Lamb waves generated by a

circular magnetostrictive patch transducer, Appl. Phys. Lett. **90**, 054102 (2007)

[83] J. S. Lee, S. H. Cho and Y.Y. Kim, Beam-focused shear-horizontal wave generation in a plate by a circular magnetostrictive patch transducer employing a planar solenoid array, Smart Mater. Struct. **18**, No. 1 (2009)

[84] H. Tada, P. C. Paris and G. R. Irwin, The stress analysis of cracks handbook, 3rd Ed., Del Research Corp, Hellerton, PA (1973).

[85] P. K. Mallick, Effects of hole stress concentration and its mitigation on the tensile strength of sheet moulding compound (SMC-R50) composites, Composites **19**, No. 4, 283-287 (1988)

[86] Z. Yang, C.-B. Kim, C. Cho and H. G. Beom, The concentration of stress and strain in finite thickness elastic plate containing a circular hole, Int. J. Solids. Struct. **45**, 713-731 (2008)

[87] J. R. Rice, A path-independent integral and the approximate analysis of strain concentration by notches and cracks, J. Appl. Mech. **35**, 376-386 (1968)

[88] E. F. Rybicki and M. F. kanninen, A finite element calculation of stress intensity factors by a modified crack closure integral, Engng. Fracture. Mech. **9**, 931-938

(1977)

[89] K. Kishimoto, S. Aoki and M. Sakata, On the path independent integral, J. Engng. Fracture Mech. **13**, 841-850 (1980)

[90] K. Kishimoto, S. Aoki and M. Sakata, Dynamic stress intensity factors using J-integral and finite element method, Engng. Fracture. Mech. **13**, 387-394 (1980)

[91] T. Nishioka and S. N. Atluri, Path-independent integrals, energy release rates, and general solutions of near-tip fields in mixed-mode dynamic fracture mechanics, Engng. Fracture. Mech. **18**, 1-22 (1983)

[92] T. Nishioka, R. Murakami and Y. Takemoto, The use of the dynamic J integral (J') in finite-element simulation of Mode I and missed-mode dynamic crack propagation, Int. J. Pres. Ves. & Piping **44**, 329-352 (1990)

[93] S. H. Eslami and F. Amini, Dynamic stress intensity factors due to scattering of harmonic waves by a crack in a infinite medium, Fatigue Fract. Engng. Mater. Struct. **31**, 918-927 (2008)

[94] B. Gommerstadt, The time-averaged elastodynamic J-integral, Int. J. Fracture 101, L15-L20 (2000)

[95] S. A. Cummer, M. Rahm and D. Schurig, Material parameters and vector scaling in transformation acoustics, New J. Phys. **10**, 115025 (2008)

[96] H. Chen and C. T. Chan, Acoustic cloaking and transformation acoustics, J. Phys. D: Appl. Phys. **43**, 113001 (2010)

[97] Z. L. Mei, J. Bai, T. M. Niu and T. J. Cui, Design of arbitrarily directional cloaks by solving the Laplace's equation, J. Appl. Phys. **107**, 124502 (2010)

[98] B. Vasic and R. Gajic, Self-focusing media using graded photonic crystals: focusing, Fourier transforming and imaging, directive emission, and directional cloaking, J. Appl. Phys. **110**, 053103 (2011)

[99] J.-C. Hong, K. H. Sun and Y. Y. Kim, Dispersion-based short-time Fourier transform applied to dispersive wave analysis, J. Acoust. Soc. Am. **117** (5), 2949-2960 (2005)

Abstract (Korean)

변환 탄성 기법을 이용한 유도초음파 클로킹의 설계와 응력 차단에의 응용

이 민 경

서울대학교 대학원

기계항공공학부

본 연구는 변환 기법을 이용한 탄성 클로킹의 설계와 이를 이용한 응력 차폐를 다루었다. 탄성 기법은 전자기파나 음향파를 조절하는 도구로서 널리 사용되어 왔으나 탄성파에 대해서는 그 응용이 아직 미미한데, 이는 탄성체가 체적탄성률과 전단탄성률을 가지고 있다는 점에서 기인한다. 특히 이 중에서 전단탄성률은 전자기파나 음파의 매질에서는 찾아볼 수 없는 특성이기 때문에, 변환 탄성 과정에서 파동의 지배방정식이 그 형태를 유지하지 못한다. 결과적으로, 변환된 탄성파의 지배방정식에서는 실재하는 물질에서는 찾아볼 수 없는 커플링 항들이 매질의 물성치로서 나타난다. 커플링 항들의 영향을 줄이기 위하여 우리는 이 항들이 실제로 장치를 구현, 응용하는 과정에서

어느 정도의 비중을 차지하는지 확인하고, 비중을 줄일 수 있는 변형식을 찾아보았다.

먼저 우리는 공형 변환식을 이용하여 탄성체를 변형시키면 커플링 항에 포함된 원소들을 구성하는 요소의 일부가 서로 상쇄시킴으로써 커플링 항의 크기를 줄일 수 있음을 수식으로 보였다. 그리고 공형 변환으로 설계된 클로킹 장치 내에서 커플링 항들의 영향이 적으며, 이 항들이 탈락되어도 장치의 성능이 우수함을 시뮬레이션 및 실험으로 증명하였다. 클로킹 장치를 구현하기 위해서 다양한 포노닉 크리스탈을 복합적으로 사용하였다. 다음으로는 이 결과의 연장선상에서, 구현된 클로킹을 응력 분산에 응용하였다. 일반적으로 평판에 인장 응력이 가해지면 평판 내에 위치한 구멍이나 결함 끝부분에 큰 응력이 집중되어 구조물의 파괴를 일으킨다. 그리고 탄성파 또한 구멍 또는 결함에 반복적으로 응력을 가할 수 있다. 이때, 구멍 또는 결함을 클로킹 내부에 위치하도록 하여 클로킹을 구조물 표면에 부착하면 탄성파의 일부가 클로킹의 영향을 받아 그 경로가 바뀌며, 결과적으로 구멍 또는 결함에 가해지는 응력의 크기가 줄어든다. 이를 시뮬레이션 및 실험으로 증명함으로써, 탄성 변환 기법을 이용하여 설계된 클로킹이 구조물의 안정성을 도모할 수 있음을 확인하였다.

주요어 : 탄성 변환 기법, 탄성 클로킹, 공형 변환, 응력 차폐, 파동 제어

학 번 : 2010-31318